The development of 3D colorectal cancer models to test cancer therapies.

Miss Michelle Anneka Johnpulle

Submitted in accordance with the requirements for the degree of Doctor of Medicine (M.D.)

The University of Leeds

School of Medicine

March 2024

Intellectual property and copyright statement

I confirm that the work submitted is my own and that appropriate credit has been given where reference has been made to the work of others.

Acknowledgements

I would firstly like thank the generous funding, kindly awarded by the charity organisation Rays of Hope. Without this and the opportunity of fellowships funded by the Royal College of Surgeon England and Bowel Cancer UK this research would not have been possible. I would also like to thank my academic supervisors Dr Fiona Errington Mais and Dr Victoria Jennings who without their patience and support this work would not have been completed. Special thanks should also be given to my clinical team who supported me during my time in Leeds. I'd like to thank the inspirational Professor Giles Toogood for his knowledge and words of encouragement during my time in research.

Throughout my research project I would like to thank my family, my husband Jonathan, mum and sister Andrea as well as my mother and father -in -law who looked after my boys Henry and Oscar, who I had during my time in research, so that I could complete my project and continue clinical work. Their words of encouragement and advice were invaluable. They have all been on this journey with me.

I would also like to thank my friend Jen who introduced me to Leeds and the world of research. She made my time at Leeds enjoyable and unforgettable.

Finally, I would like to dedicate this work to my late father Dr Antoninus Johnpulle who without him I would not be where I am today. His hard work and determination were an inspiration. He always told me never to miss opportunities to better myself and to help others. Thank you for being the best father and a role model.

Abstract

In 2015 there were an estimated 2.5 million people living with cancer in the UK. This number will rise to 4 million by the year 2030. 1.1 million of these deaths will be due to colorectal cancer. For those patients who have progressive metastatic disease, that is not amenable to surgery, less than 10% of patients will survive 5 years. The standard regime for advanced or metastatic colorectal cancer is chemotherapy. This can take the form of mono-therapy with Capcitebine or oxaliplatin, in combination with 5-fluorocil (5-FU) and folinic acid. However, acquired drug resistance is a major issue and this can result in a decrease in therapeutic efficacies in cancer treatments.

Oncolytic viruses (OV) have been used to treat a variety of different cancers and are safe and well tolerated in cancer patients. They can be used independently or in conjunction with more traditional treatments such as chemotherapy and radiotherapy. Most notably, the US Food and Drug Administration (FDA) has licensed the OV, Talimogene laherparepvec (T-VEC), for patients with inoperable melanoma. OVs preferentially infect and kill cancer cells by two differential methods. Firstly, the cancer cells are destroyed by viral replication causing the release of viral progeny, which go on to destroy the additional tumour cells. Secondly, OV's induce cell death by activating the human immune system, thereby acting as a cancer immunotherapy.

To date, 2-Dimensional (2D) cell cultures models have been utilised to test the efficacy of OV against CRC. However, 2D cell layers lack many features that are exhibited in human cancer cells, such as the complex cellular heterogeneity, or cell-to-cell interactions, that are present in clinical tumours. By contrast, 3-dimensional (3D) multicellular models are more likely to represent the complex tumour microenvironment (TME) as they develop cell-cell interactions, hypoxic areas, and from physical barriers for drug penetration. Therefore, 3D structures provide a more realistic pre-clinical model for testing of novel therapeutic agents.

.

MiRNAs are small, non-coding regulatory RNAs that bind to mRNA sequences and decrease mRNA stability prevent translation of specific target proteins. Significantly, miRNA aberrations have been associated with drug resistance in CRC. Dysregulation of miRNAs has been associated in a variety of solid tumours including gastric, breast and lung cancers. Pivotally, miRNA-145 is down regulated in CRC. If this miRNA can be re-introduced we can aim to restore chemo-sensitivity in CRC by normalizing gene expression. Evidence shows that over-expression of miR-145 can inhibit cell proliferation, migration and invasion.

As OV specifically target the TME, they can preferentially replicate in malignant cells and are also well tolerated in the patient population. Therefore, they are ideal vehicles to deliver miRNA species into malignant cells. Moreover, the ability of OV to synergise with chemotherapy is well established and therefore this approach would hopefully build on current studies and identify a novel approach to overcome drug resistance.

In this project we aim to develop and characterise superior 3D models of CRC, and test the efficacy of the OV, Maraba virus (MG-1), as a direct cytotoxic agent. We will also explore miRNA delivery using MG-1 and perform initial studies to investigate the ability miRNA-expressing MG-1 to potentiate the cytotoxic capabilities of the chemotherapy agent, 5-FU.

Abbreviations

2D	2 Dimensional
3D	3 Dimensional
5FU	5- Fluorouracil
AJCC	American Joint Committee on Cancer
AKT	Protein Kinase
ANOVA	Analysis of Variance
ATCC	American Type Culture Collection
ATP	Adenosine triphosphate
BCL	B cell lymphoma-2
BMJ	British Medical Journal
BRAF	V-Raf murine sarcoma viral oncogene homolog B1
BUB1	Budding uninhibited by benzimidazoles 1
CAF	Cancer associated fibroblasts
CD14	Cluster of differentiation 14-human protein made of macrophages
CD163	Cluster of differentiation 163
CEA	Carcinoembryonic antigen
CIN	Carcinoma in situ
CMV	Cytomegalovirus
CRC	Colorectal cancer
CSC	Cancer stem cells
CTG	Cell titre glow assay
CTL	Cytotoxic T lymphocytes
DMEM	Dulbecco's modified eagle's medium
DMSO	Dimethyl sulfoxide
DNA	Deoxyribonucleic acid
DROSHA	Double stranded RNA-specific endoribonuclease
EBV	Epstein-Barr virus
ECM	Extracellular matrix
ELISA	Enzyme linked immunosorbent Assay

EMT	Epithelial mesenchymal transition
EPC	Endothelial progenitor cells
FACS	Fluorescence activated cell sorting
FDA	Food and drug administration
FZD10	Frizzled class receptor 10
GFP	Green fluorescent protein
HBSS	Hanks' balanced solution
HFF	Human foreskin fibroblasts
HIV	Human immunodeficiency virus
IFN	Interferon
IHC	Immunohistochemistry
IL	Interleukin
KRAS	Ki-ras2 Kristen rat sarcoma viral oncogene homolog
MAGE	Melanoma antigen gene
MAPK	Mitogen activated protein kinase
MCTS	Multicellular tumour spheroid
MDSC	Myeloid derived suppressor cells
MMP	Matrix metalloproteinases
MOI	Multiplicity of infection
MSC	Mesenchymal stem cells
MSI	Microsatellite instability
MTT	4,5-dimethylthiazol-2-yl)-2,5-diphenyltetrazolium bromide
NF	Nuclear factor
NK	Natural killer
NOX4	NADPH oxidase 4
NP	Nanoparticles
NSCLC	Non-small cell lung cancer
OV	Oncolytic virus
PAMP	Pathogen associated molecular patterns
PBMC	Peripheral blood mononuclear cells
PBS	Phosphate buffered saline

PCR	Polymerase chain reaction
PDGF	Platelet derived growth factor
PFA	Paraformaldehyde
PFU	Plaque forming unit
PI3K	Phosphoinositide 3-kinase
PKC	Protein kinase C
PKR	Protein kinase receptor
PLT	Platelets
PMN	Polymorphnuclear
PMS2	Postmeiotic segregation increased 2
PRR	Pattern recognition receptor
PTEN	Phosphatase and TENsin homolog deleted on chromosome 10
RAD18	E3 ubiquitin-protein ligase
RAF	Rapidly accelerated fibrosarcoma
RAS	Rat sarcoma
RFS	Relapse free survival
RISC	RNA induced silencing complex
RNA	Ribonucleic acid
ROS	Reactive oxygen species
RPMI	Roswell Park Memorial Institute
RT	Room temperature
SA-PE	Streptavidin phycoerythrin
SD	Standard deviation
SEM	Standard error of the mean
SFRP	Secreted frizzled related protein
SMAD	Staphylococcal morphology determinant A
SNAIL	Zinc finger protein
SOX9	Sex determining region Y box 9
STR	Short tandem repeat
TAM	Tumour associated macrophages
TCR	T cell receptor

TGF	Transforming growth factor
TK	Thymidine kinase
TME	Tumour microenvironment
TNF	Tumour necrosis factor
TNFSF	Tumour receptor superfamily
TP53	Tumour protein 53
TRAIL	TNF-related apoptosis inducing ligand
TSLP	Thymic stromal lymphopoietin
TTP	Thymidine triphosphate
TUSC3	Tumour suppressor candidate 3
T-VEC	Talimogene laherparepvec
TWEAK	TNF-related weak inducer of apoptosis
UK	United Kingdom
USA	United States of America
VEGF	Vascular endothelial growth factor
VSV	Indiana vesiculovirus
VV	Vaccinia virus

Table of Contents

List of Figures

List of Tables

Chapter 1: Introduction

1.1 Background

For centuries cancer research has focused on the tumour centric model of cancer. However, as early as 1863 it was recognised that tumour cells interact with their environment. It was Rudolph Virchow who first observed that leukocytes infiltrated tumours. This led him to postulate a link between cancer and inflammation. [1] However, it was not until the 1970's that the role the tumour microenvironment (TME) played in the development and progression of cancer was widely studied. Today the TME is recognised as a highly complex and heterogenous ecosystem that not only contains malignant cells, but also other cells from the hosts such as endothelial cells, fibroblasts, and a variety of immune cells. These TME interactions play a pivotal role in cancer progression, local resistance, immune evasion and metastasis. Moreover, it has been demonstrated that certain features of the TME can predict better clinical outcomes in melanoma, ovary and colorectal cancer (CRC), in particular, the extent of tumour infiltration by cytotoxic T lymphocytes (CTLs) is associated with a better prognosis. [2] Understanding cellular interactions within the TME, and identifying the factors that influence tumorigenesis, initiation, progression, metastasis, immune evasion and drug resistance will aid the development of novel therapeutic modalities to halt tumour progression and overcome drug resistance. [3] Furthermore, identifying what drives infiltration of CTLs and harnessing this phenomenon could also lead to improved outcomes in cancer patients.

1.2 Colorectal Cancer (CRC)

1.2.1 Pathogenesis

The formation of CRC from normal colonic mucosa is a multistep process outlined in **Figure 1.1.** This process involves genetic and epigenetic changes that result in the conversion from normal glandular epithelial cells to invasive adenocarcinoma. Fearon and Vogelstein first postulated the theory that tumour progression occurs from benign neoplasms such as adenomas and sessile polyps to more invasive cancer. [4]

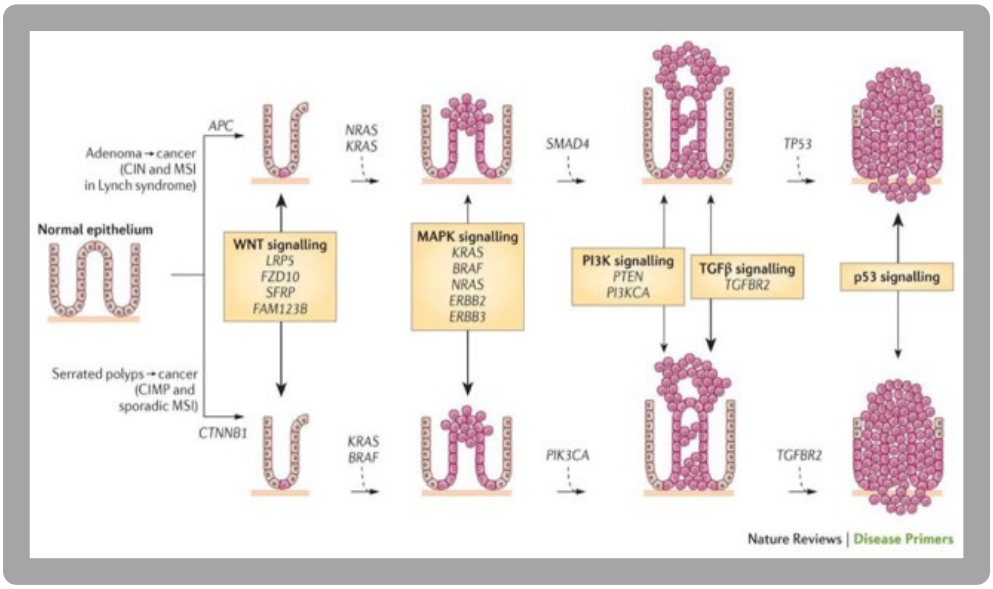

Figure 1-1. Progression from benign polyp to CRC. The progression from a benign polyp to CRC can occur by two distinct processes. Normal colonic epithelial cells transform from aberrant crypt foci to early and advanced polyps which progress to cancer. The classical pathway demonstrated at the top depicts the transformation of tubular adenoma to adenocarcinoma. The alternative pathway demonstrated at the bottom depicts serrated polyps and the progression to serrated CRC. The genes involved in each pathway are indicated. Some genes are involved in both pathways whereas others are unique to that specific pathway. The signalling pathways involved during cancer progression are also shown. The length of the arrow represents the significance of the pathway. Abbreviations: APC, adenomatous polyposis coli; CIN, chromosomal instability; CTNNB1, catenin-β1; FAM123B, family with sequence similarity 123B (AMER1); FZD10, frizzled class receptor 10; LRP5, low density lipoprotein receptor-related protein 5; MAPK, mitogen activated protein kinase; MSI, microsatellite instability; PI3K, phosphatidylinositol 3-kinase; PI3KCA, phosphatidylinositol =-4,5- bisphosphate 3-kinase catalytic subunit-α; PTEN, phosphate and tensin homologue; SFRP, secreted frizzled-related protein; SMAD4, SMAD family member 4; TGFβ, transforming growth factor-β; TGHBR2, TGFβ-receptor 2. This image taken from Kupiers et al (2015).*[5]*

Neoplastic cells differ from normal colonic mucosa as they are genetically unstable. A variety of genetic instability features have been described in CRC, these include, chromosomal instability (CIN), microsatellite instability (MSI), non-MSI hypermutability, aberrant DNA methylation and global DNA hypomethylation. [6] CIN occurs in the majority of CRCs and has been reported in up to 85% of CRC patients. [7] CIN is usually recognisable due to structural chromosome abnormalities, including the acquisition or loss of a whole arm of a chromosome. This can occur due to the dysregulation of mitotic checkpoint regulators, such as budding uninhibited by benzimidazoles 1 (BUB1). Smaller structural abnormalities are caused by dysregulation of DNA repair. CIN can play a role in the progression of a polyp to CRC therefore, chromosome abnormalities have been identified in colonic adenomas. [8]

The remaining 15% of CRC exhibit MSI. Although rare, MSI can be found in serrated polyps, except in Lynch syndrome, where it is prevalent in tubular adenomas. The mechanism of MSI can be attributed to inactivation of DNA Mismatch Repair genes (MMR) which include MLH1, MLH2, MSH6 and PMS2. In the majority of CRC, the MLH1 gene is inactivated by two main mechanisms: 1) by uncontrolled DNA methylation; or 2) by somatic mutation. Lynch syndrome patients develop CRC due to mutation in MMR genes and are therefore almost always MSI. [9] MSI CRC commonly harbour a genetic mutation in the oncogene BRAF (BRAFV600E) which is associated with worse prognosis. [10] Unregulated DNA methylation is apparent in the majority of CRCs; however, a decrease in DNA methylation can also occur. Whilst the mechanism for this hypomethylation is unclear, research suggests that this can be attributed to the expression of oncogenes such as Kristen rat sarcoma virus (KRAS). [11] [12] KRAS is a proto-oncogene. In normal physiological conditions KRAS initiates signal transduction pathways that are initiated when epidermal growth factor receptors (EGFR), hepatocyte growth factors (HGF) and insulin-like growth factors (IGF) bind to their corresponding receptors as is demonstrated in **Figure 1.2.** Wild-type KRAS can cause the activation of multiple effectors such as RAF, BRAF and MEK1 and 2. These effectors induce a multitude of effects on cell function such

apoptosis suppression, cell growth initiation, transformation, angiogenesis, cell migration and differentiation. As mentioned earlier, 60% of CRC patients exhibit activating mutations in the KRAS gene. Unfortunately, this subset of CRC is associated with an aggressive tumour and reduced survival. [13] There have been multiple studies that have shown that patients with KRAS mutations demonstrate a shorter overall survival compared to patients with wild-type KRAS mutations. [14] The median overall survival of patients with wild-type KRAS was 35.1 months compared to 25.8 months for those with mutant KRAS (p=0.006). [15] BRAF mutations occur in 7-10% of patients with CRC. These patients have a median survival of less than 12 months. [16] BRAF exerts its effect downstream from KRAS in the Mitogen activated protein kinase (MAPK) pathway, coding for a serine/theroine kinase. The BRAF oncogene activates mitogen activated protein kinase kinase (MAPKK/MEK) and promotes uncontrolled cell proliferation in an EGFR independent manner. The BRAFV600E mutation is the most common and contributes to ~90% of BRAF mutations. [17]

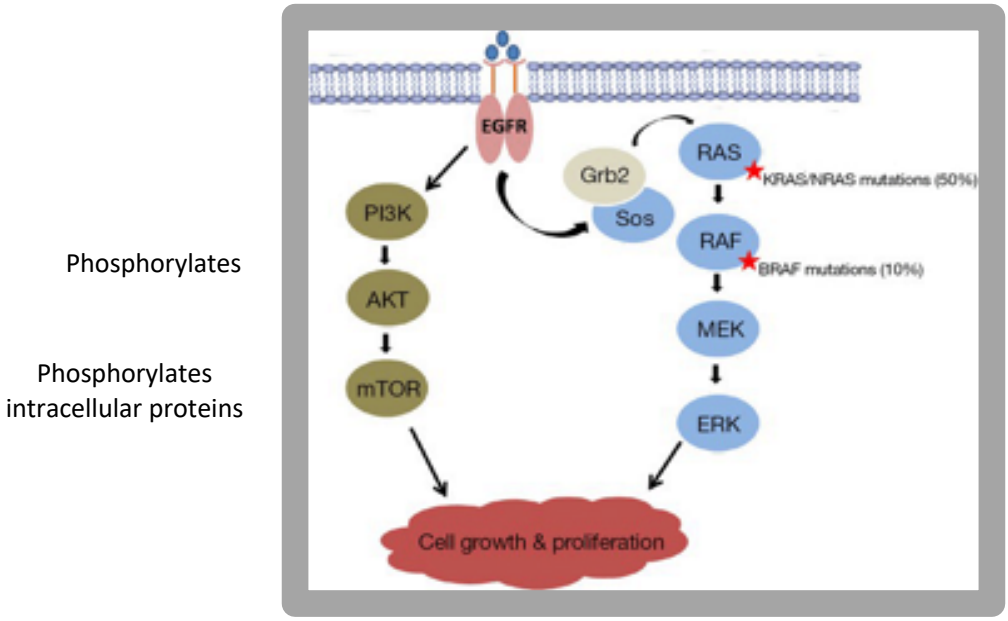

Figure 1-2. **MAPK signalling in the formation of CRC.** Mutations in genes such as KRAS and BRAF result in uncontrolled cell proliferation and tumorigenesis due to the activation of a signalling cascade. The main effects can occur downstream from the EGFR (epidermal growth factor) receptor. Tumours that rely on anti-EGFR treatments are resistant. PI3K activation phosphorylates and activates AKT (protein B kinase). Activated AKT, via mTOR, can phosphorylate intracellular proteins to promote cell growth and survival. This image adapted from Clarke et al 2015. [17]

1.2.2 Epidemiology

CRC is the 4th most common cause of cancer in the UK and accounted for 12% of new cancer diagnoses in 2015. It is the 2nd most common cause of cancer death in the UK, with 10% of all cancer deaths being attributed to CRC. Every day there are 110 new cases of CRC diagnosed in the UK. Unfortunately, this number is expected to rise with the ageing population, where incidence rates are at their highest in people aged 85 to 89 (2013-2015) (Cancer Research UK). **Figure 1.3** demonstrates the increasing incidence of CRC in both males and females over their lifetime. Currently, the aging male population show an increased incidence of CRC compared to females. Although the incidence of CRC is on the rise, survival has more than doubled in the last 40

years. This encouraging increase in survival can be attributed to a number of factors including early diagnosis, excellent screening methods, increased patient awareness, and better treatment modalities. [18] However, despite these improvements patients with advanced metastatic disease (stage 4 disease) have poorer outcomes and, in this setting, less than 10% of patients survive 5-years post diagnosis. (Cancer Research UK)

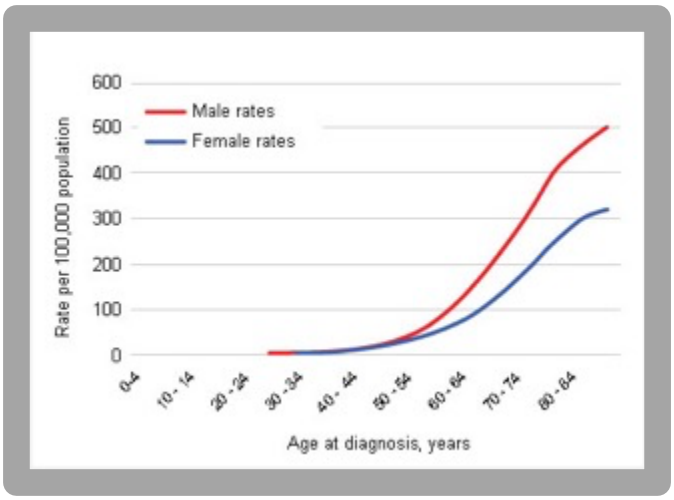

Figure 1-3. Incidence of CRC in the UK depending on age group. Chart shows incidence of CRC increases as the age of the population increases. More males are diagnosed as the population ages, compared to females. Image taken from BMJ 2018. [19]

1.2.3 Staging

To determine how far the CRC has spread, and therefore what treatment modality should be offered to patients, CRC is staged according to different parameters **(Figure 1.4).** Currently, there are a number of different classification systems used. These include the Duke's classification system, tumour, node, metastasis system (TMN) outlined in **Table 1.1** or the simplified numbered staging system. The TMN classification system is the most detailed classification system used in CRC.

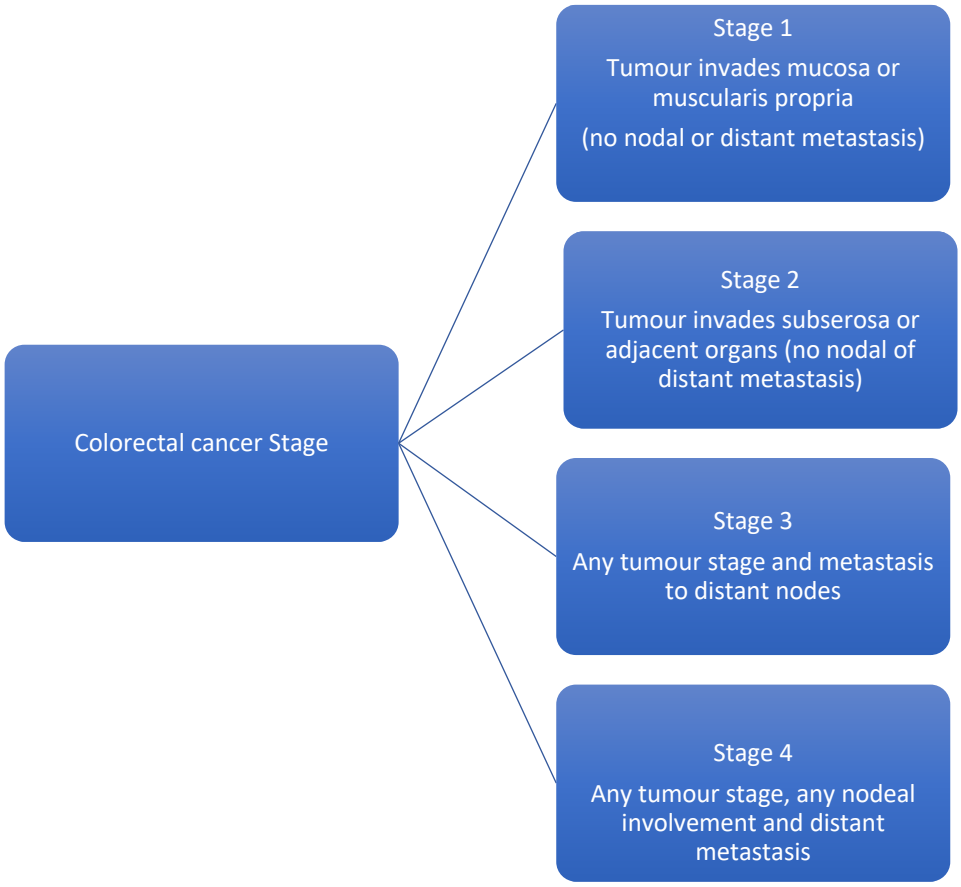

Figure 1-4. American Joint Committee on Cancer (AJCC) staging. Demonstrates the histological definition at different stages of CRC. The higher the stage the worse the prognosis. Adapted from Church et al 2013. [20]

Stages (AJCC)	T	M	N	Dukes' Classification
Stage 0	Tis (carcinoma in situ)	N0 (no regional lymph nodes involved)	M0 (no distant metastasis)	
Stage I	T1(invades submucosa)	N0	M0	A
	T2 (invades muscularis propria)	N0	M0	B1 (invades muscularis propria)
Stage II	T3 (invades muscularis and peri-colorectal tissue)	N0	M0	B2 (transmural extension)
	T4 (invades peritoneum and adjacent organs)	N0	M0	B2
Stage III	T1, T2	N1 (metastasis in 1-3 regional lymph nodes) or N2(metastasis in 4 or more lymph nodes)	M0	C1 (T2 with enlarged lymph nodes)
	T3, T4	N1 or N2	M0	C2 (invasion of adjacent organs)
Stage IV	Any T	Any N	M1(metastasis to one or more distant sites)	D (distant metastasis)

***Table* 1-1. AJCC, TMN and Duke's Classification of CRC.** This figure demonstrates the different CRC classification systems. The TMN is the most detailed system and depends on tumour (T), nodal involvement (N) and distant metastasis (M). T1 (invades submucosa), T2 (invades muscularis propria), T3 (invades muscularis and peri-colorectal tissue), T4 (invades peritoneum and adjacent organs), N0 (no lymph node involvement), N1 (metastasis in 1-3 regional lymph nodes), N2 (metastasis in 4 or more lymph nodes), M0 (no distant metastasis) and M1 (metastasis to one or more distant sites). Adapted from Buturovic et al 2014. [21]

1.2.4 Metastatic Disease

Cancer death can be directly attributed to the development of metastatic disease and the widespread disseminated nature of metastatic disease can limit treatment options. Tumours tends to metastasise to specific organs. For example, primary CRC tumours commonly metastasises to the liver and lungs. Over the years there have been many theories postulated regarding the 'site selectivity' of metastasis. These include adhesion molecules between tumour cells and the organ and/or the response to chemokines and growth factors. However, the most interesting explanation regarding distant tumour growth is the idea that metastatic cells interact with the specific organ's environment. [22] For example, tumour cells bind to endothelial cells present in the organ's vasculature, where endothelial cells express specific cell-surface receptors to allow tumour engagement. [23] This 'seed and soil' theory of metastatic disease was first hypothesised as early as 1889 by an English surgeon named Stephen Paget (1855-1926). [24] Paget hypothesised that for metastatic disease to occur, tumour cells that exhibit metastatic activity ('the seed') are attracted to certain organs based on their growth promoting milieu ('the soil'). The site of metastatic disease is therefore dependent on the tumour and its microenvironment. Gaining a greater understanding of the TME, and how to target it therapeutically, could help to reduce morbidity associated with metastatic disease in the future. [25]

1.2.5 Prognosis

As mentioned in **Section 1.2.4**, patients who present with metastatic disease have a worse prognosis and **Table 1.2** illustrates the five-year survival rate of patients who present with Duke A to Duke D stage of disease**.** Patients with Duke D CRC have a 5-year survival of only 6.6%

Stage of Disease	5-year relative survival (%)
Duke A	93.2%
Duke B	77%
Duke C	47.7%
Duke D	6.6%

Table 1-2. Five-year survival of CRC patients diagnosed 1996-2002 by stage at diagnosis. Those patients with a later stage of disease have a worse 5-year prognosis. Statistics taken from the NCRAS (National Cancer Registration Analysis Service) 2006. [26]

Unfortunately, 25% of patients presenting with localized disease will go on to develop distant metastasis within five years of diagnosis. [7] Of patients who present with metastatic disease, 30% of patients present with liver metastasis and these account for 66% of all CRC-related deaths. [27] Distant metastasis can also occur in the lungs (50%) and bones (30%).

1.2.6 Treatment

The treatment of CRC is dependent on a number of factors. These include location of disease, stage of disease and patient factors. In patients with hepatic metastasis, surgical resection of the metastasis may improve overall survival. Moreover, recent advances have redefined surgical resection where surgery aims to resect all visible hepatic metastasis, while preserving at least 20-25% of the remnant liver. Patients that undergo complete surgical resection of hepatic metastasis have improved survival rates of 50% at five years and 17-25% at ten years. [27]

1.2.7 Chemotherapy Agents

In addition to surgery, radiotherapy and chemotherapy are treatment modalities that can be used alone or in conjunction with surgical management. Currently chemotherapy remains a mainstay of treatment. Chemotherapy can be used neo-adjuvant or adjuvant, in combination with radiotherapy to shrink the tumour or in

the palliative setting, to slow the spread of advanced cancer and reduce disease-related symptoms.

Chemotherapy agents such as Oxaliplatin and Irinotecan are often used in combination with 5-Fluorouracil (5-FU); 5-FU has been used for the treatment for metastatic CRC for the last fifty years. The efficacy of 5-FU was first confirmed in 1988, where a meta-analysis demonstrated the benefit of using 5-FU in combination with surgery, over surgery alone (odds ratio of death 0.83, 95% CI 0.70 - 0.98). [28] A randomised control trial conducted by the European Organisation for Research and Treatment of Cancer (EORTC) Intergroup (Trial 40983) also concluded that perioperative FOLFOX4 (5-FU, leucovorin and oxaliplatin) reduced the risk of cancer progression by a 25%, when compared to surgery alone. [29]

Various sequences of chemotherapy can be offered to patients with advanced lymph node disease or metastatic CRC, as demonstrated in **Figure 1.5**. Overall performance status, organ function and patients' co-morbidities are considered when choosing either first line or second line chemotherapy regimens. Second line agents are reserved for patients that have been previously treated for CRC.

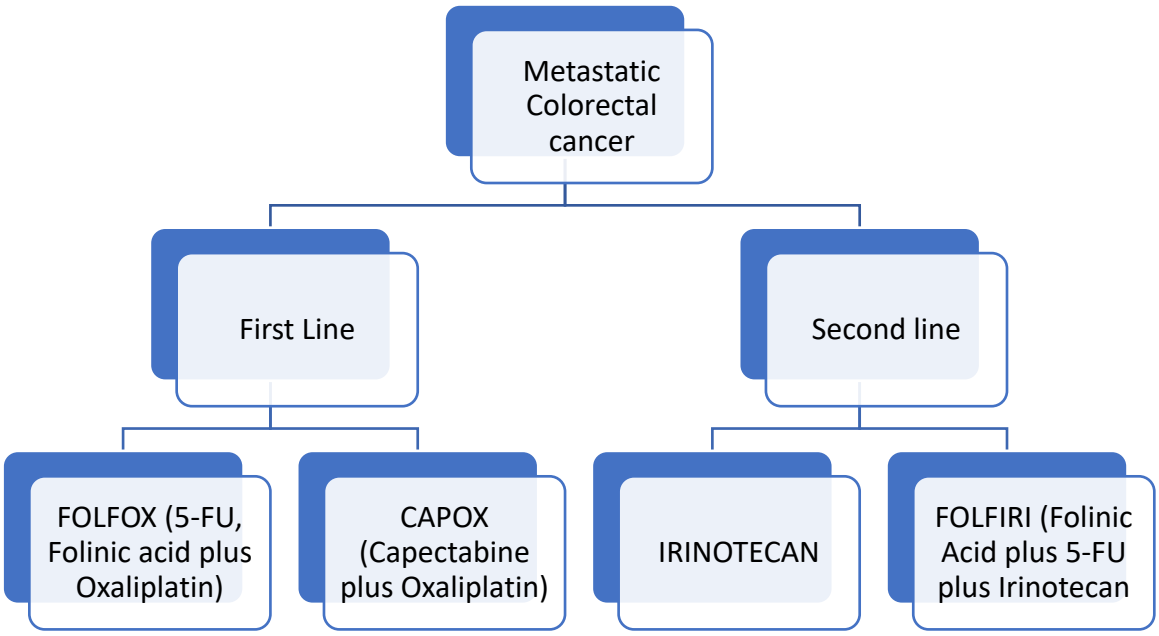

Figure 1-5. ***First or second line chemotherapy treatments*****.** Regimens depend on patient co-morbidities, organ function and performance status. First line treatment is reserved for patients who are newly diagnosed with CRC. Second Line agents are for patients previously treated for CRC. Figure recreated from [30]

1.2.8 5-FU Chemotherapy

5-FU is a pyrimidine analogue with antineoplastic properties. 5-FU and pyrimidines are structurally similar. The differ in that a hydrogen molecule is replaced with fluorine. The mechanism of action of 5-FU is outlined in **Figure 1.6.** *In vivo* 5-FU is converted to the active metabolite 5-fluoroxyuridine monophosphate (F-UTP). This metabolite replaces uracil and incorporates into RNA, inhibiting RNA processing and cell growth. Another active metabolite is 5-5-fluoro-2'-deoxyuridine-5'-O-monophosphate (F-dUMP), which inhibits thymidylate synthases and subsequently depletes thymidine triphosphate (TTP), a nucleotide triphosphate used in the synthesis of DNA. [31] [32]

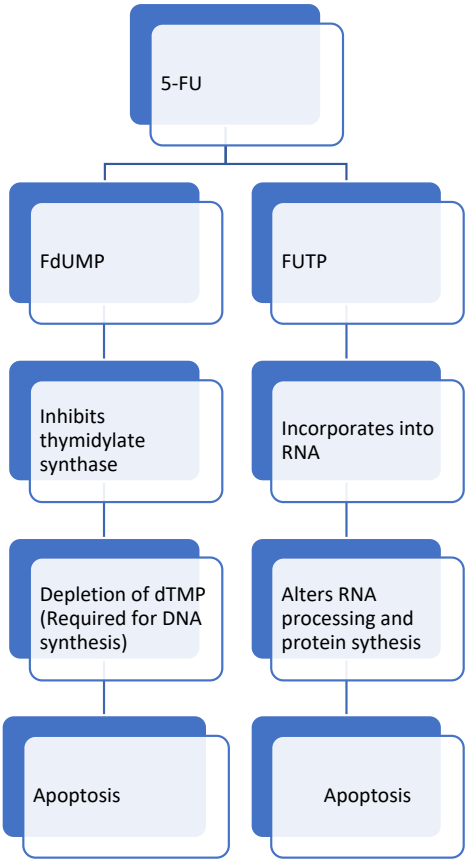

Figure 1-6. ***Mechanism of action of 5-FU.*** F-UTP replaces uracil and prevents RNA processing. 5-FU also inhibits the enzyme thymidylate synthases and the conversion of deoxyuridine to thymidine, therefore the conversion of deoxyuridine to thymidine does not take place. The action blocks DNA synthesis and leads to cell apoptosis. Figure recreated from [31].

Currently, 5-FU based chemotherapy is the first line agent in the treatment of CRC. However, in patients with advanced disease, response rates remain poor, at approximately 15%, due to chemoresistance. [33]

1.3 Chemoresistance

Drug resistance in CRC is a common problem leading to the decreased efficacy of many anticancer agents, including 5-FU. The response rate of current chemotherapy agents is approximately 50%; however; nearly all patients develop drug resistance

following prolonged treatment, and most cancer-related deaths are due to chemotherapy resistance. [34] Intrinsic resistance can be due to a variety of factors such as the support the TME provides, as well as tissue heterogeneity, as cancer tissue is made up of a variety of different molecular sub-clones, some of which are not responsive to treatment. By contrast, acquired resistance follows an initial response to chemotherapy and can occur in combination with intrinsic mechanisms of resistance. Drug resistance can be caused by an inability of the drug to reach the target cell, the presence of drug-efflux pumps, up-regulation of anti-apoptotic proteins and mechanisms that can de-toxify drugs and/or up-regulation of enzymes that are integral for DNA repair. [35]

The initial discovery that drug resistance directly correlated to levels of P-glycoprotein (P-gp) was first investigated and reported in 1976 in ovarian cancer cell lines. P-gp, a trans-membrane protein, removes cytotoxic molecules from the cell and is usually expressed in tissues at low levels. However, the expression of P-gp is up-regulated in epithelial cells and overexpression has been associated with a drug resistance. [33] Meads *et al (2009)*, reported that the chemotherapy resistance could also be mediated by cytokine cross talk between the tumour cells and their TME. [36] For example, the pro-inflammatory cytokine CCL21 interacts with CCR7 that is expressed on immune cells. CCR7 promotes cell migration and immune tolerance by targeting T cells and dendritic cells (DC) to lymph organs. In CRC cells, CCL21 promotes 5-FU resistance by activating the PI3K/AKT pathway thereby inhibiting GSK3b activity which upregulates SNAIL expression. [37] SNAIL expressing fibroblasts have been shown to demonstrate cancer associated fibroblast (CAF) like properties that contribute to 5-FU chemoresistance in CRC cells. [38]

Furthermore, certain signalling events within the TME also help tumour cells to escape apoptosis induced by chemotherapy agents. [39] For example, the balance between cell death and survival is strictly governed by pro-apoptotic signals and anti-apoptotic signals. Pro-apoptotic mediators include proteins such as TRAIL and TNF-α and anti-apoptotic mediators include BCL-2. [40] Anti-apoptotic proteins such as BCL-2 show variable levels of expression in CRC. For example, BCL-2 expression was lower

in CRC compared to the anti-apoptotic proteins, BCL-XL and BCL-W (which belong to the BCL-2 family). [41] An alternative mechanism of chemotherapy resistance in cancer is dysregulated expression of microRNA (miRNA). MiRNAs are dysregulated in CRC and play an important role in drug resistance, for example, upregulation of miR-21 has been reported to promote resistance to 5-FU while miR-145 is downregulated in chemo-resistant CRC; discussed in more detail in **Section 1.4.1.** [42] [43]

1.4 MicroRNA

MiRNAs are small, non-coding RNA molecules. They are approximately 18-25 nucleotides in length and can act as gene modulators. MiRNA bind to the 3' untranslated region of target mRNA sequences leading to mRNA degradation or translational repression; each miRNA can potentially target hundreds of mRNA transcripts. [44] **Figure 1.7** illustrates the biogenesis of miRNA. Initially, miRNA synthesis takes place in the nucleus where RNA polymerase II synthesises pri-miRNA. Cleavage of pri-miRNA occurs via DROSHA and its co-factor, DGCR8, to generate premature miRNA (pre-miRNA). The next step occurs in the cytoplasm as pre-miRNA is transported out of the nucleus via Exportin-5 where it undergoes further processing by DICER to form mature miRNA that can be incorporated into the RNA-induced silencing complex (RISC). [44] Importantly, miRNA have been implicated in the pathogenesis of many diseases, including CRC. [45] This is discussed in more detail in **Section 1.4.2**.

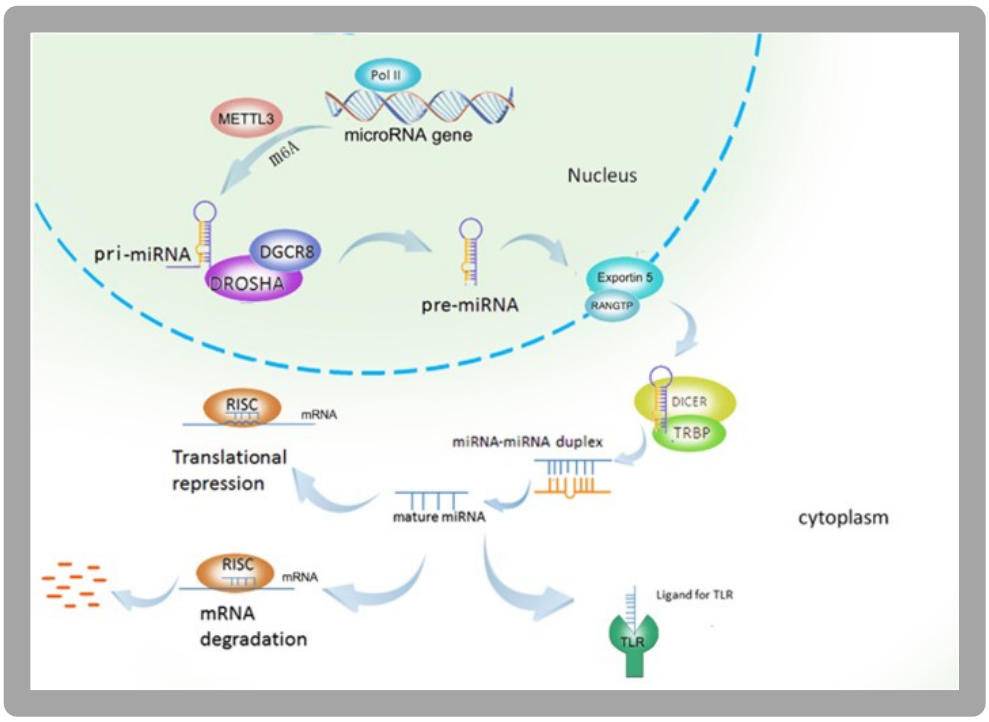

Figure 1-7. ***Mechanism of action of microRNA's.*** MiRNA's undergo transcription via RNA polymerase II and produce primary transcripts called pri-miRNAs. These are then cleaved by a microprocessor complex (RNA-binding protein DGCR8 and type III RNase Drosha) to produce a loop structure called pre-miRNA. This complex is then transported out of the cell nucleus to the cytoplasm via a transported called Ran/GTP/Exportin 5 complex. Pre-miRNA is then processed by a RNase III enzyme Dicer to a miRNA-miRNA duplex complex. The duplex undergoes unwinding and this mature miRNA is incorporated into a protein complex called RISC. The miRNA-RISC complex undergoes gene silencing via mRNA cleavage and degradation or translational repression. MiRNA's can also function as ligands and can bind to Toll-like receptors (TLR). Image taken from Peng *et al*. [46]

1.4.1 MiR-145

MiRNA's are important moderators in the development of a variety of malignancies. One such miRNA is miR-145 that can play an integral part in tumour progression. MiR-145 is located on the fragile region of chromosome 5q and was first identified in the heart muscle of mice. [47] Following this discovery, miR-145 was subsequently

detected in a range of human organs including the ovaries, uterus, prostate, testis, spleen and heart. However, research has also demonstrated that miR-145 can be downregulated in a variety of cancers such as CRC, non-small cell lung cancer (NSCLC) and breast cancer. Therefore, investigation of miR-145, and the role it plays in tumour progression, invasion and migration, are important. [48]

1.4.2 MiR-145 and CRC

The link between miRNAs and CRC was first postulated by Michael *et al (2003),* and decreased levels of MiR-143 and MiR-145 were reported in CRC compared to healthy colonic tissue. [47] Importantly, miR-145, a tumour suppressor miRNA, plays an integral role in inhibiting the proliferation, invasion, migration and angiogenesis of tumour tissue. For example, miR-145 can down-regulate RAS and MAPK expression thereby decreasing cell growth and proliferation. [49] [44, 50] Furthermore, the importance of miR-145 in CRC has also been attributed to its ability to inhibit cell migration and invasion. Overall, miR-145 exerts its anti-cancer effects by suppressing multiple target genes including P21-activated kinase 4 (PAK4), tumour suppressor candidate 3 (TUSC3), ribosomal protein S6 kinase beta-1 (p70S6K1), sex-determining region Y-box 9 (SOX9), myosin V1 (MY06), insulin receptor substrate-1 (IRS-1), SMAD-interacting protein 1 (SIP1) and fascin-1 (FSCN1) as described in **Table 1.3**. [48]

Target Genes	Function
PAK4	Regulator of glucose metabolism therefore regulates tumour growth and proliferation
TUSC3	Induces drug resistance and cellular stemness
P70S6K1	Mediates tumour growth, angiogenesis and VEGF expression
SOX9	Transcription factor linked to stem cell maintenance
MY06	Role in cellular transport, cell endocytosis and tumour cell migration
IRS-1	Protein scaffold that organises intracellular pathways for tumour progression
FSCN-1	A cytoskeleton protein enhances movement, metastasis and invasion of tumour cells.

Table 1-3. Target genes suppressed by MiR-145. This table demonstrates the different target genes that miR-145 can suppress in order to provide anti-cancer properties. [51-56]

1.4.3 Mir145 combined with chemo/radiotherapy

As mentioned earlier, 5-FU has been used as a neo-adjuvant treatment modality for CRC for many years; however, chemotherapy resistance in CRC remains poorly understood. Research that has focused on identifying targets involved in CRC resistance is continuingly evolving. Epithelial-to-mesenchymal transition (EMT)-associated phenotypes that encourage motility and invasion are evident in CRC cells; moreover, EMT mediators also play a positive role in cell survival. These include zinc finger E-box binding homeobox 1 (ZEB1), ZEB2 or SNAIL. [57] In CRC, EMT mediators, such as SNAIL, have been attributed to poor prognosis in CRC. [58] Findlay *et al* hypothesised that 5-FU resistance in CRC was regulated by SNAIL, which inhibited miR-145 expression. [59] Zhu *et al (2018)* further demonstrated a relationship between radiotherapy resistance in CRC and miR-145, and they postulated that rectal cancer tissue with elevated levels of SNAIL would be resistant to radiation. [60] Importantly, following the introduction of miR-145 to CRC SW620 cells, they became sensitive to radiation, compared to control cells. Moreover, delivery of miR-145 also sensitised SW620 cells to the chemotherapy agent, oxaliplatin. [60] Therefore, there findings suggest a role for miR-145 in regulating the response to standard of care therapies such as chemotherapy and radiotherapy.

1.5 Cancer and the Immune system

1.5.1 Innate immunity

The innate immune system can be described as the body's first line of defence to any abnormal situation. This is a generalised defence system and is not antigen or pathogen specific. In order to provide this defence system a variety of cells are recruited to infected sites such as natural killer (NK) cells, macrophages (M1) (M2), myeloid-derived suppressor cells (MDSCs), neutrophils, DCs and mast cells. Immunity is provided via phagocytosis of pathogens or immune-mediated killing of infected cells. NK cells are one of the main cells involved in providing innate immunity and do so via granule exocytosis therefore ensuring apoptosis and cytokine secretion. [61] NK cells also secrete interferon-gamma (IFN-γ) which aids the maturation of antigen presenting cells (APCs), such as DCs, to facilitate the adaptive immune responses.

In order to recognise incoming pathogens, the innate immune system relies on pattern recognition receptors (PRRs). These receptors are found on a variety of cell surfaces including the surface of monocytes and macrophages. They can also be located in the cytoplasm of cells or within endosomes. [62] Once these receptors are engaged, they can trigger phagocytosis alongside cytokine and chemokine release.[63] These act to recruit immune cells to sites of inflammation and infection. Key cytokines include tumour necrosis factor (TNF), interleukin 1 (IL-1) and interleukin 6 (IL-6). [64] Following phagocytosis, antigens are processed by APCs and presented to cells of the adaptive immune system (**Section 1.5.2**). [65]

1.5.2 Adaptive Immunity

APCs such as macrophages and DCs belong to the mononuclear phagocyte system and are the most common APCs. DCs and macrophages survey the environment and detect and phagocytose pathogens, including cancer cells, and also release inflammatory cytokines. DCs and macrophages present antigens to the adaptive

immune system and therefore, provide an important link between the innate and adaptive immune system. [66]

Adaptive immunity works in conjunction with innate immunity and much of the actions of the adaptive immune system are facilitated by the innate immune system. However, the adaptive immune system serves to protect the host against specific antigens that the innate immune system cannot eliminate and as such it recognises and eliminates specific pathogens and forms long-term immunological memory. [64] The main cellular components involved in the adaptive immune system are antigen specific T and B lymphocytes. [64, 67]

T cells possess unique antigen-binding receptors, specifically the T-cell receptor (TCR). In order for T cells to recognise a specific antigen they rely on APCs, which express major histocompatibility complex (MHC) molecules, categorised as class I or class II. MHC Class I proteins are present in all nucleated cells and present endogenous peptides to CD8+ T cells, by contrast, class II MHC molecules are only present on APCs such as macrophages, DCs and present exogenous peptides to CD4+ T cells. [64]

The innate and adaptive arms of the immune system play a pivotal role in cancer progression and treatment.

1.5.3 The Role of the immune system in cancer development

As cancer develops the innate immune system, and then subsequently the adaptive immune system, is activated. The role the immune system plays in cancer is commonly referred to as immunoediting and encompasses three main phases: elimination, equilibrium and escape.

Elimination occurs when the immune system (via innate and adaptive immunity) eradicates the tumour cells as they develop. However, if tumour cells are not completely eradicated in the elimination phase, these tumour cells enter the equilibrium phase. During the equilibrium phase, the immune system can limit

tumorigenesis and tumours can remain in a dormant state. Finally, for clinical signs of malignancy to occur tumour cells must 'escape' from immune control and proliferate without restriction. This step is subject to a variety of mechanisms including decreased immune recognition, resistance to immune cell attack and modulation of the TME which becomes highly immunosuppressive. [68]

- Elimination

The innate and adaptive immune system recognises and eliminates cancer cells. This occurs via the secretion of perforin and granzyme (via cytotoxic granules) from immune cells such as natural killer cells (NK), NK T cells and cytotoxic CD8+ T cells.

- Equilibrium

In this phase the immune system plays a role in controlling the growth of cancer cells and the cancer cells remain in a dormant state; this phase is considered to be the longest phase of immunoediting. Unfortunately, due to tumour heterogenicity and genetic instability cancer cells eventually escape the equilibrium state.

- Escape

Immunosuppression is a key component of this phase. Numerous mechanisms of immunosuppression exist, including downregulation of MHC class I on the surface of cancer cells, thereby escaping the cytotoxic effects of CD8+ T cells. Anti-apoptotic pathways and suppression of tumour antigen expression allow cancer cells to escape and therefore aid cancer progression. [69] Immune cells, such as T regulatory cells (Tregs) and MDSCs, also secrete inhibitory cytokines that act to suppress the function of cytotoxic effector immune cells such as NK and T cells. [70] [71]

1.5.4 Immune surveillance and re-editing

The complex interaction between cancer and the immune system has been a topic of wide discussion for many years. It was in 1909 that Ehlirch hypothesised that the immune system offers protection against cancer by eradicating cancer cells before

they have a chance to mount any clinical signs. However, in 1970 Burnet developed this theory further, and concluded that genetic mutations acquired for malignancy allow the immune system to recognise cancerous cells and eradicate them. [72] In line with this theory, malignancy is more common in immunosuppressed patients. For example, in organ transplant patients taking immunosuppressant medications there is a higher incidence rate of malignancies, such as melanomas, Kaposi's sarcoma and Non-Hodgkin's lymphoma. [70]

1.6 CRC tumour microenvironment

CRC and immunity are especially important as the bowel has commensal bacteria which is evaded by the immune system, however the immune system, within the colon, can still recognise a foreign pathogen. The selective nature of bowel mucosa occurs due to the cell-to-cell interactions that take place between the bowel epithelia, bacteria and immune cells such as DCs, monocytes and macrophages. In CRC, there is a fine balance between cells that exert an anti-tumour response, like effector T cells, and those cells that exert a pro-tumour effect such as regulatory T cells (Tregs). [73]

Tumour progression and drug sensitivity is influenced not only by tumour cells, but also by other cells within the TME, therefore understanding the TME in CRC is essential. Progression from colonic epithelial mucosa to invasive colonic carcinoma is a multi-step process supported by the TME. The TME consists of a variety of different cell types such as tumour-infiltrating immune cells and vascular cells alongside extracellular matrix (ECM) and matrix associated molecules. Tumour infiltrating immune cells can include both innate and adaptive immune cells such as, tumour-associated macrophages (TAMs), MDSCs, NK cells, neutrophils, mast cells, CD8+ T lymphocytes and Tregs. Other cells that exist within the TME include mesenchymal stem cells (MSCs), CAFs (cancer associated fibroblasts), endothelial progenitor cells (EPCs) and platelets (PLTs). [74] Cytokines, chemokines and growth factors are also secreted and these promote an optimum environment for tumour proliferation. Cancer cell interactions with the ECM are also important to promote

metastasis. This mechanical process is heavily dependent on the expression of cellular adhesion molecules (e.g., E-cadherin) and matrix degrading enzymes (e.g. Metalloproteinases). Stromal cells therefore play an integral part in the TME and as such have been a target for therapeutic agents. For example, CAFs in CRC express a high level of platelet-derived growth factor receptor (PDGF-R) and blockade of PDGF-R signalling is the basis of Imatinib treatment in CRC. [75, 76] A study has shown that combination therapy of Imatinib with Irinotecan for four weeks inhibited tumour growth when compared to single agent therapy in mouse models. [77]

1.7 Immune cells that play a role in the TME

1.7.1 Tumour associated macrophages (TAMs)

Macrophages have a wide range of functions in the TME. Macrophages within the TME can be polarised into two different sub-types, termed M1 (classically activated) or M2 (alternately activated). T helper (Th)1 cells, secrete a variety of cytokines including IFN-γ, which can activate macrophages and DCs. Once M1 macrophages are activated they can initiate the innate host defence and aid in tumour killing. They exert their direct killing effects by phagocytosis, or the production of pro-inflammatory cytokines (IL-1b, IL-6 and tumour necrosis factor-alpha;TNF-α) and reactive oxygen/nitrogen species (ROS/RNS). M1 macrophages can also act as an APCs and present antigens to T cells to prime adaptive T cell anti-tumour immunity. Therefore, M1 macrophages are considered to have anti-tumour properties. By contrast, M2 macrophages exert pro-tumour properties and Th2 cytokines, such as, IL-4, IL-10 and IL-13, act to stimulate M2 polarisation. In normal physiology, M2 macrophages are important in wound healing, tissue remodelling and humoral immunity. M2 macrophages produce immunosuppressive cytokines (e.g., IL-10, IL-13 and TGF-B) whereby, IL-10 and TGF-β inhibit DC differentiation and function resulting in ineffective induction of anti-tumour T cells. [78] TAMs also play an integral role in tumorigenesis, growth, development and metastasis and M2 polarised TAMs constitute approximately 50% of the cell mass in CRC, breast, lung, ovarian and prostate cancers. [79] TAM recruitment is mediated by chemokines, such as CC-chemokine ligands 2 and 5 (CCL2 and CCL5), as well as cytokines including

colony stimulating factor 1 (CSF1).[80] In CRC, studies have suggested a high density of macrophage is associated with a more advanced stage of cancer and a poor prognosis. [81] Despite this, the role TAMs play in CRC is controversial as two theories exist. For example, Forssell *et al (2007)* concluded that a higher proportion of macrophages at the site of tumour invasion indicated better prognosis. [82] Conversely, Kang *et al (2010)* concluded that a higher proportion of macrophages enhanced cell invasion and tumour progression. [73, 83] The role TAMs play in the response to therapy is also evident in a retrospective study of 123 CRC patients with advanced disease treated with bevacizumab combined with chemotherapy. This study concluded that patients with a lower proportion of TAMs had higher relapse free survival (RFS) and overall survival (OS) rates. Therefore, suggesting that a higher proportion of TAMs may reduce the efficacy of this combined therapy. [84]

MDSCs are also found in abundance in the tumour microenvironment. Initially they are produced in bone marrow from myeloid progenitor cells. MDSCs can be grouped into two different subtypes, polymorphonuclear MDSC (PMN-MDSCs) are derived from granulocytes and monocytic MDSCs (M-MDSCs) are derived from monocytes. [85] The metastatic potential and stage of solid tumours, including CRC, has been reported to be directly influenced by the number of circulating MDSCs. [86] High levels are associated with later stage CRC and disease progression. Pivotally, MDSCs suppress immune responses such as T cell proliferation through the secretion of immunosuppressive cytokines, e.g.,IL-10 and TGFβ. [87][64] MDSCs also upregulate molecules such as arginase-1, nitric oxide and reactive oxygen species, which abrogate T cell proliferation. [88] [89] MDSCs have been targeted in CRC as a potential treatment option. One such method decreased the number of circulating MDSCs using all-trans-retinoic acid (ATRA). This study confirmed that the number of MDSCs decreased and their function was inhibited in tumour bearing mice (B16 melanoma and CRC) therefore reducing the growth of tumours. [90]

1.7.2 CD4 T cells and Tregs

Along with CD8 cytotoxic T cells, CD4 T cells play a role in the adaptive T cell immune response. CD4 T cells have a variety of roles and functions. They can provide 'help' to other immune cells to co-ordinate an immune response and they can also exert a direct cytotoxic effect to tumour cells.[91] A recent study from 2019, demonstrated the ability of CD4 T cells to enhance the anti-tumour role of CD8 T cells, specifically, interleukin-21 (IL-21) derived from CD4 T cells promoted the differentiation of CD8 T cells with enhanced anti-viral and anti-tumour activity in a murine model of melanoma. [92]

Tregs are CD4+ T cells which suppress an immune response by effecting the cellular activity of effector immune cells within the TME. There are two subsets of Tregs cells; nTregs that occur naturally in the thymus and are present from birth and Tregs, which occur in the periphery and work to halt tissue inflammation. Specifically, Tregs interfere with the priming of T cells by producing immunosuppressive cytokines such as TGF-β and IL-10. [93] High numbers of Tregs have been identified in CRC which act to inhibit anti-tumour immune responses and promote tumour progression. [94] Moreover, in CRC, studies have reported that higher levels of Foxp3+ Tregs are evident in late-stage cancer and that they are a biomarker of poor outcomes. [95]

1.7.3 CD8 T cells

In CRC there is evidence to suggest that there is a link between prognosis and the number of CD8+ T cells. For example, a higher proportion of CD8+ T cells correlated with an improved prognosis, suggesting that CD8+ T cells exert an anti-tumour response that could halt disease progression. [96] CD8+ T cells exert their cytotoxic effects by recognising tumour-associated antigens (TAAs) bound to MHC class I. Common TAAs in CRC include mucin 1 (MUC1), carcinoembryonic antigen (CEA), human epidermal growth factor receptor 2 (HER2), epidermal growth factor (EGFR), epithelial cell adhesion molecule (EpCAM), telomerase, heparanase and tumour protein p53 (TP53). TAAs expressed on CRC can be recognised by T cells to facilitate tumour eradication. [97]

1.7.4 Cancer associated fibroblasts (CAFs)

In normal benign tissues few fibroblasts exist and they mainly reside in the vascular extracellular matrix to maintain structural integrity; they do this by secreting extracellular matrix (ECM) components (e.g. Type I and III collagens, elastin and fibronectin) and ECM remodelling enzymes. [98] However, in tumours there is often a greater proportion of fibroblasts. Fibroblasts can be derived from a different precursor cell depending on the organ. For example, in the pancreas and liver they are derived from stellate cells, whereas in the gastrointestinal tract they are derived from peri cryptal myofibroblasts.[99] Within the tumour, fibroblasts undergo physiological changes to become CAFs due to the presence of tumour-derived cytokines such as TGF-β.[98, 100] Hypoxia and oxidative stress are environmental factors that also contribute to CAF activation. [101] Due to their heterogenous nature and ability to secrete a variety of cytokines and growth factors (e.g., HGF, EGF, connective tissue growth factor (CTGF), IL-6 and ECM remodelling enzymes) CAFs play an important role in modulating the TME to aid tumour progression, as such they have been described as the 'architects of cancer pathogenesis'. [102] These properties pose an interesting target for therapeutics and there have been recent advances in using CAF-targeted therapies to reduce the number of CAFs, decrease their tumour enhancing effects or reprogramme CAFs to a more quiescent state. [103] This is apparent in colitis-induced CRC where Yuan *et al* (2021*)* proposed that by inhibiting MyD88 signalling in CAFs, using synthetic inhibitor TJ-M2010-5, prevents colitis-induced CRC in mice; inhibition of the MyD88 signalling pathway encouraged M1 macrophage polarization. [104] [105]

Importantly, the abundance of CAFs is also a marker of prognosis in CRC where a higher proportion of CAFs within the TME is indicative of a poor prognosis and chemotherapy resistance. [106] For example, recent studies have demonstrated that higher numbers of IL-11+ fibroblasts were associated with reduced disease- free survival. Here, IL-11 enriched fibroblasts expressed genes that aided tissue repair and

proliferation via the secretion of growth factors. [107] This suggests that tumour growth and progression in CRC can be attributed to CAFs. [73]

CAFs have also been implicated in the development of chemoresistance in gastrointestinal cancers. Ham *et al* (2021) described a variety of CAF related factors that could attribute to chemoresistance. [108] This theory was confirmed by Gu *et al* (2019) who demonstrated that CRC patients with CAFs induced factors, such as alpha-smooth muscle actin (a- SMA), phosphorylated (p)-AKT, p-ERK and survivin were more likely to show resistance to oxaliplatin and 5-FU chemotherapy. [109]

CAFs also secrete cytokine and chemokines which encourage tumour stimulating pathways that facilitate metastasis and tumour growth. [108] For example, IL-6 is a pro-inflammatory cytokine that has been associated with worsening disease and poor prognosis. [110] In order to promote tumour progression, IL-6 enhances tumour cell survival by inducing the production of vascular endothelial growth factor (VEGF) within tumour. VEGF subsequently promotes angiogenesis and tumour migration and metastasis. The production of IL-6 is greater in CAFs than in tumour cells, further highlighting the role for CAFs in CRC progression. [73] In addition, CAFs produce degradation enzymes, known as metalloproteinases (MMPs). [111] MMPs are involved in tumour progression and their main role is to destroy the ECM to allow tumour cells to invade neighbouring blood vessels and lymph nodes, thereby promoting tumour spread. High levels of MMPs (1, 2, 9, 11 and 16) have been identified in CRC cells. [112]

1.8 Immunotherapies in CRC

The TME as described above is highly immunosuppressive but despite this, immunotherapies have been considered in the treatment of CRC and some have shown promising outcomes. For example, immune checkpoint inhibitors (ICIs) are effective against metastatic CRC that is mismatch-repair-deficient (dMMR) or microsatellite instability-high (MSI-H). The FDA have therefore approved pembrolizumab and nivolumab (anti-PD-1 antibodies) with or without Ipilimumab(an anti-CTLA-4 antibody) for the treatment of metastatic CRC.[113] However, this ICI

therapy depends on the MSI status of CRC patients. For example, CRC patients can be grouped according to microsatellite instability from high, low and stable, with ICI therapy being more effective in patients with a high MSI, due to the high tumour mutation burden. However, despite these promising effects 90-95% of metastatic CRC tumours are microsatellite stable (MSS) and unfortunately do not respond to ICI therapy. For this reason, there is need to harness alternative immunotherapies, such as oncolytic viruses (OVs), in the treatment of CRC. [114]

1.9 Oncolytic virotherapy

1.9.1 Background

Viral therapy to treat cancer has been a phenomenon since the last century. It was first noticed that young patients suffering from leukaemia experienced a short period of remission following exposure to viral infections. [115] Following on from this, in the 1950's and 1960's a case series of cancers treated with viruses was produced which included wild type viruses such as hepatitis and Epstein-Barr (EBV). Unfortunately, these viruses produced side effects that were intolerable; however, one virus that showed some promise with minimal side effects was Adenovirus when used to treat cervical cancer. Cervical cancer patients received adenovirus by various routes and within 10 days of treatment two thirds of patients showed tumour necrosis while sparing healthy cells. Despite this breakthrough it took nearly thirty years for the term 'oncolytic virotherapy' to become widespread. [116]

1.9.2 Mechanism of action

OVs are an exciting and unique anticancer therapy. OVs can occur naturally or be genetically modified for improved selectivity and safety. OVs exert their anti-cancer properties by two main mechanisms. Firstly, they induce their cytotoxic effect by direct tumour lysis (via viral propagation); here, OVs replicate in tumour cells and release viral progeny to infect and kill adjacent tumour cells. Secondly, OVs enhance the host's anti-tumour immune response by inducing immunogenic death in host

cells which ultimately activates both innate and adaptive immune response, as illustrated in **(Figure1.8).** [117]

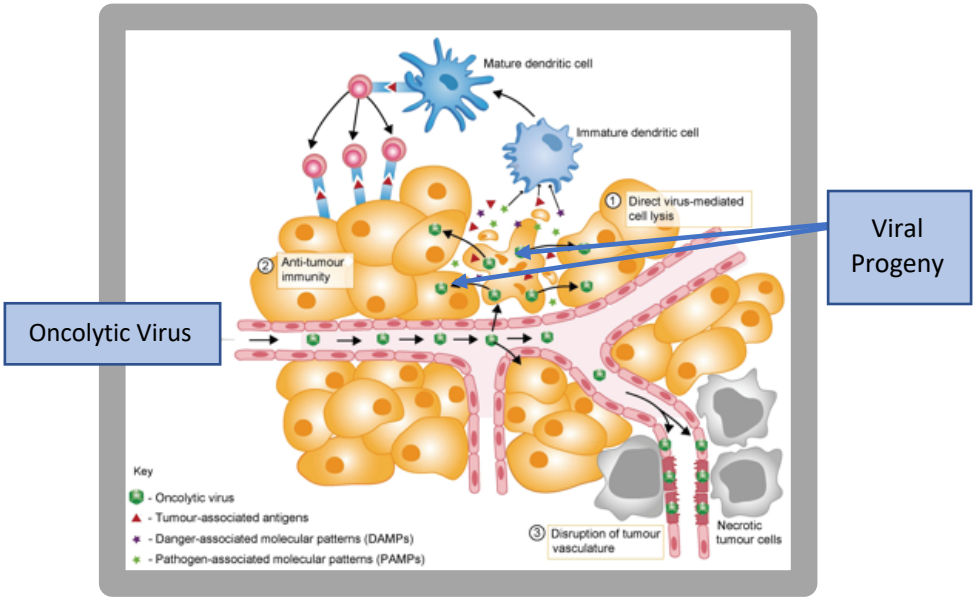

Figure 1-8. ***Mechanism of action of OV's.*** OV's induce cell death by direct infection. Progeny viral particles are released to infect adjacent cells and amplify the response. OV's induce immunogenic cell death and release tumour associated antigens, pathogen associated molecular patterns (PAMPs) and danger associated molecular patterns (DAMPs). TAA, PAMPS and DAMPs are engulfed by antigen presenting cells, such as DC and the inflammatory environment stimulates DC to become mature and migrate to lymph nodes. Here, DC present TAA to T cells and anti-cancer CD4+ and CD8+ effector T cells are generated which can kill infected and uninfected tumour cells. Ischemia and necrotic death of the uninfected tumour cells can also occur by OV's disrupting the vasculature surrounding the tumour. Image adapted from Marchini *et al*. (2016) [118]

In 2015, the US Food and Drug Administration (FDA) approved the clinical use of an HSV-1-based virus OV, called T-Vec, for the treatment of advanced metastatic melanoma. The approval of this OV has paved the way for more clinical trials to investigate alternative OV's. For example, Pexa-Vec (pexastimogene devacirepvec, JX-594) is a thymidine kinase gene inactivated oncolytic vaccinia virus, that has been

used intravenously in phase 1 clinical trials for the treatment for patients with metastatic liver tumours. This virus was well tolerated and demonstrated a dose response in survival benefit. [119] Fukuhara *et al* (2016) describes a number of OVs that have progressed to clinical trials, including those mentioned above, and importantly, they have been extremely safe and well tolerated. [120]

1.9.3 Oncolytic viruses clinical trials in colorectal cancer

Oncolytic virotherapy has produced promising results both in the pre-clinical and early phase clinical trial settings in the treatment of CRC. OV's can exert direct or indirect cytotoxic effects either in monotherapy or in combination with standard therapies. [121] Specific OV's used in CRC include herpes simplex virus (HSV), Vaccinia virus (VV) and reovirus (Reo), which will be discussed below. An alternative OV that could be considered for the treatment of CRC is Maraba virus (MG-1-Maraba virus encompassing mutations in the M and G protein). Although preclinical data needs to be generated to support clinical progression.

1.9.4 Herpes simplex virus (HSV)

HSV is a double stranded DNA virus. A multicentre phase I/II trial by Geevarghese *et al* (2010) evaluated the anti-tumour effects of repeated doses of the genetically modified HSV-1 virus, NV102, in patients with advanced CRC that had metastasised to the liver. In this study, patients received a weekly hepatic artery infusion of NV102, delivered prior to the standard chemotherapy regime. Notably, the results showed that NV1020 could stabilise CRC liver metastasis with 50% of patients demonstrating stable disease with a one-year survival of 47.2%. [122]

1.9.5 Vaccinia Virus

Modified vaccinia viruses can exert cytotoxic effects on CRC cells. [123] Pexa-Vec (JX594, a thymine kinase deactivated VV expressing GMCSF) was given intravenously, as a single dose, to patients, 14 days prior to surgical resection of CRC liver metastasis. Results concluded that Pexa-Vec initiated both an innate and adaptive immune response which was associated with tumour necrosis. [124] Interestingly,

there have also been early phase I/II studies that have combined JX594 with immune checkpoint inhibitors (Trial number NCT03206073) to treat peritoneal metastases. Peritoneal metastases occur at the end stage of CRC and signify a poor prognosis. JX-594 can selectively infect and lyse peritoneal tumour cells and activate DCs and CD8 T cells thereby promoting anti-tumour immunity. [121] To assess the effects of JX-594 on peritoneal CRC, MC38 colon cancer cells were treated intraperitoneally with JX594 and peritoneal tumour burden, vascular leakage and malignant ascites formation were assessed to determine anti-tumour response. This study confirmed that this combination therapy suppressed the progression of peritoneal metastasis and malignant ascites in CRC. [125]

1.9.6 Reovirus

Reovirus can exert direct oncolysis in CRC. Reolysin (Pelareorep) is a wild type strain of reovirus that has been used in early phase trials. In normal cells reovirus can cause protein kinase receptor (PKR) activation which results in halting of viral replication. However, in tumour cells with Ras mutations (such as in CRC) PKR is inactivated and viral replication can continue to induce cell lysis. [126] A phase I clinical trial by Fogel *et al* (2021) reported a positive effect of reovirus in KRAS mutated CRC, which was encouraging given that approximately 45-50% of CRC harbour KRAS mutations. Here, PBMCs were isolated from CRC patients pre and post intravenous administration of reovirus. The biological response was determined by assessing the gene expression pathways in the RAS-signalling pathway. Administration of reovirus occurred as a sixty-minute infusion for five consecutive days every twenty-eight days. Results showed a regression in tumour mediators and an increase in tumour apoptosis combined with a decrease in tumour angiogenesis. Reovirus also lead to an increase in immune response. [127] Adair *et al* (2014) investigated the replication of reovirus in CRC patients following administration of weekly intravenous reovirus pre-surgery to resect CRC metastasis in the liver. Analysis of the liver specimens demonstrated that there was a greater expression of the reovirus protein in malignant cells compared to healthy liver tissue. [128]

1.9.7 Rhabdoviruses

Rhabdoviruses are bullet shaped virions that are enveloped by a membrane and contain single stranded RNA (ssRNA). There are more than two hundred and fifty rhabdoviruses that are divided into six subtypes depending on pathology. Some rhabdoviruses are pathogenic such as the Rabies virus. However, some viruses are not pathogenic to humans, for example, vesicular stomatitis virus (VSV) and MG-1 virus. Rhabdoviruses are simple ssRNA viruses and generally code five proteins, including the nucleocapsid (N), phosphoprotein (P), matrix protein (M), glycoprotein (G) and large polymerase (L). [129]

Rhabdoviruses possess many properties that make them attractive oncolytic agents in the treatment of cancer. For example, viral replications take place in the cytoplasm therefore genotoxicity cannot occur as there is no DNA intermediate. [130] Moreover, Rhabdoviruses can be genetically modified to incorporate transgenes to improve their anti-tumour activity, including tumour antigens such as MAGE-A3.[131, 132] Furthermore, Fernadez *et al* (2002) reported that VSV could be genetically modified to incorporate the suicide genes thymidine kinase (TK) or cytokines (e.g., interleukin 4; IL-4) to induce apoptosis of cancer cells. [133] The structure of Rhadboviruses is such that transgene insertions can occur at various points, upstream of the N gene, in between genes or downstream of the L gene. [130] [134] The ability of the virus to allow insertion of transgenes at various points make them an ideal expression vector, allowing multiple antigens to be expressed from a single virus platform. Rhabdoviruses are also highly immunogenic and exert both a strong humoural and cellular immune response following infection. Moreover, as the majority of Rhabdoviruses are insect or animal viruses and transmission to humans is low, humans rarely have pre-existing antibodies. [129]

Another virus that belongs to the Rhadbovirus family is the MG-1 virus. Le Boeuf *et al* (2017) initially demonstrated the efficacy of MG-1 against sarcoma, with MG-1 promoting the generation of a memory anti-tumour immune response *in vivo*, which protected against a further tumour insult. Furthermore, the efficacy of MG-1 has been compared with Vaccinia virus, demonstrating that MG-1 replicates more

effectively in *ex vivo* human sarcoma tissue than Vaccinia virus. Additionally, Sarcoma-bearing mice treated with MG1 demonstrated increased survival and provided protection against tumour challenge also suggesting its ability to mount a memory anti-tumour immune response. [135]

In addition to work in sarcoma, Brun *et al* (2021) also demonstrated that the MG-1 had potent oncolytic activity against a number of different cancer cell lines, including CRC. Interestingly, it was also concluded that MG-1 was effective at blocking the hosts IFN antiviral response; MG-1 was reported to block the cytoplasmic transport of mRNA and therefore blocked IFN-β mRNA transport to the cytoplasm thus blocking induction of the IFN cascade. Similar to VSV, MG-1 can also deliver transgenes (including miRNA) to further enhance its anti-cancer activity. [136] For example, Wedge *et al* (2022) investigated the use of exosomes to deliver MG-1 miRNA transgenes to uninfected cells to promote viral replication. This study confirmed that exosomes can transfer MG-1-expressing miRNA's to cancer cells; miRNA targets included immune checkpoint protein such as PDL-1. [137] To date, the clinical experience with MG-1 is limited. A clinical trial using MG-1 expressing the TAA, MAGE-A3, in combination with an adenovirus expressing MAGE-A3 in a prime-boost strategy, has been tested for the treatment of MAGE-A3 expressing solid tumours, such as melanoma and non-small cell lung cancer. However, this trial is still in progress and results have not been reported. [120] Therefore, due to its ability to render itself to genetic manipulation, high replication rate and ability to block IFN antiviral responses, MG-1 is a promising virus for investigation in the context of CRC cells. [130]

1.10 OV in combination with chemotherapy

Despite some clinical efficacy with single agent OV treatments in cancers such as melanoma and sarcomas, in general terms the clinical benefits have been disappointing for the majority of patients. This is also true for CRC patients, therefore investigating novel combination strategies with enhanced efficacy remains a priority.

Due to the advantageous properties of the MG-1 this is an attractive virus to consider in combination with standard chemotherapy regimes in CRC.

For OV's to transition to the forefront in cancer therapy it would be beneficial for them to work in conjunction with therapies that are already in clinical use. Chemotherapy, unlike OVs, act on rapidly dividing cells, including healthy cells. It is for this reason chemotherapy agents, regardless of class, are toxic and induce many side effects, including hair loss and nausea. [138] The use of OVs in combination with chemotherapy has been previously investigated and have antitumour potential. Moreover, viral replication was enhanced following combined exposure of colon and pancreatic cells to 5-FU and HSV-1. [32] Combination therapy can also be used to promote cancer cell apoptosis. For example, in a pancreatic cancer model, gemcitabine was used in combination with a genetically modified adenovirus, engineered to express Relaxin (an extracellular matrix protein) to induce apoptosis. By contrast, monotherapy with Gemcitabine alone, and Adenovirus alone, showed limited cytotoxic effects towards pancreatic cancer. [139] In addition to apoptosis, some chemotherapy agents, such as Temozolomide, induce autophagy and increase cell death by increasing adenovirus viral replication. [140, 141]

As discussed above, combination therapies ca be used to augment anticancer responses; **Table 1.4** displays the current clinical trials of OV's used in combination with standard therapies. As mentioned above trials including the JX-594 and NV1020 trials have shown promising results when combined with chemotherapy. However, OV combination therapies in CRC remain underexplored. Importantly, OV activity can be promoted by multi- cellular cross talk. For example, normal fibroblasts are epigenetically regulated following exposure to tumour secreted factors, such as TGF-B, and develop into CAFs. Ilkow *et al (2015)* confirmed that when grown in isolation normal human fibroblasts were not infected with OVs; however, when cultured with cancer cell-conditioned media, or TGF-B, fibroblasts became sensitive to virus infection. Moreover, tumour cell susceptibility to viral infection was also enhanced. [142] However, in order to rationally design combination therapy, the effect of the TME on OV activity need to be better understood.

Virus	Name	Phase	Tumour	Combination
Adenovirus	ONYX-015	II	SCCHN	Cisplatin
Herpes simplex virus	NV1020	I/II	CRC liver mets	5-FU, oxaliplatin or irinotecan
Reovirus	RT3D	I/II	Advanced cancers	Carboplatin/paclitaxel
Vaccinia	JX-594(Pexa-vec)	I/IIa	CRC	Irinotecan

Table 1-4. Clinical trials of OV's used in combination with other therapies in CRC. Adapted from Filley *et al* (2017). [143]

1.11 Modelling CRC *in vitro*

Cancer drug approval rates are relatively low at <5% despite investment in research and pre-clinical drug development. One potential reason for this low drug approval rate are the limitations of the cellular models used to test the efficacy of novel treatments. In particular, cancer cell line models are not a true representation of human solid tumours and better models of human cancer are required. [144]

To date, *in vitro* pre-clinical data focussing on CRC has been generated using 2-dimensional (2D) cell culture models and *in vivo* xenograft mouse models which lack the intact immune cell repertoire that exists in human tissue. Murine cancer models are also well established in CRC; however, these models fail to accurately model disease heterogeneity. For example, these models are deficient in the high tumour mutation load present in human cancers. [145]

Cells in 2D monolayers also lack the tissue heterogeneity and behaviour that exists *in vivo* [146] and 2D cell culture models do not incorporate the cell-to-cell interactions that occur between different cell types present within the TME. As reported by Kimlin *et al* (2013), 3D cell culture models possess more TME features,

such as complex cell-to-cell interactions, hypoxia, reduced drug penetration and drug resistance **(Figure 1.9).** [147] 3D culture models shift the balance of growth away from unrestricted proliferation, as seen in the 2D models, and generate cellular pressures that are more representative of human cancer. [144]

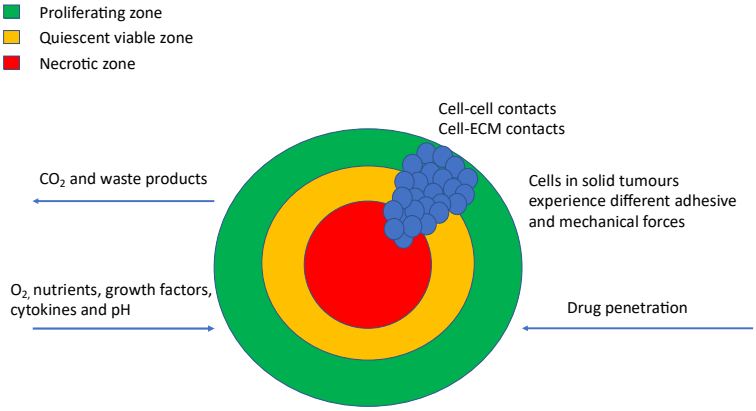

Figure 1-9. Tumour cells in the 3D model. Cells culture in this model develop complex cell to cell interaction, oxygen gradients and nutrient gradients. These regulate cell function and overall cellular behaviour. Compared to cells cultured in 2D, 3D cell cultures are exposed to different mechanical forces. This 3D tumour microenvironment can alter a variety of cellular activities such as gene expression, protein expression and drug metabolism. They exhibit different zones of proliferation, viability and hypoxia. Figure adapted from Sant *et al* (2017). [144]

Previous research by Sato and Clevers *et al* (2016) successfully developed a 3D epithelial organoid culture with human intestinal stem cells that developed crypt-like structures, this model accurately represented organ structure, cell differentiation and physiology. [148] Moreover, a recent study by Lee S *et al* (2015) demonstrated that 3D tumour spheroids, derived directly from tissue samples of CRC patients, maintained the molecular profile of original tumours; STR analysis showed no alterations in the genotype of 3D tumour spheroids and their parental tumours. Importantly, genes that were mutated in the parental CRC tumours (*K-RAS, APC, MLH1 and TP53*) were also found to be mutated in the tumour spheroids. [149]

Generation of a more complex 3D model of human CRC could bridge the gap between simple 2D cell culture models, more expensive animal models and technically challenging organoid systems. This model could enable the cheap and effective screening of drugs prior to animal testing and testing in the more precious organoid cultures. [150] With this in mind, co-culture spheroid models incorporating stromal fibroblasts and immune cells may represent a more realistic model of human cancer, as they will mimic certain elements of the TME. However, the size of the 3D spheroid would also be important as this could influence drug cytotoxicity. For example, a culture of 48 hrs will generate a small spheroid (200µm in diameter) whereas a longer culture at >4days will produce a larger spheroid (>500µm in diameter). These larger spheroids are more suitable for drug screening as they contain cells with different proliferation kinetics as well as a hypoxic core. Cells that are resistant to chemotherapy are more aggressive and can metastasis under hypoxic conditions, therefore, larger spheroids, with a hypoxic core, are likely to be more representative of human tissue and a better model to test novel therapies. [33]

1.12 Hypothesis

Successful treatment options for advanced CRC are limited, therefore novel treatment strategies are urgently required. Our overarching hypothesis is that the OV, MG-1 could be used as an effective therapy for the treatment of CRC. It could also be used to deliver transgenes such as miRNA species and restore drug sensitivity and /or modulate the TME to make it more receptive to anti-cancer therapies. However, to determine the effectiveness of any novel therapeutic strategy it is important to test these in more advanced pre-clinical models, beyond simple 2D cell culture models.

Therefore, to test this hypothesis the following aims have been devised:

1. Generate a 3D multicellular colorectal cancer model (3D MCTS) which incorporates elements of the TME, including both immune cells and stromal fibroblasts.
2. Assess the sensitivity of MCTS to MG-1 infection and standard of care chemotherapy (5-FU) compared to traditional 2D cell culture models.
3. Perform proof of principle studies to see if we can use MG-1 to deliver miRNA (using miR-145 as a model miRNA species), to CRC tumour cells and test its efficacy in combination with 5-FU.

Chapter 2: Material and Methods

2.1 Cell culture

2.1.1 Cell line

Four colorectal (CRC) cell lines were selected to use in *in vitro* experiments, HCT116, HT29, HCA7 and LOVO (metastatic adenocarcinoma). Further details regarding cell lines used are provided in Table 2.1. CRC cell lines were a gift from Dr. Mark Hull, University of Leeds. Human foreskin fibroblasts (HFF) and VERO cells were purchased from ATCC.

Cell Line	Origin	Location	Histology	Stage	Derivation
HCT116	48 year old male	Ascending colon	Poorly differentiated colon cancer	Dukes D	Primary Tumour
HT29	44 year old female	Colon	Moderately differentiated colon adenocarcinoma	Dukes C	Primary Tumour
LOVO	56 year old male	Colon	Poorly differentiated colon adenocarcinoma	Dukes C	Primary Tumour
HCA7	58 year old female	Colon	Moderately differentiated colon adenocarcinoma	Dukes B	Primary Tumour

Table 2-1. CRC cell line library. A summary of the demographics, site, histology and stage of the CRC cell lines used in subsequent experiments.

2.1.2 Cell culture

HCT116 were cultured in glutamine containing Rosewell Park Memorial Institute medium (RPMI) and supplemented with 10% foetal calf serum (FCS) (both Sigma-Aldrich Ltd). HT29, HCA7, LOVO and HFF cell lines were cultured in glutamine containing Dulbecco's modified eagles medium (DMEM) (Sigma-Aldrich Ltd) supplemented with 10% FCS.CD14+ (monocytes) were isolated from PBMC after lympho-prep density gradient centrifugation (performed by Dr V Jennings) and cryopreserved as in **Section 2.3** then stored at -80°C. These cells were thawed in a water bath at 37°C and re-suspended in glutamine containing RPMI supplemented

with 10% FCS. All cells were cultured in a Sanyo CO_2 incubator at 37ºC in a humidified atmosphere of 5% CO_2 in air. All experiments and maintenance of cell lines were performed under strict aseptic conditions using a Nuaire Class II Microbiology Safety Cabinet.

Cells were maintained in plastic vented tissue culture flasks (75cm² and 150cm²;Corning® Costar®). 50mL or 15mL sterile polypropylene tubes (BD Falcon) were used for harvesting and washing cells. Depending on the experiment, cells were plated in 12 well or 96 well plates (Corning®Costar®). For routine passaging, cells were checked for confluency and once cells reached the desired confluence (~80%), adherent cells were harvested by washing with sterile phosphate buffered saline (PBS) (PBS tablets; Sigma-Aldrich Ltd.) dissolved in distilled H_20). Once washed, cells were de-attached using trypsin (10x stock trypsin solution diluted to 1:10 using Hanks' Balanced Salt Solution [HBSS]; Sigma-Aldrich Ltd.) and cultured at 37°C for one minute. Cells were then harvested in the appropriate culture medium. Viable cell counts were performed using trypan blue exclusion (0.2% Trypan blue in PBS, Sigma-Aldrich Ltd.) with an Improved Neubauer haemocytometer. Cells were pelleted by centrifugation at 400 *x g* for 5 mins using an Eppendorf Centrifuge 5810R, unless stated otherwise. All cells were routinely tested for *mycoplasma* contamination using the EZ-PCR detection kit (Geneflow Ltd.) and found to be free from contamination.

2.1.3 Cryopreservation

To maintain and preserve cell lines, cells were harvested and re-suspended in freezing media (90% FCS; 10% dimethyl sulphoxide (DMSO; Sigma-AldrichLtd.) and aliquoted into cryovials (NUNC®) before being transferred to -80°C for short term storage. Cryovials were then transferred to liquid nitrogen for the long-term storage.

2.2 Generation multi-cellular tumour spheroids (MCTS)

Three-dimensional cultures were generated either in monoculture (tumour cells alone), double culture (tumour cells and fibroblasts) and triple culture (tumour cells, fibroblasts and monocytes). Cells were seeded in clear walled 96-well ultra-low binding U bottom plates (Corning®Costar®) or for viability assays **(Section 2.8)** cells were plated in black 96 well ultra-low binding U-bottom plates (Corning®Costar®). **Table 2.2** demonstrates the number of cells seeded for each 3D spheroid culture. Cultures were fed every 48 hrs by removing 100µL of media from each well and replacing it with 100µL fresh growth media.

	Tumour Cells	Fibroblasts	Monocytes
Monoculture	$2.5x10^4$	nil	nil
Double Culture	$2.5x10^4$	$1.25x10^4$	nil
Triple Culture	$2.5x10^4$	$1.25x10^4$	$1.25x10^4$

Table 2-2. Cell numbers used to generate MCTS. Cells seeded into 96 well ultra-low binding plates for mono, double and triple spheroids.

2.2.1 Fluorescent Microscopy

Bright-field and fluorescent images were acquired using an EVOS Fl cell imaging system microscope (Thermo Fisher Scientific) at indicated timepoints. These images were used to visualise GFP expression following MG-1-GFP infection or to quantify spheroid diameter using Image J software.

2.2.2 Immunohistochemistry

To process spheroids for IHC analysis the MCTS were fixed in 10% neutral buffered formalin, for 24 hours, and then embedded in Histogel (Richard Allen Scientific HistoGel Specimen Processing Gel, Thermo Fischer Scientific), fixed in 4% paraformaldehyde (PFA) overnight and then embedded in paraffin. Once embedded

in paraffin the blocks were sectioned using a microtome (Leica). For antibody staining, these sections were rehydrated with alcohol and antigen retrieval was performed in Tris Base Buffer (pH 7.6). The following antibodies were used for immune-histochemical analysis: α smooth muscle actin (α SMA) (1 in 500 dilutions;D21H3 XP Rabbit monoclonal antibody) and CD68 (1 in 200 dilutions;KP1 Anti-mouse monoclonal antibody); both antibodies were obtained from Cell Signalling Technologies. Haematoxylin and Eosin (H&E) staining was also performed. IHC and H&E was kindly performed by Dr Gemma Migneco.

2.3 Oncolytic viruses

2.3.1 Maraba virus

Maraba virus (MG-1) vectors were provided by Turnstone Biologics. All virus stocks used throughout this project were kindly prepared and titred by Dr Victoria Jennings. Green fluorescent protein (MG-GFP), MiRNA 145 (MG1-MiR-145) or miRNA non-targeting control MiRNA (MG-NTC) had been previously engineered into the viral back bone between the G and the L protein. Genetically engineered MG-1 virus stocks were titred using standard plaque assay techniques **(Section 2.6.2)** and stored at -80°C. Once thawed the virus was used immediately.

2.4 2D Cell viability assay

2.4.1 3-(4,5-dimethylthiazol-2-yl)-2,5-diphenyltetrazolium bromide (MTT) assay

An MTT assay was used as a method for assessing metabolic activity, a commonly used indicator of cell viability and proliferation, in CRC cells following infection with virus and treatment with 5-FU. CRC cell lines were seeded at 2.5 x 10^4 cells per well in a 96-well flat bottom plate in 100μL of growth media and incubated at 37°C for 24 hrs. Cells were then treated with MG-1, 5-FU (R&D Systems) or a PBS control. MG-1 virus expressing GFP, MiR-NTC or MiR-145 were added at various MOIs (0, 0.001, 0.01, 0.1, 1 and 10) for 24 and 48hrs and 5-FU was used at various concentrations (0,

2, 5, 10, 25, 50, 100, 200 and 800μM) for 96 hours in a total of 200μL/well. After the appropriate incubation time, 20μL/well of MTT (5mg/mL, Sigma-Aldrich Ltd) was added to each well and incubated at 37°C for 4 hrs. Cell supernatant was carefully removed from each well and 150μL of DMSO was added to each well before measuring optical density using Thermo Multiskan Ex ™ with an optical filter of 540nm.

2.5 3D Cell Viability Assay

2.5.1 CellTiter-Glo® 3D Cell Viability Assay

To analyse cell viability in 3D cell culture models the CellTiter-Glo® (CTG) 3D Cell Viability Assay (Promega Corporation) was used following the manufacturer's instructions. Briefly, 3D MCTS were seeded as previously described (**Section 2.2)** and treated with either MG-1 virus expressing GFP, MiR-NTC or MiR-145 at various MOIs (0,0.001, 0.01, 0.1, 1 and 10) and incubated for 72 hours or 5-FU at (10, 25, 50, 100, 200, 400 and 800μM) for 96 hrs. After the appropriate incubation time, all reagents and plates were equilibrated at room temperature, then 150μL of media was removed from each well and 100μL of CellTiter-Glo® 3D Cell reagent was added. The plates were then placed on a plate shaker (Heidolph, Unimax 2010) for 5 minutes and equilibrated for a further 25 minutes at room temperature before reading on a luminescence plate reader (BertholdTech Mithras).

2.6 GFP quantification following MG-1 infection

To assess GFP expression following MG-GFP infection, fluorescence microscopy and flow cytometry was used. Cells were seeded at $1x10^5$ cell/well in a 12 well flat-bottomed plate and incubated for 24 hours. Following this, cells were treated with MG-GFP at various MOIs (0.01, 0.1 and 1.0). 24 hours post infection images were acquired using the EVOS microscope (as described in **Section 2.2.1**). To further quantify the level of GFP flow cytometry was performed. Here, cells were harvested by transferring media (and detached cells) into a FACS tube (BD Falcon™). 1mL of PBS was added to each well and excess PBS removed and discarded before adding 0.5mL

of trypsin to each cell well. Media from the appropriate FACS tube was then used to wash each well and transferred back to the FACS tube. Following this, the FACS tubes were centrifuged at 400 *x g* for 5 minutes to generate a cell pellet. Excess media was then removed and cells were fixed with 200μL of 1% paraformaldehyde (PFA). FACS tubes were stored at 4°C in the dark prior to acquisition using a CytoFLEX S (Beckman Coulter) flow cytometer. Analysis was carried out using CytExpert software to quantify the percentage of GFP positive cells.

2.7 Assessment of MG-1 replication

2.7.1 Sample collection

LOVO CRC cells were cultured in mono, double and triple culture in a 96 well U-bottomed plate as described in **Section 2.2.** Supernatants were collected at 24 hours post-virus infection (MG-GFP, MG-NTC and MG-MiR-145,MOI of 0.1) and frozen immediately at -80°C.

2.7.2 Plaque assay

VERO were seeded into 6 well plates at $7x10^5$ cells per well in growth media. Plates were then incubated at 37°C for 24 hours to allow cells to adhere. Ten-fold serial dilutions of LOVO thawed sample supernatants and stock virus (MG1-GFP, MG-NTC and MG-MiR-145) were prepared in a 96 well flat-bottomed plate using serum free DMEM containing glutamine. Dilutions ranged from $1x10^{-3}$ to $1x10^{-9}$. Growth media was carefully removed from VEROs and 500μL/well of serum free media was then added followed by 100μL of the 10- fold serial dilutions of the LOVO cell supernatants and stock virus in duplicate and incubated at 37°C for 1 hour. After 1 hour the LOVO cell supernatants were removed and 2mL of 1% (w/v) agarose (Sigma-Aldrich Ltd.): 1xDMEM10% FCS (diluted 1:1) was added to each well; the agarose was allowed to set and then plates were incubated for 24 hrs at 37°C.

After 24 hours, 1mL of 1% PFA was added to each well and plates were left for 20 minutes to fix the cells. Plates were then washed with cold water to wash off the agarose and cells were stained with 0.5mL 1% methylene blue (4g methylene blue in 400mL: 200mL ddH_20 in 200mL of ethanol). A further wash with cold water was carried out to remove the remaining methylene blue. Plates were left to dry at room temperature and plaques were counted. The concentration of virus (pfu/mL) was calculated using the following formula:

Pfu/mL = Number of plaques/DxV*

D= the dilution plaques counted, V= the volume of diluted virus added (mL).

2.8 Cytokine Detection

2.8.1 Bio-Plex Pro ™ Human Inflammation Assay (LUMINEX assay)

To assess the levels of thirty-seven inflammatory cytokines/chemokines produced from MCTS (HCT116, LOVO, HT29 and HCA7 cells) generated as per **Section 2.2** a Bioplex Luminex assay (BioRad) was used; MCTS were treated with MG-1 variants (MG-MiR145, MG-NTC and MG-GFP) at an MOI of 0.1 for 24 hrs. After 24hrs, supernatants were harvested from these plates and used for the multiplex assay. The Bio-Plex Pro ™ Human Inflammation assay was performed following the manufacturer's instructions. Briefly, standards were reconstituted with standard diluent and a three-fold standard dilution series was prepared. The Bio-plex assay buffer was used to dilute the coupled magnetic beads and then 50μL/well was added to the plate. Following plate washing with 100μL Bio-Plex wash buffer, 50μL/well of diluted standards or MCTS samples were added. Detection antibodies were vortexed and then added to the plate at 25μL/well. Plates were then incubated in the dark at room temperature (RT) (850± 50 rpm for 30 minutes at RT) and Streptavidin-phycoerythrin (SA-PE) 50μL/well was added to the plate. Following a further three

washes with wash buffer, 125μL/well of assay buffer was added to re-suspend the beads. A Bio-Plex 100 plate reader with Bio-Plex Manager software was used to analyse and quantify the levels of cytokines/chemokines produced.

2.9 miRNA expression using RTqPCR

2.9.1 MCTS Generation

LOVO and HCT116 cells in triple culture were seeded in 96 well U-bottomed plates to generate MCTS as in **Section 2.2.** These plates were incubated at 37°C for 7 days and treated with MG-NTC and MG-MiR-145 at an MOI of 1 at 24 hours. At 24 hours, the MCTS were harvested by placing them in a 15mL falcon tube, allowing them to settle, then media was removed and MCTS were washed with 5mL of PBS. Excess PBS was removed and 1mL of TRIzol™ Reagent (Invitrogen) was added directly to the MCTS and incubated for 5 minutes at RT; samples were either processed straight away or stored at -80°C.

2.9.2 Isolation of RNA

To isolate RNA, 200μL of chloroform (Sigma-Aldrich Ltd) was added to 1mL TRiZol and samples were incubated at RT for 2-3 minutes followed by centrifugation at 12,000 *x g* for 15 minutes at 4°C using an Eppendorf 5415D microcentrifuge. The aqueous layer was collected and placed in a new 1.5 mL Eppendorf tube. The aqueous layer was then mixed with 500μL isopropanol and incubated for 10 minutes at RT, then centrifuged for 10 minutes at 12,000 *x g* at 4°C. The RNA pellet was washed with 1mL 75% ethanol prior to another centrifugation at 7500 *x g* at 4°C for 5 minutes. The ethanol was aspirated, and the pellet was left to air dry before re-suspending in 20 μL RNA free water. To determine the final RNA concentration in each sample a NanoDrop ™ 1000 spectrophotometer (ThermoFisher Scientific) was used.

2.9.3 MicroRNA cDNA synthesis

To convert miRNA to cDNA, using the isolated RNA **(section 2.9.2)** the qScript™ microRNA cDNA Synthesis Kit (Quanta Biosciences™) was used and performed according to the manufacturer's instructions. Firstly, 1 μL PolyA tail was added to RNA species, (up to 7μL of RNA) and samples were incubated at 37°C for 60 minutes, followed by 5 minutes at 70°C. The cDNA synthesis reaction was performed by adding the poly (A) tailing reaction with a specific adaptor primer (sequence unknown) and a reverse transcriptase. Volumes are documented in **Table 2.3.** Samples were incubated for twenty minutes at 42°C followed by 5 minutes at 85°C.

2.9.4 RTqPCR Amplification

Real time SYBR Green RTqPCR amplification of miRNA was then performed on the generated miRNA cDNA. 2 x SYBR Green SuperMix (ThermoFisher), microRNA assay primer (5'-GTCCAGTTTTCCCAGGAATCCC-3'), universal reverse PCR primer (sequence unknown) were used to perform the PCR amplification and volumes used are documented in **Table 2.5.** Thermal cycling was performed using the QuantStudio ™ 5 Real-Time PCR system (Applied Biosystems™) with the following 2-step cycling protocol: two minutes at 95°C, followed by forty cycles of five seconds at 95°C, fifteen seconds at 60°C and fifteen seconds at 70°C.MiR-145 expression was normalized with the RNU6 housekeeping gene (5'-TGGCTTCGGCAGCACATATAC-3') to give the delta CT (ΔCT) value. Relative gene expression was quantified using the $2^{-\Delta\Delta CT}$ method.

Component	Volume
Poyl (A) Tailing Buffer (5x)	2µL
RNA (up to 1µg total RNA)	up to 7µL
Nuclease-free water	variable
Poly (A) Polymerase	1µL
Final volume	10µL

Table 2-3. Poly (A) tailing reaction volumes.

Component	Volume
SYBR Green Supermix (2X)	25µL
microRNA Assay Primer (10µM)	1µL
Universal PCR Primer (10µM)	1µL
MicroRNA cDNA	up to 23µL
Nuclease-free water	variable
Final Volume	50µL

Table 2-4. Real-time SYBR Green qRT-PCR Amplification of MicroRNA volumes.

2.10 Statistical Analysis

All statistical analysis was performed using Graphpad Prism for MacOS (version 8.4.1, Graphpad Software Inc). Data was represented graphically using mean ± standard error of the mean (SEM). To determine statistical significance when comparing two or more groups *p* values were calculated using the Student's *t*-test with two tailed distributions. When comparing two or more groups the one-way analysis of variance (ANOVA) or two-way ANOVA was used. Results were considered statistically significant if $p<0.05$. Figure legends describe which statistical tests were used in all experiments.

Chapter 3: Characterisation of the multi-cellular colorectal cancer (CRC) tumour spheroid model

3.1 **Introduction**

To date, CRC spheroids have been successfully used to study tumour growth, proliferation, invasion, micro-metastasis, immune cell interactions, as well as being used as a drug screening tool. [151-153] Gene expression analysis has also been performed on CRC spheroids containing hypoxic and necrotic regions demonstrating that these spheroids mimic the gene expression profile of *in vivo* tumours. [154] Furthermore, studies have shown that incorporating stromal cells, such as fibroblasts, into CRC spheroids alters specific pathway expression in the co-cultures versus the mono-culture spheroids, these include the RAS and nuclear factor-kappa B (NF-κB) signalling pathways. [155] NF-κB is associated with inflammation and CRC progression, therefore, incorporating stromal cells into CRC spheroids has the potential to better mimic certain aspects of the TME. More recently, the incorporation of myeloid linages, has also been investigated in CRC HCT116 spheroids, to further recapitulate key aspects of the TME. [115] Bauleth-Ramons *et al* (2020) confirmed that the CRC cell line, HCT116, can form MCTS: however, to generate multicellular 3D models, agarose micro-moulds were used incorporating fibroblasts and monocytes, at differing ratios. Immunohistochemistry analysis confirmed the development of a necrotic core in the centre of the spheroid, with the presence of proliferative cells at the edge of the spheroid at day seven. Fibroblasts were localised to the core whereas monocytes were located at the periphery of the MCTS. [156] Expanding on this work with HCT116 cells, this work aimed to build on these studies and examine the ability of a panel CRC cell lines to generate 3D spheroids grown in isolation (monoculture), with fibroblasts (double cultures) or with fibroblast and monocytes (triple cultures) using ultra-low binding plates. The morphology, size, histology and cytokine production of these 3D cultures was also investigated.

3.2 The formation of 3D CRC spheroids in a monoculture.

The use of ultra-low binding culture plates ensures little to no cell attachment to the tissue culture plastic, supporting the establishment of 3D spheroids via cell-to-cell aggregation through naturally secreted extracellular matrices. Spheroids grown by this methodology are of similar size resulting in the reproducible generation of uniform 3D spheroids. [157] This method of generating 3D cultures was selected for investigation due to this important characteristic, as well as ease to establish at relatively low cost and high through-put method. Furthermore, the spheroids are directly plated into the tissue culture-well used for downstream assays and hence require no further handling once generated. The ability of four CRC tumour cell lines (HCT116, LOVO, HCA7 and HT29) to form spheroids as monocultures was initially investigated. HCT116, LOVO, HCA7 and HT29 were seeded at $2.5x10^4$ cell/well in a 96-well ultra-low binding plate and imaged by bright field microscopy on day two, four and six post seeding. **Figure 3.1a** shows a representative brightfield image of all CRC cell lines, and demonstrates that HCT116, LOVO, HCA7 and HT29 were capable of forming 3D spheroid structures. However, there was distinct differences in how quickly the individual cell lines formed spheroids, and how compact they became. HCT116, HCA7 and HT29 formed tight spheroids from day two post seeding, while at the same timepoint LOVO cultures appeared as a large aggregate of cells. By day six, HCT116, HCA7 and HT29 spheroids, much like day 2, displayed a dense spherical composition, while LOVO cultures remained as a large aggregate of cells. The shape of the HCT116 spheroid remained uniform at all time points, while HT29 spheroids at day six and HCA7 at day four demonstrated a much more spherical shape, when compared to earlier timepoints.

The size of the 3D spheroid is important and can influence drug cytotoxicity. Large spheroids of >500μm in diameter, are more suitable for drug screening as they contain cells with different proliferation kinetics. [158] Therefore, the diameter of the four tumour cell spheroids was measured using Image J software on day six of cell culture. **Figure 3.1b** shows the mean diameter of spheroids for all four cell lines from three different wells over three independent experiments. The LOVO cell line

generated the largest spheroid based on an average diameter of 992.42 μm. The remaining cell lines generated a spheroid diameter of approximately 650 -700 μM. Specifically, HCT116 generated a mean spheroid diameter of 694.92μM, HCA7 of 667.99μM and HT29 of 675.14μM. In summary, all four CRC cell lines have the ability to generate 3D spheroids with a diameter >500μm.

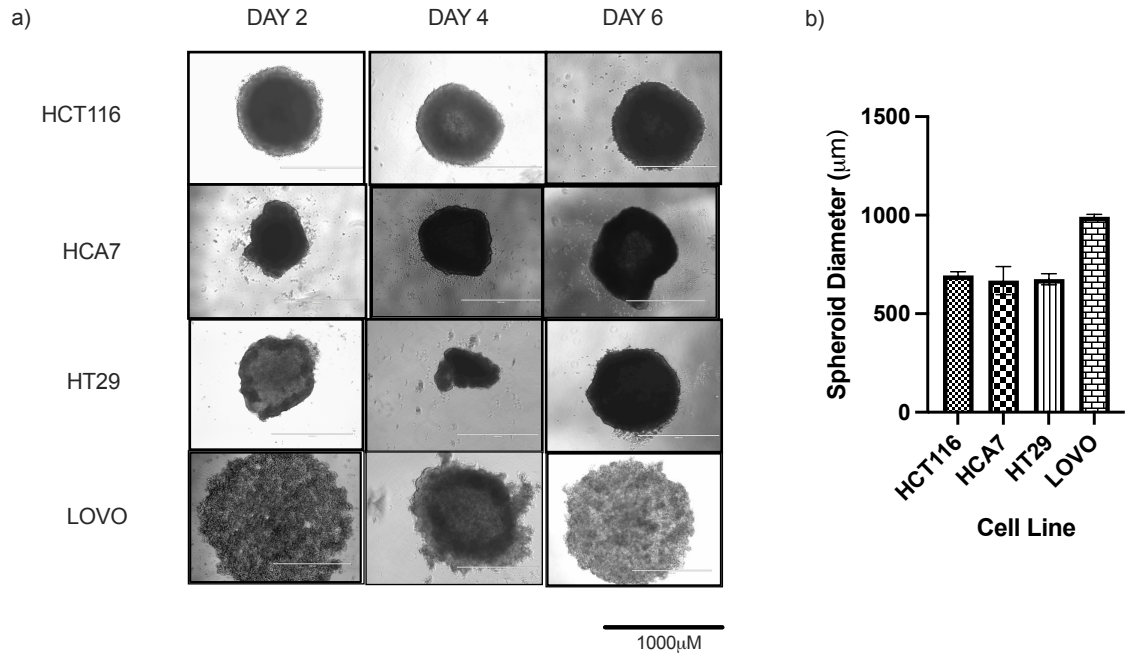

Figure 3.1. **HCT116, HCA7, HT29 and LOVO cells form 3D spheroids in monoculture**. **(a)** HCT116, HCA7, HT29 and LOVO cells were seeded at $2.5x10^4$ cells per well in a 96 well ultra-low binding U bottom plate. After 2, 4 and 6 days, bright field images of the MCTS were acquired using the EVOS microscope, magnification 4x. **(b)** represents the average diameter of spheroids in monoculture at day 6 using Image J software. Data shows mean diameter ± SEM (n=3)

3.3 Incorporation of fibroblasts in 3D CRC model

Having established that tumour cells alone were able to form spheroids in **Figure 3.1,** it was next investigated if fibroblasts could successfully be incorporated within the tumour spheroid. HCT116, HCA7, HT29 and LOVO were seeded at $2.5x10^4$ cell/well in combination with human foreskin fibroblasts (HFF) at a 2:1 ratio in a 96-well ultra-

low binding plate and imaged by bright field microscopy on day two, four and six post seeding. **Figure 3.2a** shows representative brightfield images of CRC cell lines in combination with fibroblasts. All CRC tumour cells (HCT116, HCA7, HT29 and LOVO) in combination with fibroblasts could form 3D spheroid structures. By contrast to the monocultures, images in **Figure 3.2a** show that the addition of fibroblasts with the LOVO cell line generates a more compact spheroid, which was evident across all time points. The shape of spheroids generated with all four cell lines remained uniform throughout all three time points with the most consistent shape evident in the HCT116 cell line. The HCA7 cell line generated the least spheroidal shape of all four cell lines as time progressed.

Similar to **Figure 3.2b**, the average spheroid diameter was measured with image J software. **Figure 3.2b** shows the average diameter of double culture spheroids from three different wells from three independent experiments. The addition of fibroblasts to the four cell lines resulted in an average diameter of 642.62μM for HCT116, 571.9μM for LOVO, 484.4μM for HCA7 and 455.4 μM for HT29. Although, the addition of fibroblasts decreased the diameter across all four cell lines, compared to monocultures, the greatest change in average diameter was seen in the LOVO cell line where the diameter reduced by 350.4μM with the addition of fibroblasts.

In summary, these results show that fibroblasts can be incorporated into 3D cultures for all four CRC cell lines investigated, and initial observations suggest that the addition of fibroblasts in the HCA7, HT29 and LOVO cell lines generated a much smaller double culture spheroid compared to monoculture spheroids ($p= 0.8788$, $p=<0.0001$, $p=0.0007$ respectively). The HCT116 cell line did not generate a significantly smaller double culture spheroid when compared to monoculture spheroids ($p=0.1542$).

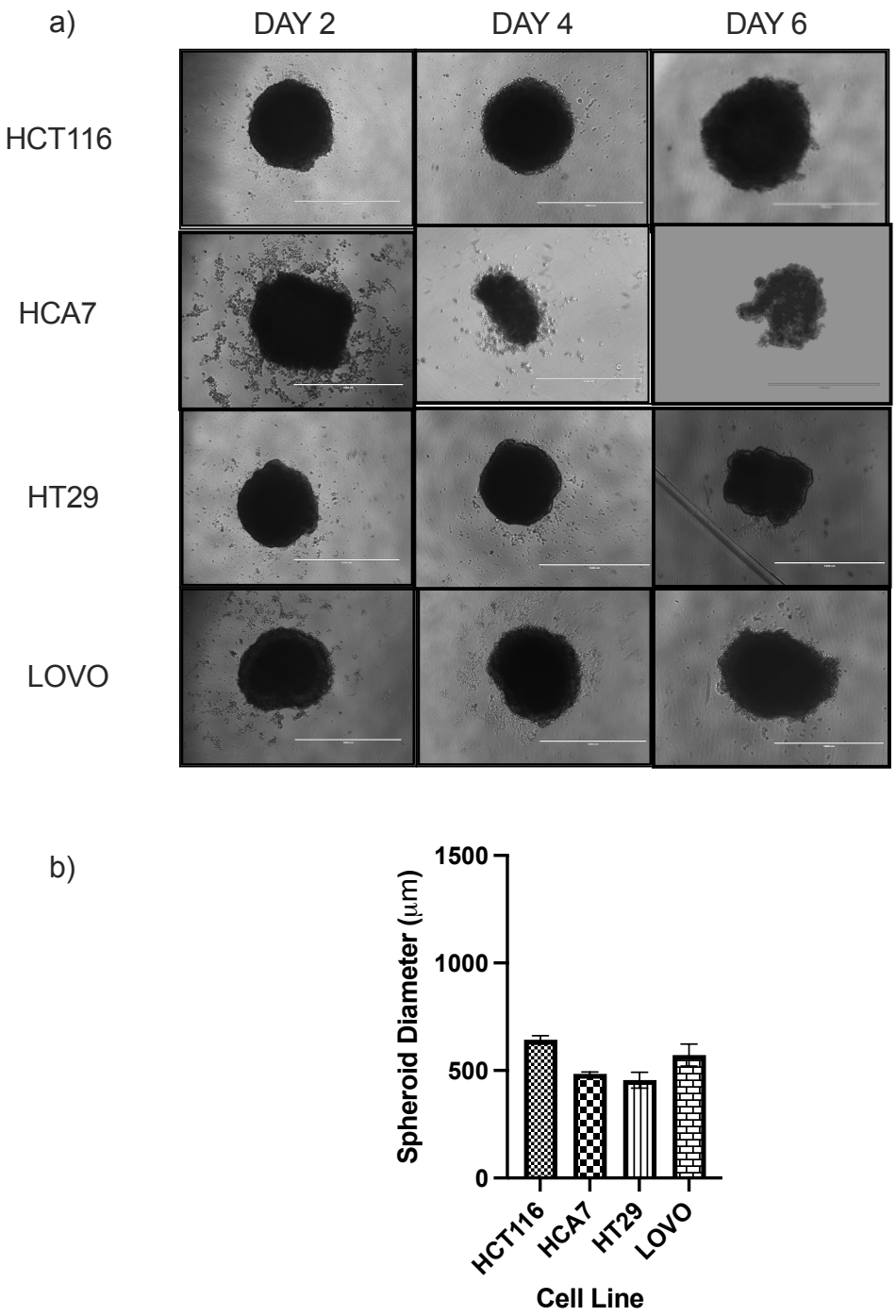

Figure 3.2. **3D spheroids with fibroblasts. HCT116, HCA7, HT29, LOVO and HFFs were seeded at a 2:1 ratio in a 96 well ultra-low binding U bottom plate. (a)** After 2, 4 and 6 days, images of the MCTS were acquired using the EVOS microscope, magnification 4x. **(b)** Illustrates the average diameter of spheroids in double culture at day 6 using Image J software. Data shows mean diameter ± SEM (n=3).

3.4 Optimisation and incorporation of monocytes in the 3D CRC model

To further increase the complexity of our *in vitro* model we next assessed whether monocytes (CD14+ cells) could be incorporated into the 3D CRC model along with fibroblasts (HFF). CD14+ cells were isolated from PBMC using magnetic bead selection. In order to visual the migration/location of monocytes in spheroids, monocytes were fluorescently labelled with a cell membrane dye. Red fluorescently labelled monocytes were combined with HCT116 and fibroblasts, either at the same time or 16 hours post seeding; cell densities ranging from $5x10^4$ to $1x10^6$ were used. **Figure 3.3** shows a merged bright field and fluorescence image of the HCT116 tumour spheroids. Red fluorescently-labelled monocytes were observed within the centre of the 3D spheroid, at all cell densities tested and regardless of the time of addition.

To establish if monocytes could also be successfully incorporated into spheroids for the remaining CRC cell lines, all CRC cell lines were investigated for their ability to form this triple cell culture 3D spheroid structure. As timing was not a factor in monocyte incorporation, all three cell types were seeded together at a 2:1:1 ratio of tumour cells: fibroblasts: monocytes. **Figure 3.4a** shows representative bright field images of the triple culture spheroids on day two, four and six post seeding. Images were screened from three independent experiments. **Figure 3.4a** shows that all four cell lines formed spheroids two days post seeding and morphologically these looked similar to the double culture images shown in **Figure 3.2a.** Again, the diameter of spheroids was evaluated using the Image J software and mean diameters at day six are shown in **Figure 3.4b.** The addition of monocytes to the double cultures resulted in an average diameter of 636.8μM for HCT116, 456.52 μM for LOVO, 468.06 μM for HCA7 and 436.89μM for HT29. The addition of monocytes to the double culture model decreased the diameter of the spheroids significantly in the LOVO cell line ($p=0.03$). The decrease in diameter of double culture spheroids compared to triple culture spheroids was not statistically significant in the HCT116, HCA7 and HT29 cell lines ($p=0.99$, $p=0.99$ and $p=0.98$, respectively). As is demonstrated in **Table 3.1,**

when comparing double and triple culture models to monoculture models, a statistically significant difference was seen in the HT29 and LOVO cell lines.

Of note, it is also important to mention that currently, MCTS were generated using CD14+ monocytes isolated from blood donations obtained from the national blood service and there is some variation in spheroid formation depending on the donor used. Future monocyte donors will be screened on HT29 and LOVO CRC cell lines, prior to MCTS formation, as MCTS formation is less reproducible with these cell lines.

Given that HCT116 in triple culture generated the largest spheroid and was >500μM (based on Image J calculations) and the most spheroidal shape (based on bright field images), this cell line was chosen to be taken forward for further characterisation in subsequent experiments. Larger spheroids are preferred for drug screening due to different proliferation kinetics that exist in larger spheroids. The presence of a hypoxic core within a 3D MCTS is also beneficial as this cellular heterogenicity is more akin to what is present in the tumour. [159]

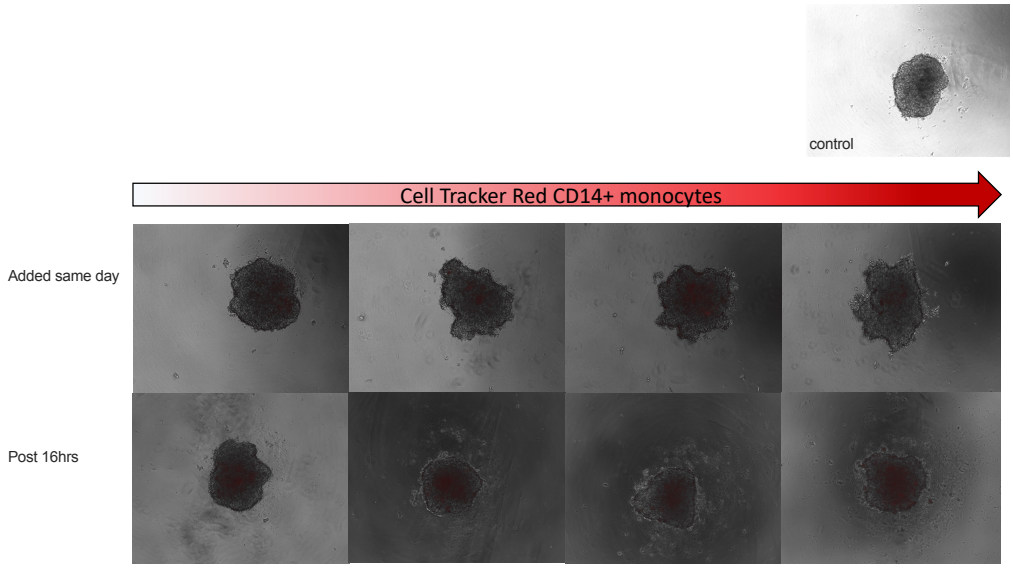

Figure 3.3. **Monocytes can be successfully incorporated into the 3D CRC spheroid model.** Fluorescently labelled monocytes (red) were seeded with HCT116+HFF at densities $5x10^3$, $1x10^4$, $5x10^5$ either at the same time or 16hrs post HCT116+HFF seeding in a 96 well ultra-low binding U bottom plates. After 16 hours bright field and fluorescent images of the MCTS were acquired using the EVOS microscope. Images shown are a representative of n=1 experiment (kindly performed by Dr Victoria Jennings).

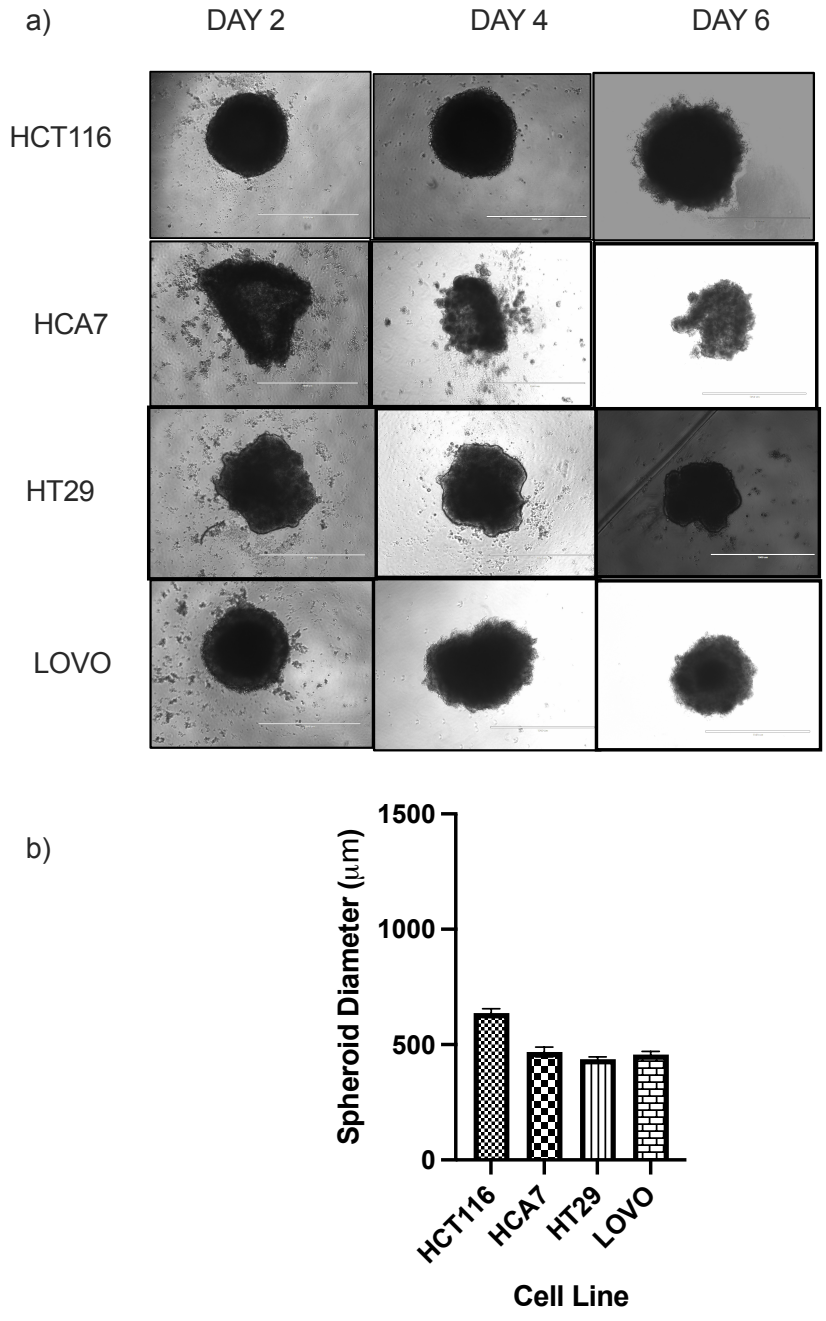

:

Figure 3.4. **3D spheroids with fibroblasts and monocytes.** HCT116, HT29, HCA7, LOVO, HFF and CD14 cells were seeded at 2:1:1 ratio in a 96 well ultra-low binding U bottom plates. **(a)** After 2, 4 and 6 days, images of MCTS were acquired using the EVOS microscope magnification 4x. **(b)** represents the average diameter of spheroids in triple culture at day 6 using Image J software. Data shows the mean diameter ± SEM (n=3).

HCT116	Mean (μm)	SD	Significance compared to monoculture
Monoculture	694.92	31.05	—
Double culture	642.62	33.06	0.1542
Triple culture	636.75	31.65	0.144

HCA7	Mean (μm)	SD	Significance compared to monoculture
Monoculture	667.99	123.5	—
Double culture	484.42	16.04	0.8788
Triple culture	468.06	36.55	0.2375

HT29	Mean (μm)	SD	Significance compared to monoculture
Monoculture	675.14	47.90	—
Double culture	455.41	64.22	<0.0001
Triple culture	436.89	17.71	<0.0001

LOVO	Mean (μm)	SD	Significance compared to monoculture
Monoculture	992.42	19.67	—
Double culture	571.98	89.36	0.0007
Triple culture	456.52	24.39	0.0016

Table 1-1. **Average diameter of spheroids.** A summary of the average diameter (μm) of spheroids at day 6 for HCT116, HCA7, HT29 and LOVO cell lines grown as mono-, double or triple cultures

3.5 **Immunohistochemistry of the 3D CRC model**

In order to visualise the location of fibroblast and monocytes within MCTS, immunohistochemistry (IHC) staining was carried out. At day six post seeding, HCT116, fibroblast and monocyte triple cultures were processed, sectioned, and haematoxylin and eosin (H&E) staining was performed to view cellular structure, furthermore antibodies against vimentin and CD68 were used to identify fibroblasts and monocytes, respectively. **Figure 3.5** shows a representative image taken following H&E staining and IHC for vimentin (red) and CD68 (brown).

H&E staining confirmed that the cells in the triple spheroid were tightly packed together. In the core of the spheroid there was an abundance of eosin staining. Eosin stains the cytoplasm of cells and due to the fact that fibroblasts have a larger cytoplasm than tumour cells or monocytes, this suggested that these pinker areas could represent fibroblast rich areas. Haematoxylin stains the nucleus of cells. Areas of small dark blue staining accompanied by little eosin staining are likely to represent the monocytic cells within the spheroid. These can be seen throughout the spheroid. Furthermore, haematoxylin has stained the cells in the periphery a darker blue. The cells in the periphery of the spheroid are likely to represent monocytes. To validate the H&E staining, regarding the localisation of the fibroblasts and monocytes, vimentin and CD68 staining was performed. **Figure 3.5b** confirms that fibroblasts (stained for vimentin) appeared to be localised in the core of the spheroid and myeloid cells (stained for CD68) were located throughout the spheroid.

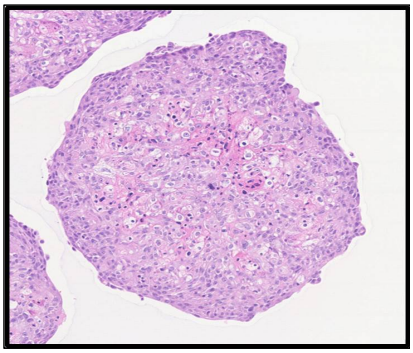

a) x16

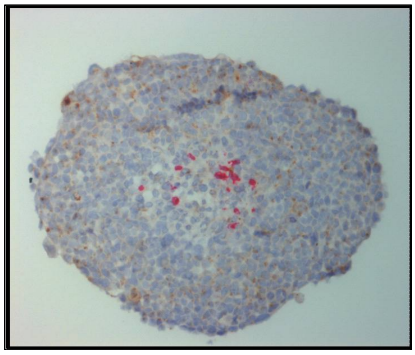

b) x16

Figure 3.5. **Immunohistochemistry of HCT116 triple culture MCTS.** MCTS were fixed in formalin then embedded in Histogel, fixed overnight in PFA and embedded in paraffin before IHC analysis took place. IHC confirms the presence and localisation of fibroblasts and monocytes with MCTS. **(a)** H&E staining of HCT116 triple culture MCTS with associated fibroblasts and monocytes at day six. **(b)** Immunohistochemistry was performed using antibodies against vimentin (red) and CD68 (brown) which are markers of fibroblasts and monocytes, respectively.

3.6 Cytokine/chemokine analysis of mono, double and triple culture MCTS

Having identified that all four CRC cell lines can generate 3D MCTS, the cytokine milieu of each of the four CRC cell lines cultured alone, with fibroblasts or with fibroblasts and monocytes was investigated. This was performed to examine whether incorporating different cell types into the spheroid model was able to functionally alter the cell to cell signalling within the MCTS, thus leading to a change in cytokine/chemokine secretion. HCT116, LOVO, HCA7 and HT29 cells were seeded to generate mono, double and triple cultures, as previously described in **Section 3.4**. On day six, cell free supernatants were collected, and a multiplex assay was performed using a predefined human inflammatory panel of 37 soluble factors (BioRad, Bio-Plex Pro Human Inflammation Assay) **Figure 3.6** heatmap shows the results for all 37 soluble factors from all four cell lines cultured either as mono (+), double (++) and triple (+++) spheroids, expressed as log10 values, from one independent experiment. The heatmaps demonstrate that all four cell lines in

monoculture (+) produce a different cytokine profile, when compared to one another. Furthermore, these profiles were additionally altered by the incorporation of fibroblasts (++) and then again by monocytes (+++). Of the 37 soluble factors tested six were not detected in either mono, double or triple culture. These include the interferons (IFN-α2, IFN-β and IFN-γ), IL-2, IL-10, LIGHT/TNFSF-14 (Tumour necrosis factor superfamily member 14), TSLP (Thymic stromal lymphoprotein) and TWEAK/TNFSF-12 (Tumour necrosis factor-like weak inducer of apoptosis). The most noticeable increase in soluble factors across all four cell lines, when comparing mono and double cultures, was the production of matrix metallopeptidase 3 (MMP3) **Figure 3.7a;** Cancer associated fibroblasts are known to secrete a wide range of dimethyl methylphosphonate (dMMPs). MMPs aid tumour cancer cell invasion and therefore encourage metastasis by degrading the extracellular matrix and promoting angiogenesis.[160] As shown in **Figure 3.7a,** MMP3 was not detected in any of the four cell lines when CRC cell lines were cultured alone, however, with the addition of fibroblasts within the spheroid, MMP3 was detected. The HCA7 double culture produced the greatest concentration, compared to the other cell lines tested. However, in the remaining three CRC cells lines (HCT116, HT29 and LOVO), the addition of monocytes led to a further increase in MMP3 production. Conversely there appeared to be a reduction in MMP3 in the HCA7 triple culture compared to mono or double cultures. MMP1 and MMP2 production were also absent in the monoculture models in all of the four cell lines but were produced in the HCA7 double culture model and the triple culture model for the HCT116 cell line. For the LOVO cell line, MMP2 was only produced in the triple culture model. Other interesting changes were observed when looking at differences across all four cell lines with the addition of fibroblasts and monocytes, two of which were changes in sCD163 **Figure 3.7b** and Pentraxin-3 **Figure 3.7c.** As sCD163 is selectively expressed in cells of the monocyte and macrophage lineages the detection of the soluble form of CD163 (sCD163) was unsurprisingly only detected in the triple culture conditions and was observed in three out of the four cell lines. This also suggests that the triple culture microenvironment expresses the necessary MMPs capable of cleaving CD163 from the plasma membrane of myeloid cells, except for the HCT116 triple culture MCTS where sCD163 was not detected. Pentraxin-3 is a glycoprotein that is involved

in acute inflammation. [161] It can be produced by both fibroblasts and macrophages and its expression in this study varies greatly across CRC spheroids tested, for example, none of the CRC cell lines express Petraxin-3 in isolation; however, with the addition of fibroblasts in both LOVO and HCT116 double cultures, Petranxin-3 was produced. By contrast, this was not observed with double cultures for the HCA7 and HT29 CRC cell lines. However, with the addition of monocytes to the 3D spheroids of HCA7 and HT29, Pentraxin 3 was observed. Interestingly, the addition of monocytes within the LOVO double cultures abolished Pentraxin 3 production, whilst conversely for HCT116 triple cultures, expression of Pentraxin 3 was enhanced compared to double cultures.

IL-34 is involved in the regulation of immune cells, including macrophages, and was detected at low levels in all CRC cell line mono, double and triple cultures; however, as demonstrated in **Figure 3.7d**, a distinct increase in IL-34 was detected in HCT116 triple culture spheroids. The addition of monocytes also showed an interesting change in the production of IL-19, which can support a Th2 immune response. [162] As demonstrated in **Figure 3.7e**, the addition of fibroblasts and monocytes to HCT116, HCA7 and HT29 cells increased the production of IL-19. However, whilst the addition of fibroblasts increased the production of IL-19 in the LOVO cell line, further addition of monocytes decreased IL-19 production. Only a few soluble factors of the 37 investigated remained consistent regardless of the cell line and culture conditions. An example of this includes sIL-6RA (soluble interleukin 6 receptor). sIL-6RA was expressed by all four CRC cell lines and expression remained at similar levels regardless of the addition of HFF or monocytes **Figure 3.7f.** In summary, results outlined here demonstrate differences in cytokine profiles within the mono, double and triple culture spheroids.

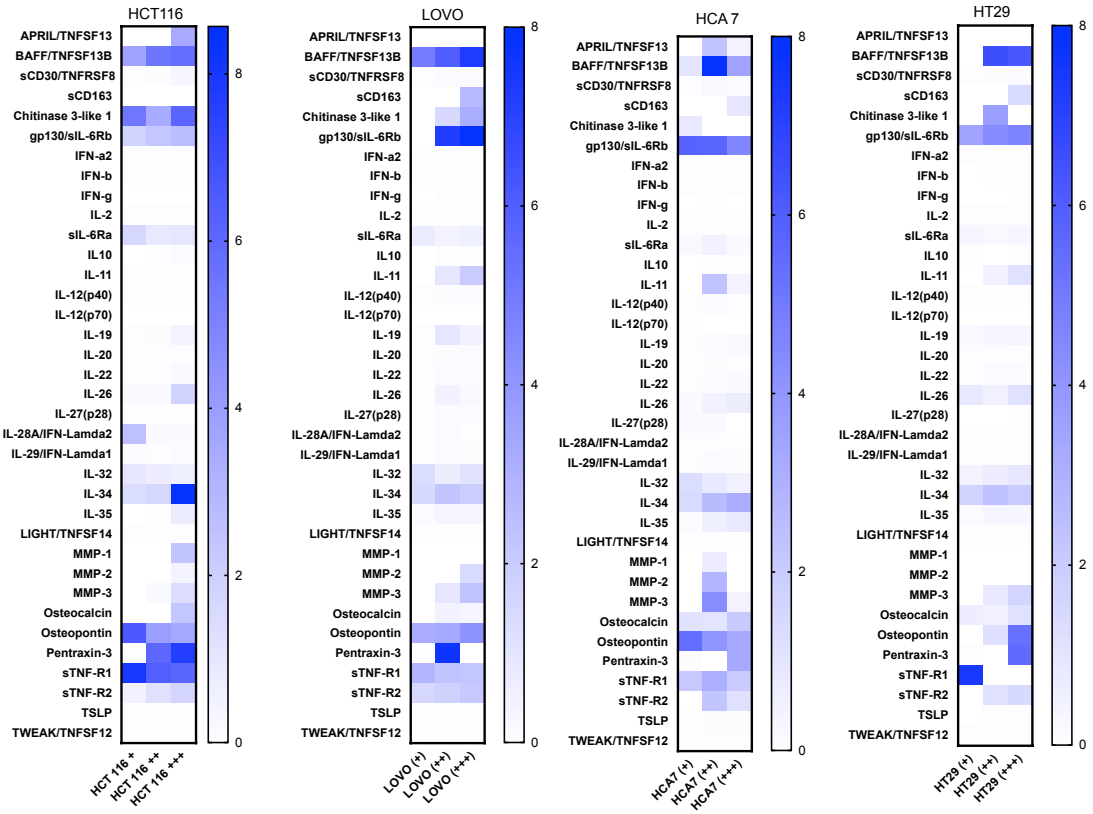

Figure 3.6. **Heatmap of cytokine production from HCT116, LOVO, HCA7 and HT29 mono, double and triple culture spheroids**. HCT116, HT29, HCA7, LOVO, HFF and CD14 cells were seeded at 2.5 x 10^4 tumour cells/ well in 96 well ultra-low binding U bottom plate to generate monoculture spheroids; 2:1 ratio to generate double culture spheroids and 2:1:1 ratio to generate triple culture spheroids. At day 6 of culture supernatants were collected and a Luminex assay was performed. Heat maps show the cytokine production as log10 values for each CRC cell line cultured as mono (+), double (++) and triple (+++) spheroids.

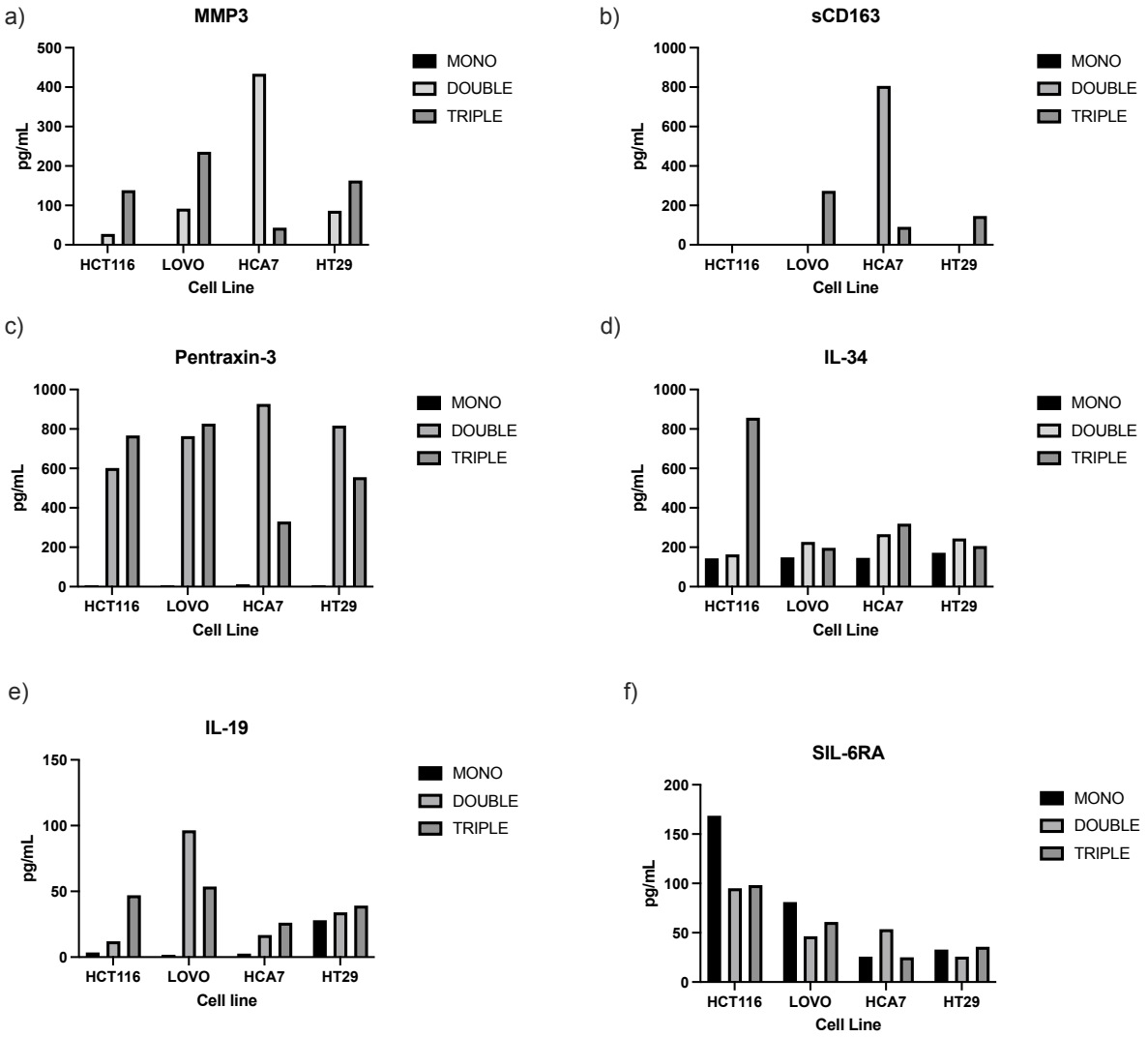

Figure 3.7. **Individual cytokine production from HCT116, LOVO, HCA7 and HT29 cells in mono, double and triple cell cultures. a)** to **f)** Illustrate the absolute concentration of cytokines for each cell line/spheroid condition. MMP3 **(a),** sCD163 **(b),** Pentraxin-3 **(c),** IL-34 **(d),** IL-19 **(e)** and SIL-6RA **(f).** Data shown is for mono, double and triple CRC cell line cultures for n=1 experiment.

3.7 Discussion

CRC is the fourth most common cancer in the UK. The roll out of the bowel cancer screening programme detects disease early; however, the incidence of CRC is on the rise due to the ageing population. [163] Despite improvements in screening and diagnosis there is less than 10% survival at five years post diagnosis. For patients who present with metastatic disease and are treated with chemotherapy, 50% go on to develop resistance. [34] It is for this reason there needs to be a greater understanding of the mechanisms of drug resistance.

There have been numerous anti-cancer treatment options that have shown encouraging results in the *in vitro* setting, however when translated to clinical trials these treatments have been disappointing. One of the potential reasons for this, is the contribution of other cell populations that can promote drug resistance within the TME. To overcome this problem, better *in vitro* models, which mimic the complexity of the TME, need to be established. From previous research we know that the TME consists of a complex mixture of tumour cells and stromal elements. By understanding these interactions, we may be able to better predict successful novel therapies, enhance standard of care therapies and ultimately improve long term patient survival. [142]

To date, the majority of anti-cancer drugs have been developed and tested in 2D cell culture models. There are two confounding issues relating to 2D cell culture. Firstly, 2D models are often monoculture models and do not contain other stromal populations that are present within the TME. Secondly, they lack the structure and organisation of more complex cancer models seen in 3D models. 3D models are therefore a better representation of human disease due to the complex oxygen and nutrient gradients that exist. [164] However, to truly represent human disease CRC cells need to exist alongside other stromal cells present within the TME, such as immune cells and fibroblasts, therefore, these need to be incorporated into new and

improved 3D models. It is well documented that cytokine mediated cross talk exists between stromal cells, such as CAFs, and cancer cells. [142] CAFs and TAMs are found in abundance in CRC, therefore any model aiming to mimic the CRC TME must include these cell populations. Importantly, TAMs have been implicated in drug resistance and conditioned media, obtained from M2 macrophages, reduced the sensitivity of CRC cells to 5-FU. Macrophages secrete cytokines such as CCL22 which regulates the PI3K/AKT signalling pathway and enhances the anti-apoptotic properties of CRC cells, thus protecting them from the cytotoxic effects of 5-FU. [165, 166] CAFs also play a role in drug resistance. Pre-clinical studies in CAF-rich mice have shown that MC38 models are resistant to OVs and PD-L1 directed therapies. It was hypothesised that this was due to CAFs excluding CD8+ T cells from tumours by producing NADPH oxidase 4 (NOX4). NOX4 expression is related to CAF accumulation in CRC patients due to regulating the differentiation of myofibroblasts to fibroblasts. [167]

There have been many studies demonstrating the different methods of generating uniform monoculture spheroids such as, using 3D hydrogels, microwells and cell suspension techniques. [168] It was decided for the purpose of these studies that spheroids would be generated using a scaffold free method, using low adhesion plates. This is similar to the hanging drop method; however, it has the advantage that there is less handling of the spheroids, once they are generated. Recently the use of low adhesion plates has become a popular method of spheroid generation due their ease of use and the fact that these plates can be used to monitor real time changes in spheroid phenotypes following the administration of drugs. [169] To date, many studies have also used this method to ensure the generation of uniform size and shape spheroids. [170-172] Not only is the quick reproducible nature of this method an advantage, but the compact uniformity of the spheroid produced is of utmost importance, as variations in spheroid shape can led to changes in the viability and the metabolic state of a spheroid. [173] It has been reported that viability and shape of 3D cultures is linked, hence the more spherical the spheroid is, the greater tumour cell viability and it was postulated that spheroids with an irregular shape had a reduction in cell-to-culture medium distance, which led to a wider zone of active cell proliferation. [172]

The aim of this work was to build on previously published data using the HCT116 cell line and examine the ability of a panel CRC cell lines (HCT116, LOVO, HT29 and HCA7) to generate 3D spheroids grown as monocultures, with fibroblasts (double cultures) or with fibroblast and monocytes (triple cultures) using ultra-low binding plates. Herein, the morphology, size, histology and cytokine production of these 3D cultures was examined.

The shape and size of the spheroids formed in mono, double and triple cultures was evaluated over six days **Figure 3.2, 3.3 and 3.4.2.** A decrease in diameter following fibroblast addition was apparent in all CRC cell lines investigated. Studies have shown that if fibroblast cells are cultured alone in 3D there is increased collagen deposition when compared to fibroblasts cells cultured in 2D. This increase in collagen, and subsequent remodelling of the ECM in the spheroid, could result in the more compact nature of double culture spheroids as observed here. [174] By contrast, Zoetemelk *et al* (2019), demonstrated an irregular shaped spheroid when fibroblasts were co-cultured with CRC cells (HCT116, SW620 and DLD1). [175] [176] Furthermore, other studies using different cell lines have reported that the addition of fibroblasts in human pharynx squamous cell cancer cells (FaDu) did not change the size of spheroids in co-culture. [177] The differences seen across different in vitro studies could be due to various factors. For example, in this published study, spheroids were generated by the liquid overlay technique. Also, the ratio of tumour cells to fibroblasts differed in that 10:1 tumour cell to fibroblasts were used, respectively, compared to the 2:1 ratio used above. As well as the differences in cell ratios, a different fibroblast line was also used. For example, published work uses MeWo cells, a malignant melanoma cell line that exhibits a fibroblast morphology. Collectively these differences might attribute to the unchanged size of double culture spheroids in this published study compared to results presented here **Section 3.3.1.** [177]

As TAMs are also a major component of the CRC TME, incorporating monocytes (the precursor cell to a macrophage) was next investigated. Reduced spheroid size was

observed when monocytes were introduced into the spheroid. This decrease in the diameter of the MCTS could be attributed to more ECM components or differing rates of growth within the spheroid. Montalban-Hernandez *et al* (2022) have demonstrated that CRC cells can be co-cultured with monocytes in 3D models, however they did not report any changes in spheroid size. [178].

There is a multitude of data to support spheroid size as a factor in drug penetration. [179] This is due to gradient shifts in oxygen and nutrients. Drug penetration in MCF-7 breast cancer cells was shown to be spheroid size dependent. The smaller the MCF-7 spheroid the more Doxorubicin was able to penetrate the cells. [180] Some studies suggest that a small spheroid (<500μm) would behave as cells in a 2D monolayer and therefore response to drug therapy would be much quicker than observed for their 3D counterparts. [181] Therefore, as mentioned, a larger spheroid provides a more realistic model to test cancer therapies. HCT116 MCTS remained >500μM. However, further evaluation of the other three cell lines would need to take place in order to generate a larger spheroid. For example, the MCTS could be cultured for longer or a change in tumour: immune cells: stromal cells ratios could be used to generate a larger spheroid. Jeppesen *et al* (2017) demonstrated a significant growth in CRC spheroids when left for longer for example seven days. (seven days). [182]

As can be demonstrated in **Figure 3.4.** the HCT116 cell line generated the most compact and spherical shape and presumably it is for this reason that multiple studies use this cell line in 3D CRC modelling. [183] [184] Furthermore, HCT116 spheroids have also been shown to closely resemble original tumours. HCT116 is a highly aggressive cell line, that contains almost only cancer stem cells (CSCs) and has therefore been used as an effective drug screening cell line. [185]

As is displayed in **Figure 3.5***,* IHC confirmed the presence and localisation of the stromal and immune cells within the HCT116 MCTS. Fibroblasts were located in the spheroid core whereas, monocytes were located at the periphery. A study by Bauleth-Ramos *et al* (2020) confirmed this localisation and postulated that monocytes were attracted to the periphery of the spheroid due to the proteolytic

enzymes TAMs produce that digest the ECM, therefore moving them closer to the edge. [156] This published study successfully optimised a MCTS, that consisted of HCT116 colon cancer cells, fibroblasts and monocytes and is one of the few studies that demonstrate this 3D model of CRC with immune and stromal cells. [156] Despite using a different method of spheroid production (microwell array techniques) and a different tumour cell: immune cell: stromal cell ratio (4:1:4) this study showed similar results to those demonstrated in **Figure 3.3.** For example, they reported that spheroid size remained consistent throughout the time course. [156]

The multiplex assay results displayed in **Figure 3.6 and Figure 3.7** demonstrates the diversity of soluble factors that are produced by the four CRC cell lines tested in monoculture, double and triple culture spheroids. Multiplex assays were performed to examine whether incorporating different cell types into the spheroid model altered the cytokine secretion and ECM factors. A difference in the cytokine milieu was apparent within the MCTS models. For example, MMP3 was only produced following the incorporation of HFFs to the tumour spheroid model. Previous studies have shown that CAFs activated in CRC (HCT116 and DLD1) can secrete MMPs to promote metastasis by degrading the ECM. [186] They also play a role in tissue remodelling and affect many signalling pathways such as proliferation pathways and apoptosis. [187, 188] The addition of monocytes into the MCTS model in three of the four cell lines further increased the production of MMP3. Previously published studies have demonstrated that increased expression of MMP3 in colon cancer cells (DLD-1) occurs following co-culture with monocytes. [189] This increase in MMP3 could be due to the production of reactive oxygen species (ROS) produced by myeloid cells as ROS has previously been shown to increase MMP3 production.[188]

CD163 is expressed on the cell-surface of myeloid cells and can be cleaved by MMP 6-8 into a soluble form, sCD163, and is therefore only present in triple culture models. TAMs express high levels of CD163 and a high level of CD163 indicates an unfavourable prognosis in CRC, and later stage disease. Therefore, CD163 (expressed on circulating monocytes or TAMs) and its soluble form sCD163, can be used as potential biomarker for prognosis. The presence of CD163 in the triple culture model

is favourable as this could suggest that this model could be used to mimic late-stage cancer and disease associated with a poor prognosis.[190]

A low level of IL-34 was detected in all four cell lines irrespective of co-culture. However, there was a distinct increase in production following the incorporation of monocytes to the HCT116 model. A rise in IL-34 production has been attributed to a number of factors present within the TME such as, pro-inflammatory cytokines including TNF-α and IL-1β, that can augment IL-34 synthesis in many cell types, including fibroblasts and epithelial cells [191]; unfortunately, TNF-α ad IL-1β were not included in the multiplex analysis performed. Moreover the IL-34 receptor, CSF-1 is expressed macrophages and CRC cells, and IL-34 has been shown to act in an autocrine manner to enhance CRC growth. [192] In a lung cancer model, IL-34 production was increased following chemotherapy treatment to promote cancer cell survival. [193] Notably, further studies have also shown that IL-34 has been associated with the survival of chemo-resistant CRC cells. [193] Given that all four cell lines produce a low level of IL-34 it is possible that this model could display chemo-resistant properties, providing an attractive model to test novel therapies aimed at (i) eradicating chemotherapy resistant disease and/or (ii) restoring chemosensitivity.

Petraxin-3 was undetected in all four of the CRC MCTS in isolation, however, the addition of either fibroblasts alone or fibroblasts in combination with monocytes induced its expression. Pentraxin-3 has been reported to be produced by macrophages and fibroblasts and can initiate tumour progression in cancers such as lung cancer.[194] Petraxin-3 is over expressed in number of cancers including, lung, prostate, glioma, melanoma and breast and has been associated with stage/grade of certain cancers such as pancreatic and ovarian cancer. [195] [196] Petraxin-3 has been reported to be involved in the onset of angiogenesis, metastatic dissemination, and immune-modulation of TME. [197] In CRC, elevated levels of Pentraxin-3 are indicative of a poorer prognosis and one study demonstrated that patients who underwent CRC resection for a primary CRC had elevated levels of Pentraxin-3 prior to surgery, when compared to healthy controls; higher Pentraxin-3 production was

associated with a reduced 5-year survival. [161] These results taken together indicate that the addition of either fibroblast or fibroblast with monocytes altered to cell environment, indicating that the addition of these cells into the MTCS could result in differential cell to cell signalling between tumour-fibroblasts-myeloid cells when grown as a MCTS.

In conclusion this chapter has demonstrated that all four CRC cell lines can generate a MCTS model. This is in keeping with other studies that have grown multicellular tumour spheroids in cancers such as ovarian and pancreatic cancer. [198] [199] This chapter expands on previous studies that cultured HCT116 cells with fibroblasts and monocytes by including further CRC cell lines. As cancer is a diverse, multifactorial and heterogeneous disease, the inclusion and characterisation of the further three CRC cell lines used in this study could lead to improved testing of anti-cancer therapies. Although data is still limited on CRC spheroids co-cultured with monocytes and fibroblasts, this chapter has demonstrated that this more complex model is more akin to human disease by the varied soluble factors they can produce. Thus, this triple culture model is likely to be more representative of human CRC. In the subsequent chapter we aim to further explore this more advanced 3D model in terms of its drug resistance properties and also test its suitability to test novel therapies such as OV's to combat chemo-resistance in CRC.

Chapter 4: Testing anti-cancer therapies in 2-dimensional and 3-dimensional colorectal cancer models

4.1 Introduction

As previously discussed in **Chapter 1**, 3D CRC models represent a more complex model of cancer and are a better model to use to test anti-cancer therapies. Although common chemotherapy agents such as 5-FU have been used to treat CRC for decades, chemotherapy resistance remains an issue for patients who present with late-stage cancer. Patients who have stage I cancer have a 90% chance of survival compared to those who present with stage IV cancer where less than 10% of patients survive. [26]

Having successfully developed and characterised the CRC MCTS, it was next investigated if the standard of care chemotherapeutic agent, 5FU or oncolytic viruses were effective at causing tumour cell death in these complex tumour models. As previously discussed in **Section 1.8,** OVs are a new and exciting development in the fight against cancer. OVs preferentially infect and kill tumour cells instead of healthy cells. There have been various pre-clinical studies supporting the application of OVs for the treatment of CRC. Specifically, OVs such Reovirus (Pelareorep) can selectively lyse CRC cells with a KRAS mutation. [121] Brun *et al* (2010) also investigated the oncolytic effect of MG-1 on SW620 (human) and CT26 (mouse) CRC cell lines. They concluded that MG1 was highly lytic against the human CRC SW620 cell line *in vitro* and when administered systemically into syngeneic CT26 CRC-bearing mice, MG-1 virus generated long term cures. [130] [201] Until recently, the oncolytic potential of OVs in vitro, including MG-1, had been limited to 2D monocultures, however, these models do not represent the complex interactions that occur within the TME. To support the importance of testing novel therapeutic agents in 3D models, a study by Tong *et al* (2015) tested the ability of a range of OVs, including MG-1, to kill ovarian cancer cell lines grown in 3D monoculture spheroids, this study showed that MG-1 cytotoxic potential remained when cells were grown in 3D; by contrast, the two other viruses tested, Vaccinia and Myxoma virus were less effective. This suggests that the oncolytic ability of MG-1 could be maintained in 3D cultures, however, the incorporation of other stromal factors was not investigated in this study. [202]

3D models of CRC are more resistant to 5-FU and drug resistance is a multistep process. CRC cells can alter cell cycle, glucose metabolism and mitochondrial behaviour in order to protect against 5-FU-induced cell death. [203] Moreover, there is a substantial body of evidence that indicates that miRNAs play a role in chemotherapy resistance via the regulation of drug resistance genes such as p53. [204] Of note, miR-145 has been shown to have tumour suppressor properties in many cancers including CRC. MiR-145 can reduce the expression of proteins involved in the EMT, such as insulin-like growth factor 1 receptor (IGF1R), fascin-1 and paxillin to stop cell proliferation and metastasis. [60] Studies have shown that miR-145 is downregulated in premalignant CRC lesions as well as CRC when compared to healthy colorectal tissue. [205] Importantly, multiple studies have reported that restoring miR-145 expression can act to reverse drug resistance in multiple tumours, including hepatocellular carcinoma (HCC) breast cancer, CRC, gastric cancer (GC) and others. [206] Specifically for 5-FU treatment, Zheng *et al* (2020) demonstrated that upregulation of miR-145 can sensitise HCC cells to the cytotoxic effects of 5-FU. [207] Liu *et al* (2015) also demonstrated that re-introducing miR-145 into HT29 and SW620 CRC cell lines sensitised cells to 5-FU. [208] Pivotally, as OVs preferentially replicate in tumour cells they are the ideal vectors to deliver therapeutic payloads, such as miRNA. Indeed, Wedge *et al* (2022) described how OV replication was enhanced in cancer cells through the incorporation of artificial miR-cargo which were disseminated via small extracellular vesicles to nearby non-infected cells. [137]

The work outlined in this chapter aimed to expand upon previously published work and investigate whether: (i) the 3D CRC models were more resistant to 5-FU than 2D CRC models and (ii) triple culture spheroids were more resistant than their monoculture counterparts. Following on from this the infection and oncolytic activity of MG-1 in a larger panel of CRC cells, cultured in both 2D and 3D MCTS was investigated and the pro-inflammatory chemokine/cytokine milieu following MG-1 treatment was explored. Finally, we sought to assess whether the addition of miR-145 altered viral replication in the 3D CRC models and whether MG-1 delivery of miR-145 could be used to restore 5-FU sensitivity, or indeed enhance OV sensitivity, in 3D CRC models.

4.2 2D cell viability following treatment with chemotherapy agent 5-FU

The commonly used CRC chemotherapy agent, 5-FU, was initially investigated for its cytotoxic potential in CRC cells using 2D cultures. Cells in 2D culture were treated with 5-FU at doses ranging from 10-800 μM and MTT viability assays were performed after 96 hours. This assay is a colorimetric assay used to measure the metabolic activity of a cell as a surrogate for cell viability. Metabolically active cells transform a water-soluble dye (3-(4,5-dimethylthiazol-2-yl)-2,5-diphenyltetrazolium bromide) into an insoluble formazan which can be quantified by measuring the absorbance at 540nm. **Figure 4.1a** shows the mean percentage of viable cells compared to PBS treated cells at 96 hrs following 5-FU treatment. **Figure 4.1a** demonstrates that treatment with 5-FU decreases the viability of each of the CRC cell lines tested, in a dose dependent manner; **Figure 4.1b** provides a table of statistical comparisons for each cell line, compared to the untreated control. In the HCT116 cell line, cell death reached significance following treatment at the higher doses of 5-FU. For example, at 200μM cell viability was reduced to 65.5% and at 800μM, only 35.6% of the cells remained viable. Similar results were observed with the HT29 cell line; cell death only reached significance at the highest dose of 800μM with 58.2% remaining. By contrast, cell death in the LOVO and HCA7 cell lines reached statistical significance at the lower doses of 5-FU, ranging from 10-100μM.

In summary these results demonstrate that all four 2D CRC cell lines are susceptible to the cytotoxic effects of 5-FU at varying degrees. The HCA7 cells were the most sensitive cell line and HT29 cells were the most resistant.

a)

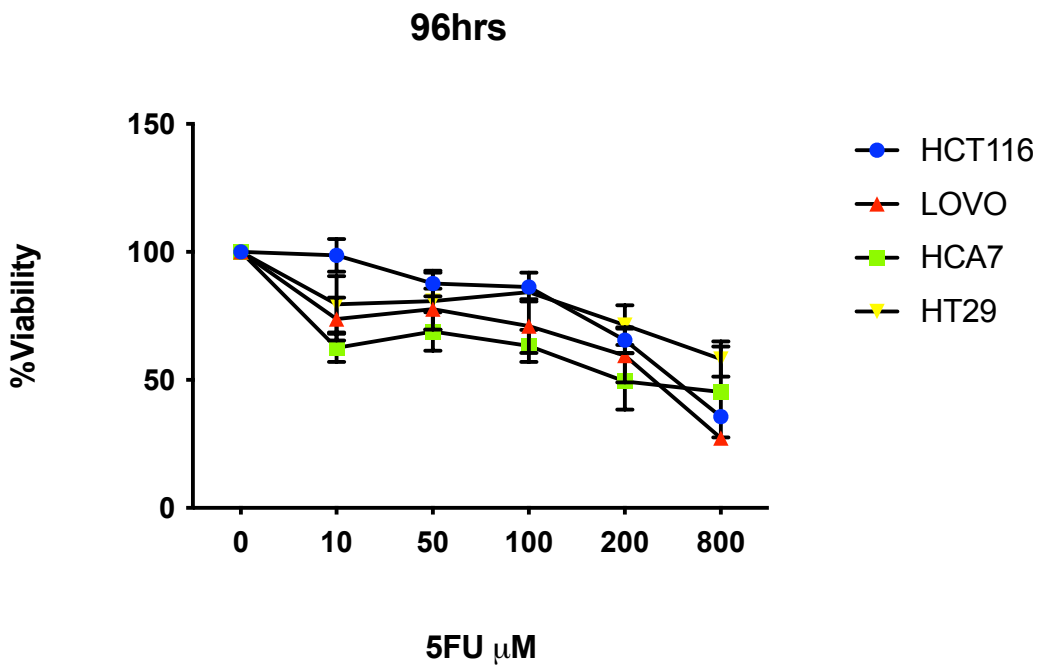

b)

	HCT116	LOVO	HCA7	HT29
0 vs 10	ns	0.0394	0.0067	ns
0 vs 50	ns	ns	0.0320	ns
0 vs 100	ns	0.0186	0.0082	ns
0 vs 200	0.0036	0.0005	0.0002	ns
0 vs 800	<0.0001	<0.0001	<0.0001	0.0021

Figure 4-1. Cytotoxicity of 2D CRC following treatment with 5-FU. HCT116, HCA7, LOVO and HT29 cells were seeded at $1.25x10^4$ cells in a 96-well flat bottom plate. **a)** Graphs show % cell viability for HCT116, HCA7, LOVO and HT29 following treatment with 5-FU for 96 hrs at doses of 0, 10, 50, 100, 200 and 800μM; cell viability was determine using an MTT assay and data shows mean ±SEM for n=4 independent experiments for HCT116 and LOVO cells and n=3 for HT29 and HCA7 cells. **b)** Statistical significance compared to control untreated was determined using a two-way ANOVA; n.s., not significant.

4.3 Comparison of 2D vs 3D cell culture viability following treatment with 5-FU

Having confirmed that 5-FU is an effective cytotoxic agent in 2D it was next investigated whether any differences in cytotoxic potential were evident between 2D and 3D monocultures following treatment with 5-FU. To investigate this 2D HCT116 cells were seeded at $1.25x10^4$ cells/ well in a 96-well flat bottom plate and 3D HCT116 spheroids were generated as a monoculture, as previously described in **Section 2.2.** To assess the cytotoxic potential of 5-FU, 2D and 3D HCT116 cells were treated with 5-FU at concentrations of 50μM, 100μM, 200μM and 800μM for 96 hours. MTT viability assays were used to investigate 2D cell viability and a 3D Cell Titre-Glo® viability assay was used to investigate 3D cell viability. This viability assay relies on the quantification of ATP and is reflective of the number of metabolically active cells. Both these assays measure metabolic activity and should be comparable.

Figure 4.2a shows the mean percentage of viable HCT116 cells in 2D and 3D (monoculture) spheroids following treatment with 5-FU at concentrations of 50μM, 100μM, 200μM and 800μM relative to untreated controls. These data demonstrate a dose dependent decrease in 2D and 3D viability; however, cell viability in the 3D models was significantly greater than in the 2D cultures. For example, at 200μM, HCT116 cells grown in 2D or 3D show a significant difference in cell viability (63.9% *vs*.89.7%) and at the highest dose of 5-FU 800μM the viability in 2D culture decreases to 35.03% compared to only 76.4% in 3D monoculture spheroids. **Figure 4.2b** provides a table of statistical comparisons of cell viability at varying 5-FU concentrations comparing 2D versus 3D cell cultures. Therefore, in summary **Figure 4.2** demonstrates that following treatment with 5-FU the tumour cells in a 3D model were more resistant than traditional 2D cancer models. These data suggest that the 3D models generated in this study would be a better model for testing novel therapeutic agents, as previously suggested in the literature. [209]

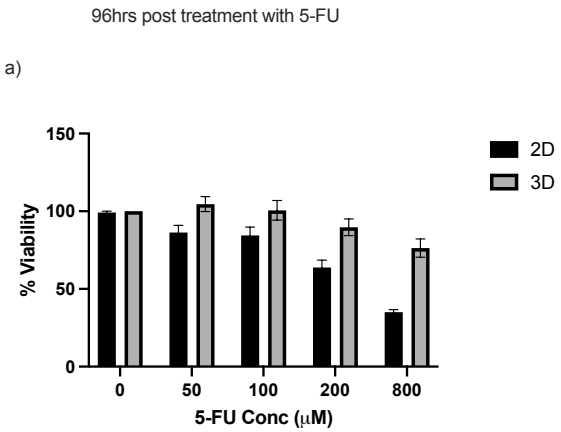

2D versus 3D	P value
50μM	0.0360
100μM	ns
200μM	0.0017
800μM	<0.0001

Figure 4-2. **Comparison of 2D versus 3D HCT116 cells following treatment with 5-FU.** HCT116 cells in 2D were seeded at $1.25x10^4$ cells/well in a 96 well flat bottom plate. HCT116 in 3D monoculture were seeded at $2.5x10^4$ cells/well in a 96 well ultra-low binding U bottom plate. **a)** Graph shows the % viability of HCT116 cells in 2D and 3D 96hrs post treatment with 5-FU at doses of 0, 50,100, 200 and 800μM, ± SEM for at least n=4 experiments, as determined using MTT (2D) and Cell-Titre-Glo® Luminescent Cell Viability Assay (3D). **b)** Statistical comparisons between 2D and cell death observed in 2D vs 3D was calculated using a two-way ANOVA test and results are highlighted.

4.4 Sensitivity to 5-FU with increasingly complex 3D CRC models

Initial results presented in **Figure 4.1 and Figure 4.2** demonstrate that traditional 2D cell culture models of CRC were susceptible to 5-FU treatment, in a dose dependent manner, and that monoculture spheroids were more resistant, as expected based on previously published literature. [164] However, 3D MCTS may represent a more realistic model of human cancer, therefore the sensitivity of MCTS to 5-FU was determined next. The viability of cell lines HCT116 and HT29, in mono, double and triple cultures was investigated using the CellTiter-Glo® 3D Cell Viability kit, following treatment with 5-FU (0 to 800 μM) for 96 hours. **Figure 4.3** shows the mean percentage viability of CRC cell lines grown in either mono, double and triple cultures relative to untreated controls, following treatment with 5-FU. **Figure 4.3b** provides a table of statistical comparison comparing each cell model against the untreated

control. This figure demonstrates that, similar to what was observed in 2D cell cultures, all four cell lines were susceptible to 5-FU, however at varying degrees. **Figure 4.3a** shows a dose dependent decrease in HCT116 viability. At the lower dose of 5-FU, 25μM, cell viability across all three cell models was comparable; 96.8%, 89.9% and 114.8% in mono, double and triple cultures, respectively. As expected, as the dose of 5-FU increased to 800μM, cell viability decreased although, again sensitivity was similar across all three cell models; 70.18%, 63.88% and 70.69% viability in mono, double and triple culture models, respectively. Following statistical analysis there was a significant decrease in cell viability at the higher doses of 200μM, 400μM and 800μM in monoculture. By contrast, a significant decrease in cell viability was only reached at the highest doses of 400μM and 800μM in the more complex triple culture model. Upon a direct comparison between monoculture HCT116 spheroids and triple culture HCT116 MCTS, the triple culture was significantly more resistant to 5-FU at 25μ ($p=0.0111$), but not the other doses, therefore it remained unclear whether triple culture MCTS represented a more drug resistant CRC model than single culture spheroids. Therefore, to explore this further we tested the viability of HT29 cells grown in 3D spheroids and treated with increasing doses of 5-FU as is demonstrated in **Figure 4.4**. There was a dose dependent decrease in viability in HT29 MCTS following 5-FU treatment; unfortunately, there did not appear to be any obvious difference in the sensitivity between mono, double and triple cultures; for example, at 200μM, cell viability was 104.8%, 73.05% and 94.14% in mono, double and triple cultures, respectively. Moreover, at the higher dose of 800μM cell viability was similar across all cultures, e.g., 64.82%, 51.36% and 65.12%.

In summary HCT116 and HT29 cell lines are sensitive to the cytotoxic effects of 5-FU in 3D culture. Moreover, the addition of HFF and/or monocytes did not significantly alter the sensitivity of CRC cells to 5-FU. However, despite this disappointing result, triple culture spheroid remains a more representative model due to the presence of different TME components. Pre-liminary data (n=1) for HCA7 and LOVO cell lines in mono, double and triple cultures show no obvious difference in cell viability between models. (see **Appendix Figure 1**)

a)

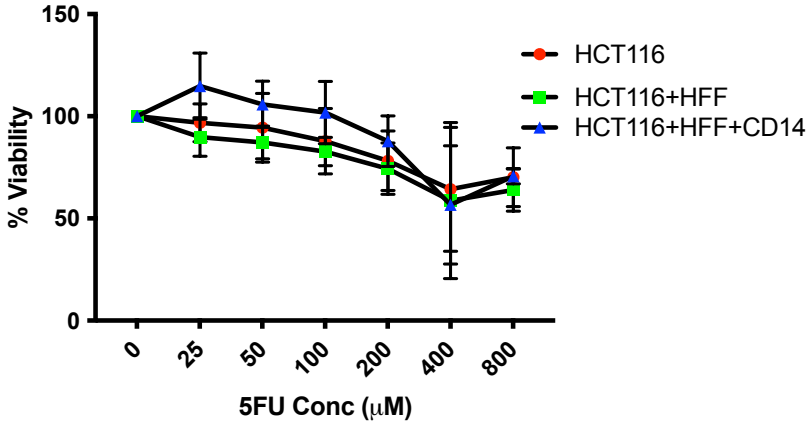

b)

	HCT116	HCT116+ HFF	HCT116+HFF+CD14
0 vs 25	ns	ns	ns
0 vs 50	ns	ns	ns
0 vs 100	ns	0.0270	ns
0 vs 200	0.0041	0.0008	ns
0 vs 400	<0.0001	<0.0001	<0.0001
0 vs 800	0.0001	<0.0001	0.0002

Figure 4-3. **Cytotoxicity of 5-FU in HCT116 MCTS.** HCT116, HFF and CD14 cells were seeded in a 96 well ultra-low binding U bottom plates. Monoculture cells were seeded at $2.5x10^4$, double culture cells were seeded at a ratio of 2:1 and triple culture cells were seeded at a ratio of 2:1:1. Following incubation at 37°C for seven days cells were treated with 5-FU at 10, 25, 50, 100, 200, 400 and 800μM and incubated again for 96 hours at 37°C for a Cell-Titre-Glo® Luminescent Cell Viability Assay was performed. a) Graph shows the mean % viability ± SEM for n=3 in HCT116. b) Statistical significance compared to control untreated was determined using a two-way ANOVA and results are highlighted (n.s., not significant).

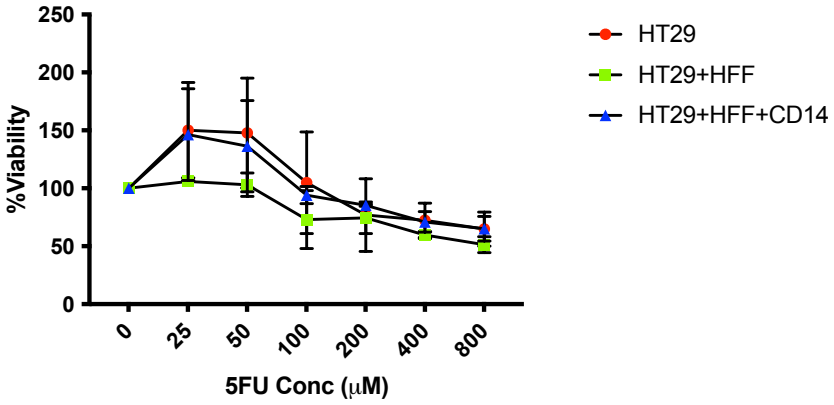

Figure 4-4. **Cytotoxicity of 5-FU in HT29 MCTS.** HT29, HFF and CD14 cells were seeded in a 96 well ultra-low binding U bottom plates . Monoculture cells were seeded at $2.5x10^4$, double culture cells were seeded at a ratio of 2:1 and triple culture cells were seeded at a ratio of 2:1:1. Following incubation at 37°C for seven days cells were treated with 5-FU at 10, 25, 50, 100, 200, 400 and 800μM and incubated again for 96 hours at 37°C for a Cell-Titre-Glo® Luminescent Cell Viability Assay was performed. The graph shows mean % viability for ± SEM for n=2 for HT29.

4.5 Virus infectibility in the 2D model

To expand on previous studies, the ability of MG-1 to infect four different human CRC cell lines was investigated. CRC cell lines HCT116, LOVO, HT29 and HCA7 were seeded at 1.25 x 10^5 cells in 12 well flat bottom plates in 1mL of appropriate media and incubated at 37°C for 24hrs. These cells were then treated with MG1-GFP (MG1 genetically modified to express GFP) for 24 hours and GFP expression was visualised using fluorescent microscopy. **Figure 4.5** shows images for all four CRC cell lines pre- and post- infection with MG1-GFP at MOI's of 0.01, 0.1, 1.0 and 10. GFP expression was clearly evident at the lower MOI of 0.01 in HCT116 cells, however for LOVO, HT29 and HCA7 cell lines GFP expression was not apparent until an MOI of 0.1.

To accurately quantify GFP expression in 2D CRC cell lines, flow cytometry was used. **Figure 4.6** demonstrates that the number of GFP positive cells increased in a dose dependent manner following MG1-GFP infection, for each cell line. As suggested using fluorescent microscopy, the HCT116 cell line was the most sensitive at the lowest MOI with 53.06% of the cells expressing GFP compared to 23.37%, 10.16%

and 6.64% in the LOVO, HCA7 and HT29 cell lines, respectively. Although the LOVO and HCA7 cell lines were the least sensitive they still displayed 47.53% and 61.7% GFP positive cells at the highest MOI of 1. In summary, these results confirmed that MG-1 can successfully infect and replicate in CRC cell lines grown in 2D models.

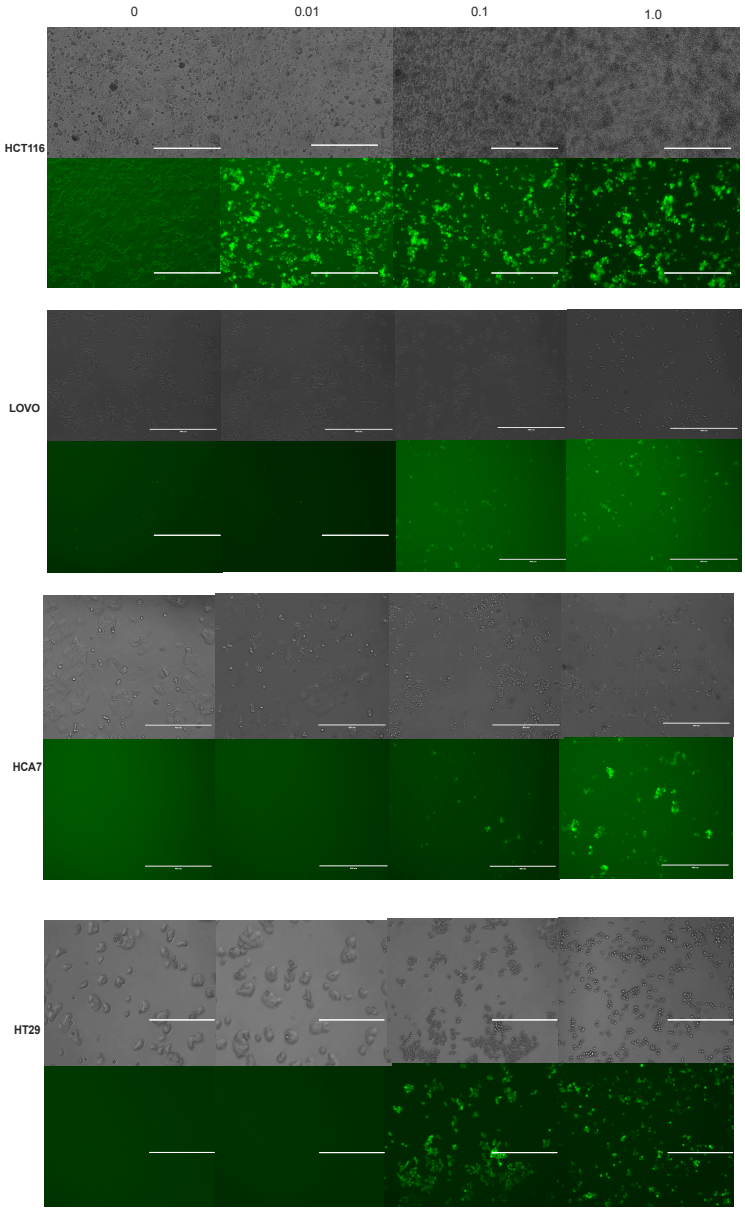

Figure 4-5. **MG-1 replication in HCT116, LOVO, HCA7 and HT29 2D CRC models.** HCT116, LOVO, HCA7 and HT29 cells were seeded at $1.25x10^4$ cells/well in a 12 well flat bottom plate and incubated for 24 hours. These cells were then treated with MG1 -GFP at MOIs of 0.01, 0.1 and 1.0 and images were acquired 24hrs post infection by the EVOS microscope, magnification x4. Images represent n=4.

a)

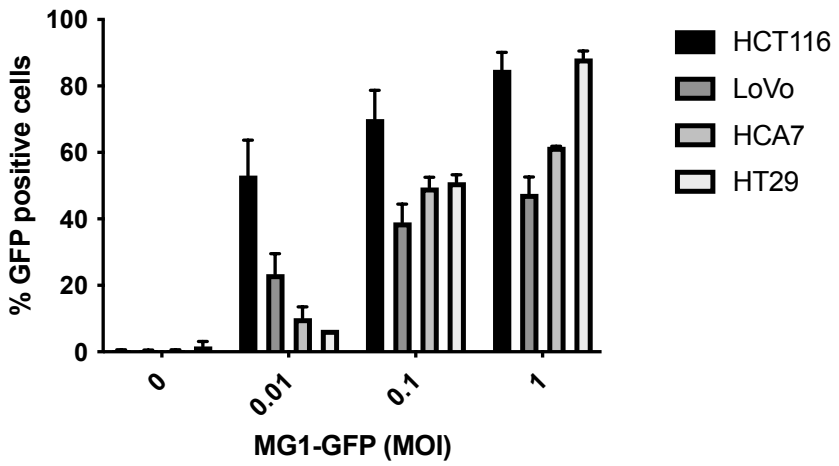

b)

	HCT116	LOVO	HCA7	HT29
0 vs 0.01	<0.0001	0.0263	ns	ns
0 vs 0.1	<0.0001	<0.0001	<0.0001	<0.0001
0 vs 1	<0.0001	<0.0001	<0.0001	<0.0001

Figure 4-6. **The percentage of GFP positive cells following treatment with MG1-GFP.** HCT116, LOVO, HCA7 and HT29 cells were seeded at $1x10^5$ cells/well in a 12 well flat bottom plate and incubated for 24 hours. These cells were then treated with MG-1 GFP at MOI's of 0.01, 0.1 and 1.0. a) The percentage of GFP positive cells were quantified by flow cytometry. Data shows mean results ± SEM (n=4). b) Statistical significance compared to the untreated control was calculated using two-way ANOVA test and results are highlighted.

4.6 2D cell viability following infection with MG-1

Having confirmed MG-1 could infect the four CRC cell lines used in this study. It was next investigated whether treatment with MG-1 resulted in loss of cell viability. To test this, the cell viability was initially determined using an MTT assay. HCT116, HCA7, LOVO and HT29 CRC cell lines were seeded in a 96 well flat bottom plate in 100μL of appropriate media and incubated at 37°C for 24 hours prior to adding MG-1 at range of MOI's, 0,0.001, 0.01, 0.1, 1 and 10. Following virus treatment, plates were incubated for 24 and 48 hrs at 37°C prior to an MTT assay being performed. **Figure**

4.7 shows the mean percentage of viable cells compared to PBS treated cells at 24 and 48 hrs post infection. This data shows that all four CRC cell lines, cultured in a 2D monolayer, were susceptible to the cytotoxic effects of MG-1 in a dose and time dependent manner. For example, MG-1 cytotoxicity was observed at 24 hrs, with a significant decrease in viability observed with MOIs as low as 0.01 (LOVO), 0.1 (HT29) and 1 (HCT116 and HCA-7), as demonstrated in the table **Figure 4.7a**. The cytotoxic effect of MG-1 was further evident at 48 hrs post infection, for example, LOVO cells treated with MOI 0.001 had a mean viability of 22.9% at 48 hrs, compared to 69.2% at 24 hrs post infection. HT29 demonstrated similar results with the same dose of MG1 at 48 hrs post infection, with a mean viability of 22.9%, compared to 64.9% at 24 hrs post infection; HCA7 cells at the same dose were 90.7% viable at 24 hours compared to 47.6% at 48 hours and HCT116 cells were 45.0% viable at 48hrs, compared to 85.2% at 24 hrs. This was not expected for the HCT116 cell line as in **Figure 4.5,** HCT116 cells were more susceptible to MG-1 infection based on the images acquired by the EVOS microscope demonstrating GFP expression. Loss of cell viability was statistically significant for all cell lines after 48 hrs post infection with MG-1 at the lowest MOI of 0.001 ($p < 0.001$ for all cell lines). Overall, these results confirmed that CRC cells grown in 2D culture conditions were susceptible to the cytotoxic effects of MG-1.

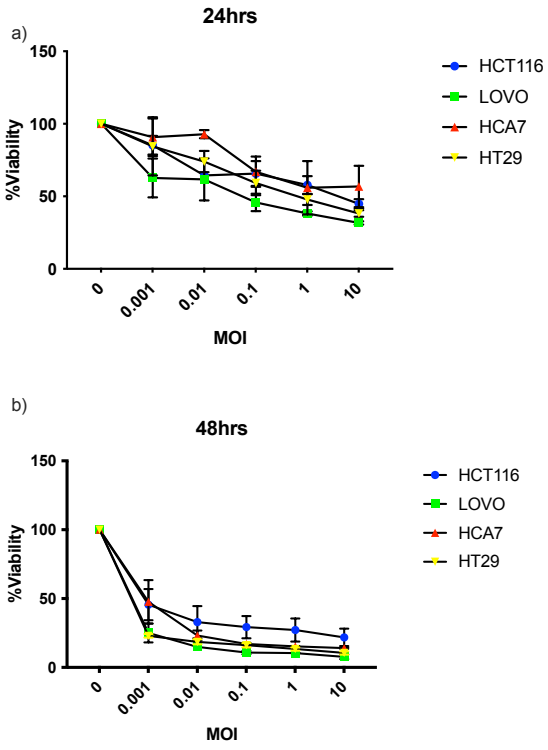

24 hrs	HCT116	LOVO	HCA7	HT29
0 vs 0.001	ns	ns	ns	ns
0 vs 0.01	ns	0.0467	ns	ns
0 vs 0.1	ns	0.0014	ns	0.286
0 vs 1	0.0212	0.002	0.0142	0.0022
0 vs 10	0.0010	<0.0001	0.0172	0.0002

48hrs	HCT116	LOVO	HCA7	HT29
0 vs 0.001	<0.0001	<0.0001	<0.0001	<0.0001
0 vs 0.01	<0.0001	<0.0001	<0.0001	<0.0001
0 vs 1	<0.0001	<0.0001	<0.0001	<0.0001
0 vs 10	<0.0001	<0.0001	<0.0001	<0.0001

Figure 4-7. **Cytotoxicity of MG-1 in 2D CRC cells.** HCT116, LOVO, HCA7 and HT29 cells were seeded at 1.25x10^4 cells in a 96 well flat-bottomed plate. They were treated with MG-FLUC for (a) 24hrs and (b) 48hrs. Graphs show % cell viability for HCT116, LOVO, HCA7 and HT29 following treatment with MG-1 at MOIs of 0, 0.001, 0.01, 1.0 and 10, determined using an MTT assay. Data shows the mean SEM for n=3 experiments. Statistically significant results are highlighted in the table adjacent to the graphs.

4.7 Virus infectibility in the 3D model

As demonstrated in **Figures 4.5 and 4.7,** MG-1 can infect and kill CRC cell lines grown in 2D cell culture models. However, once the 3D MCTS were optimised for the CRC cell lines, this model was then used to examine MG-1 infection and replication. To do this MCTS spheroids (mono, double and triple) were generated as in **Section 2.2** and cultured at 37°C for six days, MCTS were subsequently infected with MG1-GFP at an MOI 0.1 and bright field and fluorescent microscopy was preformed 24 hrs post infection, representative images are displayed in **Figure 4.8.** Images taken confirmed that MG1-GFP was able to replicate in CRC cells, despite being grown in 3D spheroids. Moreover, the incorporation of different TME cell populations, did not appear to

prevent MG-1 viral infection, as GFP expression was observed in mono- double- or triple culture spheroids. Upon further inspection of the EVOS pictures, HCT116 and LOVO cells in all cell models show GFP expression mainly at the periphery of the MCTS. By contrast, in HT29 3D models, GFP expression follows a more uniform pattern throughout the spheroid. By contrast, HCA7 cells demonstrate a more localised/punctuated pattern of GFP expression which was evident throughout the MCTS in all models. Overall, the addition of immune and stromal cells into the 3D CRC cell culture did not appear to impede MG-1 viral infection.

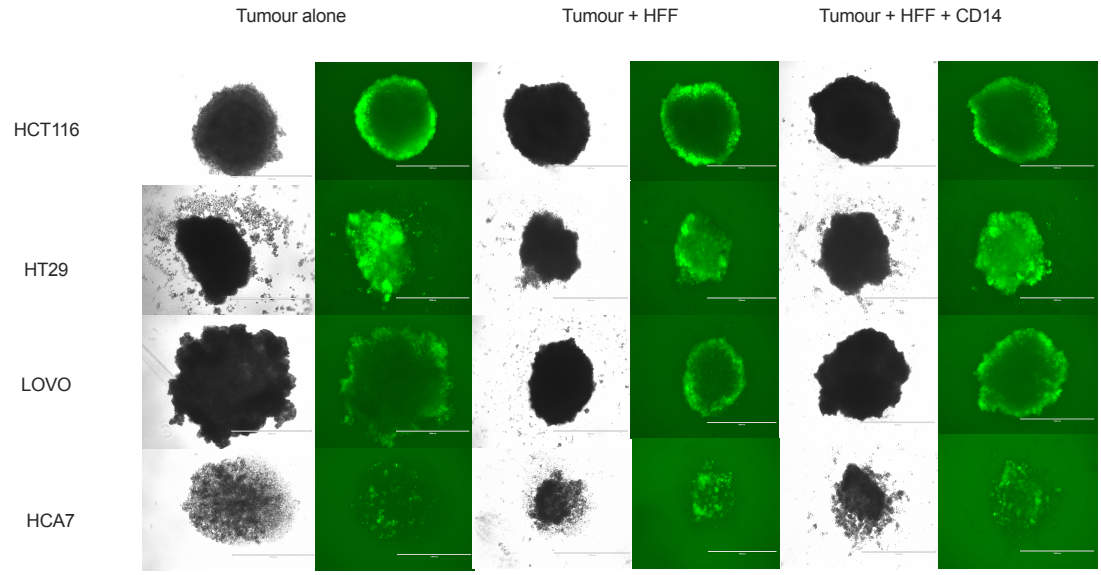

Figure 4-8. **MG-1 infection and replication in HCT116, HT29, LOVO and HCA7 3D CRC models in mono, double and triple culture models.** HCT116, HT29, HCA7, LOVO, HFF and CD14 cells were seeded at 2:1:1 ratio in a 96 well ultra -low binding U bottom plates. After incubation at 37°C for six days MCTS were infected with MG1-GFP at an MOI of 1. On day seven images were acquired with the EVOS microscope magnification x4. Images represent n=1.

4.8 3D cell viability following infection with MG-1

Once viral infection was confirmed in the MCTS model, effects on cell viability were investigated. To assess the cytotoxic effect of MG-1 in MCTS spheroids models (mono, double and triple) were seeded as previously described. MCTS were infected with MG1-GFP at an MOI 0.1 and incubated for 72hrs. A lower MOI was selected as

the images above (**Figure 4.8)** clearly demonstrated that MG-1 was able to replicate in all four cell lines despite being grown in 3D spheroid cultures. At the end of this incubation period a Cell Titre-Glo® luminescent cell viability assay was performed. Figure **4.9** demonstrates the viability of 3D CRC cells in mono, double and triple culture following infection with MG-1 at an MOI of 0.1. For the HCT116 cell line, the difference between mock versus virus was statistically significant in mono, double and triple HCT116 models. However, whilst the addition of fibroblasts appeared to decrease cell viability compared to cells grown in monoculture (53.6% of cells were viable in double culture compared to 73.4% in monoculture), this difference was not statistically significant. Moreover, the addition of monocytes into the model did not affect MG1 sensitivity compared to cells grown in monoculture.

Interestingly, pre-liminary data obtained for the LOVO, HCA7 and HT29 cells (n=1) shows potentially different results to those observed in the more commonly used HCT116 cell line data. For example, it is possible that the addition of fibroblast and/or monocytes could induce resistance to MG-1 in the LOVO and HT29 cell line models; however, these experiments would need repeating in order to confirm these initial observations. Unfortunately, time restrictions did not allow these confirmative studies to be performed.

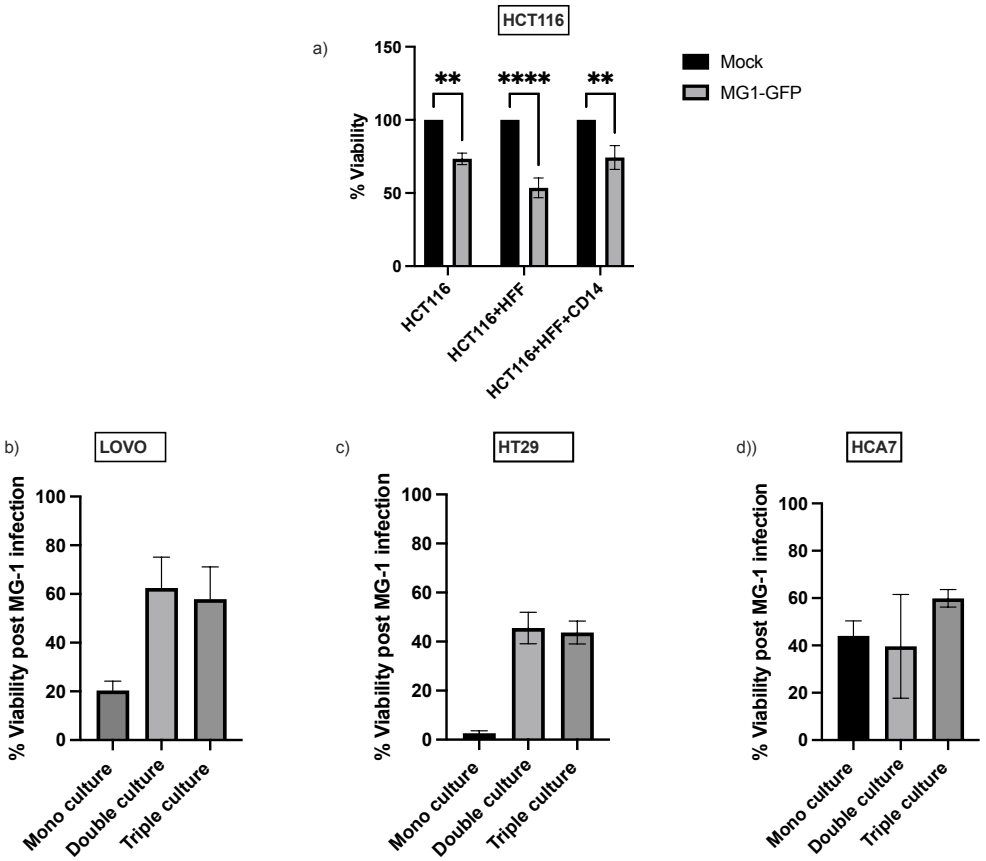

Figure 4-9. **Cytotoxicity of MG-1 in CRC MCTS.** HCT116, LOVO, HT29, HCA7, HFF and CD14 cells were seeded at a 2:1:1 ratio in a 96 well ultra-low binding U bottom plate. Following incubation at 37°C for seven days cells were infected with MG-1 at an MOI of 0.1 and incubated again at 37°C for 72hrs and a CellTitre-Glo® Luminescent Cell Viability Assay was performed. Viability of mono, double or triple culture following infection with MG-1 is shown for: **a)** HCT116 where error bars show mean, ± SEM for n=3 independent experiments and statistically significant results are highlighted on the graph. **b)** LOVO, **c)** HT29 and **d)** HCA7 where error bars show SD for triplicate replicates within n=1 independent experiment. Cell viability is shown normalised to mock treated cells in each condition.

4.9 Comparison of 2D versus 3D HCT116 cells following MG-1 infection

Having confirmed that both MG-1 and 5-FU are effective cytotoxic agents in 2D and 3D CRC cultures, it was next investigated as to whether any differences in cytotoxic potential were evident between 2D and 3D monocultures, following infection with

MG-1. To investigate this, 2D HCT116 cells were seeded at $1.25x10^4$ cells/well in a 96-well flat bottom plate and 3D HCT116 cells were generated as a monoculture**.** 2D and 3D HCT116 cells were treated with MG-1 at an MOI of 1 for 48 hours; MTT viability assays were used to investigate 2D cell viability and a 3D CellTitre-Glo® Luminescent Cell viability assay was used to investigate 3D cell viability. **Figure 4.10** shows the mean percentage of viable HCT116 cells in 2D and 3D cultures following infection with MG-1 at an MOI of 1, relative to the untreated control. This figure shows that 2D cell cultures were significantly more susceptible to the cytotoxic effects of MG-1 when compared to 3D cell cultures. For example, the average cell viability following infection with MG-1 in 2D is 33.9%, while in 3D culture viability was significantly increased to 65.9% ($p=0.04$). These data confirm that the 3D cell model is more resistant to the killing effects of MG1, as observed for 5-FU in **Figure 4.3**. Similar data was also obtained when we compared the susceptibility of 2D cultures in HCT116 cells with double and triple MCTS (see **Appendix Figure 2**).

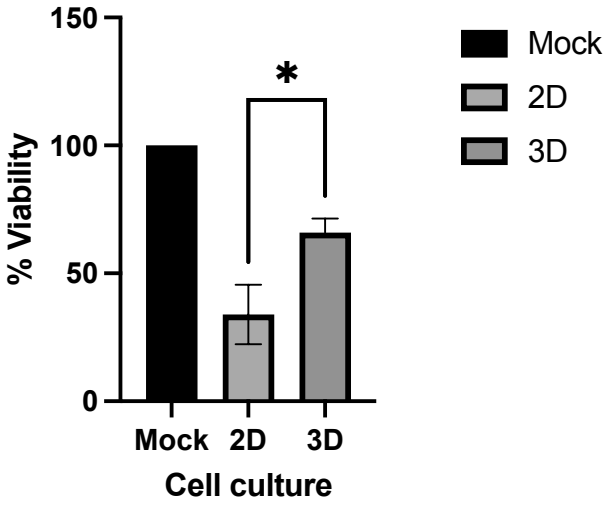

Figure 4-10. **Comparison of 2D versus 3D HCT116 following MG-1 infection.** HCT116 cells in 2D were seeded at 1.25x10^4 cells/well in a 96 well flat bottom plate or 2.5x10^4 cells/well in a 96 well ultra-low binding U bottom plate for 3D. Data shows the mean % viability of HCT116 cells in 2D and 3D 48hrs following infection with MG-1 at an MOI of 1, normalised to mock treated cells. Data shows mean ± SEM for n=4 independent experiments. Statistical significance was calculated using the unpaired t-test and * denotes a statistically significant difference ($p<0.05$).

4.10 Cytokine analysis of mono, double and triple culture MCTS for HCT116, LOVO and HCA7 following infection with MG1

Having confirmed that MG1 can successfully infect and reduce cell viability in the 3D model, albeit with some differences in mono, double and triple cultures in **Figure 4.8 and Figure 4.9**. A multiplex assay (BioRad, Bio-Plex Pro Human Inflammation Assay) was performed using a predefined human inflammatory panel of 37 soluble factors, which contained type 1, 2 and 3 IFNs, to establish if differences in the production of these anti-viral cytokines could explain potential variations in cell sensitivity to MG-1 seen in **Figure 4.9**. Double culture HCT116 cells appeared to be the most sensitive to the effects of MG-1 and preliminary data with LOVO cells suggested a more resistant phenotype in double and triple cultures, compared to mono-culture spheroids. Cell-free supernatants were collected 24 hrs post MG1 infection and

Figure 4.11 shows heatmaps for all 37 soluble factors from each CRC cell line (HCT116, LOVO and HCA7) in mono (+), double (++) and triple (+++) cultures expressed as log10 values.

Of the 37 soluble factors tested, two were not detected in either mono, double or triple culture with or without infection with MG1, these cytokines were IL-12 (p40) and IL-12 (p70).

The most noticeable difference in soluble factor production following infection with MG1 was the production of the Lambda IFNs, IL-28 and IL-29 in **Figure 4.11.** Notably, IL-28 was removed from the heat map as the concentration in HCT116 plus MG1 was high, making the other changes in cytokine profiles harder to visualise. This data is instead plotted in **Figure 4.12d-i,** alongside IL-29 and sCD163 which also demonstrated interesting changes following MG1 infection**.** sCD163, plotted in **Figure 4.12 j-l,** shows that sCD163 is produced to varying degrees in all three cell lines. In the LOVO cell line, infection with MG-1 enhances the production of sCD163 in the double culture model (204.59 pg/mL), however infection with MG-1 causes depletion of sCD163. Double culture LOVO cells produce 273.82 pg/mL whereas following MG-1 infection sCD163 levels were undetected. In the HCT116 cell line, untreated cells did not produce detectable levels of sCD163, whilst infection with MG-1 produces varying degrees of sCD163 in the mono, double and triple culture models (684.13 pg/mL 568.84 pg/mL and 387.35 pg/mL, respectively). The HCA7 cell line following infection with MG-1 also alters the production of sCD163 in the double culture model. For example, in mock treated spheroids 806.42 pg/mL is produced whereas post MG-1 infection this was increased to 1023.07 pg/mL. Although sCD163 was produced in mock treated triple culture MCTS, sCD163 was undetected following MG1 treatment.

IL-28 and IL-29 belong to the same family of IFNs and are similar to type I interferons. Infection with MG1 enhances the production of IL-28 in all three CRC cell lines, however, to varying degrees. Interestingly, the addition of fibroblasts in double culture decreased the concentration of IL-28 and this was apparent in all three CRC cell lines, while the addition of monocytes resulted in fluctuations in concentrations

depending on cell line tested. For example, in HCT116, the concentration of IL-28 in mono-, double- or triple culture were 14681.46 pg/mL, 12410.06 pg/mL and 6290.43 pg/mL, respectively; in LOVO cells they were 269.9 pg/mL, 94.27 pg/mL and 157.2 pg/mL, respectively; and in HCA7 cells they were 14.45 pg/mL, 7.71 pg/mL and 20.65 pg/mL, respectively. The HCA-7 values were below the detection limit for IL-28 which was 46.8 pg/mL, thus, induction of IL-28 in these cells remains uncertain.

Unlike IL-28, IL-29 production was only detected in the HCT116 cell line, and the concentration was lower when cells were cultured with fibroblasts and monocytes; 2851 pg/mL was detected in monoculture, 1675.2 pg/mL in double culture and 1071.34 pg/mL in triple culture. The detection limit in this assay for IL-29 was 23 pg/mL, therefore, it does not appear that LOVO or HCA7 cells induce detectable levels of IL-29 following MG-1 treatment. By contrast, none of the CRC cell lines (alone or in more complex 3D structures) produced IFNβ or IFNα2, indicating that these cell lines may be defective in these antiviral response pathways.

In summary, the results outlined here demonstrate that the HCT116 cell line produced high concentrations of IL-28 and IL-29 following MG-1 infection, and the addition of fibroblasts and/or fibroblasts with monocytes appeared to reduce this production. When comparing this to the cytotoxic effects of MG-1 demonstrated in **Figure 4.9**, the addition of fibroblasts appeared to slightly enhance the cytotoxic effects of MG-1 compared to monoculture and triple culture HCT116 spheroids. Therefore, overall, there is no obvious correlation between anti-viral cytokine secretion and susceptibility to MG-1 in the HCT116 spheroid models, or indeed the other CRC cell line models examine

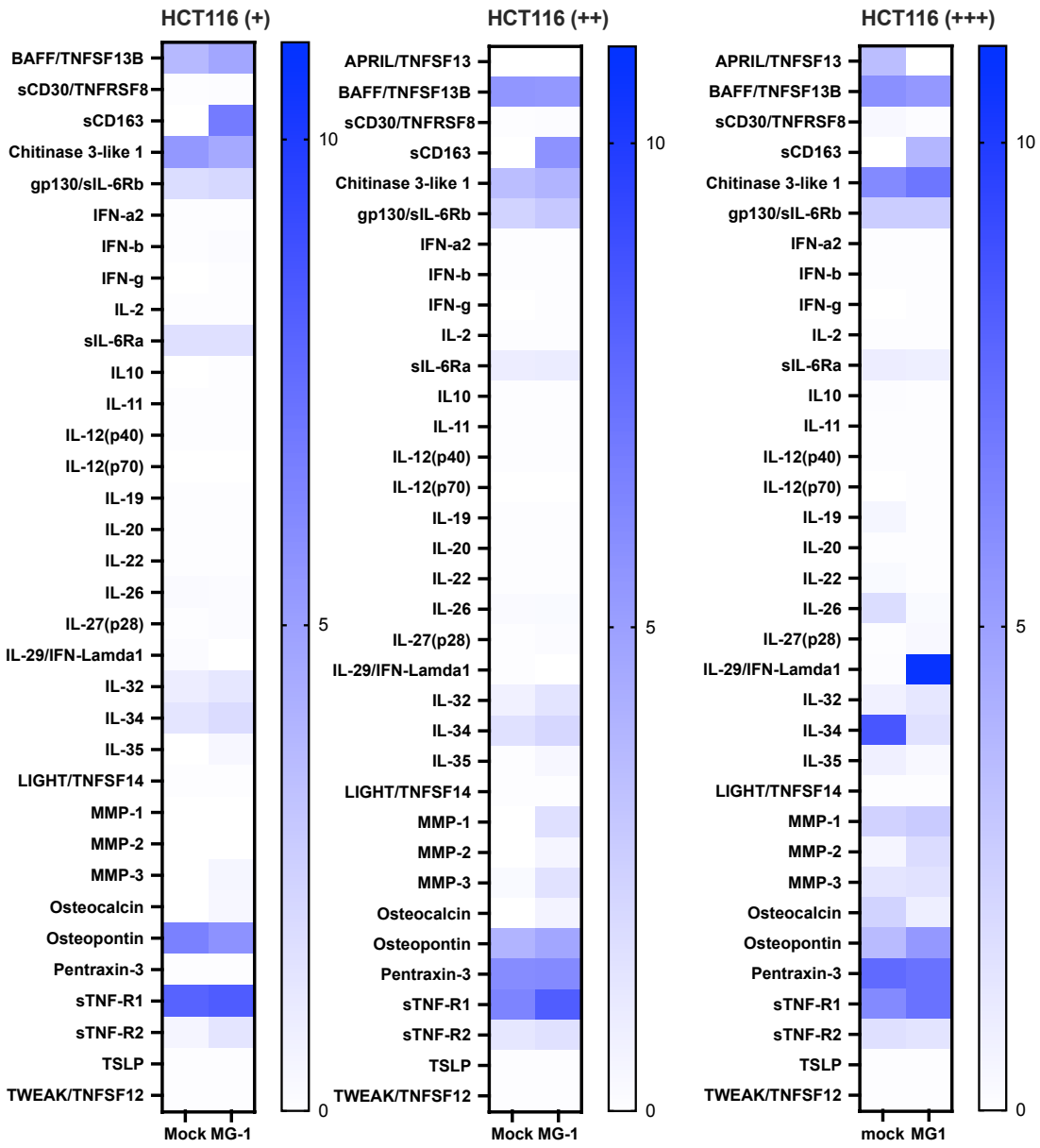
HCT116 (+)
HCT116 (++)
HCT116 (+++)
BAFF/TNFSF13B
sCD30/TNFRSF8
sCD163
Chitinase 3-like 1
gp130/sIL-6Rb
IFN-a2
IFN-b
IFN-g
IL-2
sIL-6Ra
IL10
IL-11
IL-12(p40)
IL-12(p70)
IL-19
IL-20
IL-22
IL-26
IL-27(p28)
IL-29/IFN-Lamda1
IL-32
IL-34
IL-35
LIGHT/TNFSF14
MMP-1
MMP-2
MMP-3
Osteocalcin
Osteopontin
Pentraxin-3
sTNF-R1
sTNF-R2
TSLP
TWEAK/TNFSF12
APRIL/TNFSF13
10
5
0
Mock MG-1
mock MG1

a)

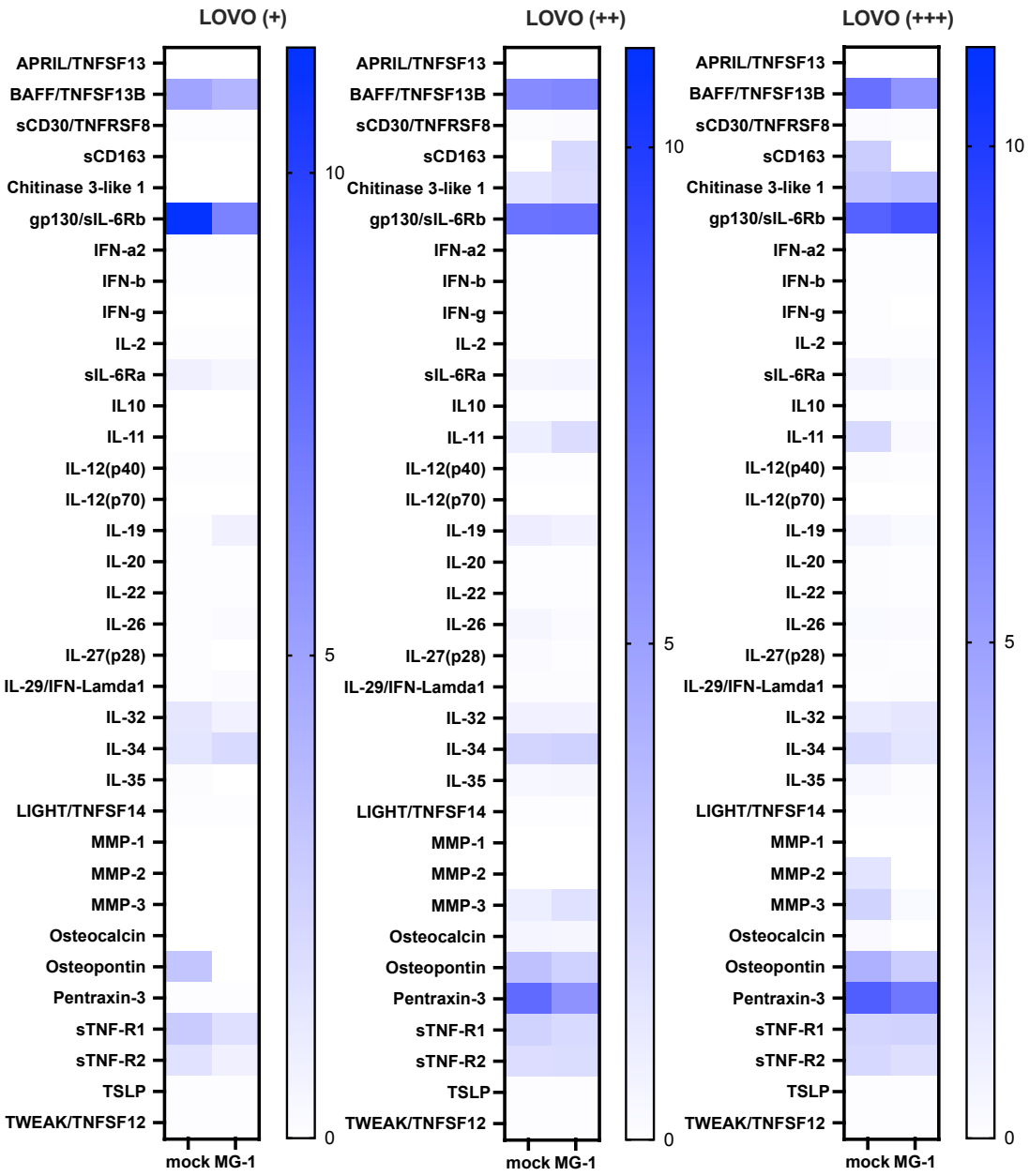
LOVO (+)
LOVO (++)
LOVO (+++)
APRIL/TNFSF13
BAFF/TNFSF13B
sCD30/TNFRSF8
sCD163
Chitinase 3-like 1
gp130/sIL-6Rb
IFN-a2
IFN-b
IFN-g
IL-2
sIL-6Ra
IL10
IL-11
IL-12(p40)
IL-12(p70)
IL-19
IL-20
IL-22
IL-26
IL-27(p28)
IL-29/IFN-Lamda1
IL-32
IL-34
IL-35
LIGHT/TNFSF14
MMP-1
MMP-2
MMP-3
Osteocalcin
Osteopontin
Pentraxin-3
sTNF-R1
sTNF-R2
TSLP
TWEAK/TNFSF12
10
5
0
mock MG-1

b)

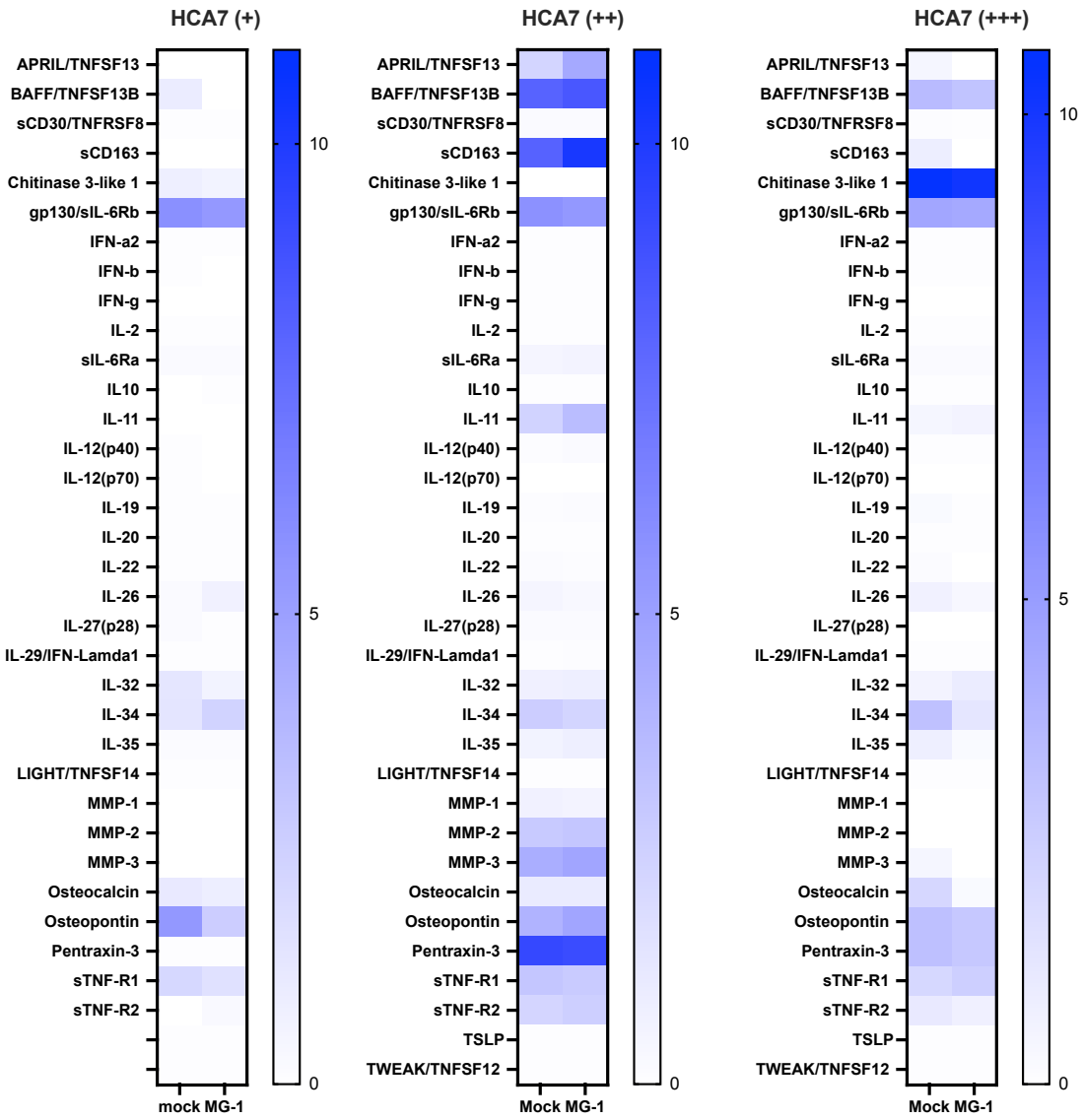

c)

Figure 4-11. **Soluble factors induced in response to MG-1 infection in the CRC spheroid model.** HCT116, LOVO, HCA7, HFF and CD14 were seeded at 2.5x10^4 tumour cells per well in monoculture, at a 2:1 ratio for cells in double culture and at a ratio 2:1:1 for cells in triple culture, in a 96 well ultra-low binding U bottom plates. Heat maps show true cytokine production of a) HCT116, b) LOVO and c) HCA7 in mono, double and triple culture. (n=1).

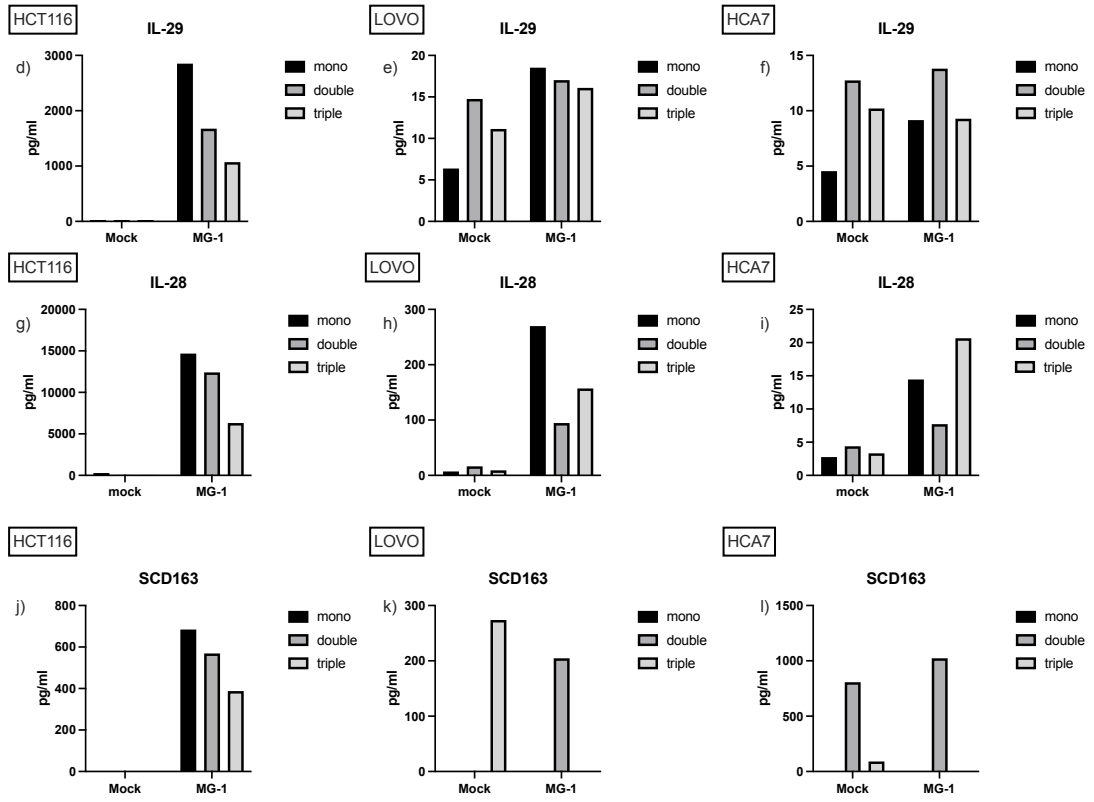

Figure 4-12. **Soluble factors induced in response to MG-1 in CRC spheroid models.** HCT116, LOVO, HCA7, HFF and CD14 were seeded at 2.5x10^4 tumour cells per well in monoculture, at a 2:1 ratio for cells in double culture and at a ratio of 2:1:1 for cells in triple culture, in a 96 well ultra-low binding U bottom plates. At day 6 of culture MG1-GFP was added at an MOI of 0.1. Supernatants were collected 24 hours post infection and a Luminex assay was performed. a-c) represents the production of sCD163. d-f) represents the production of IL-29, and g-i) represents the production of IL-28 in HCT116, LOVO and HCA7 cell lines with or without infection with MG-1 (n=1).

4.11 Expression of MiR-145 in LOVO and HCT116 cell lines

As mentioned previously, miR-145 is downregulated in CRC and it is well established that miR-145 can influence drug sensitivity in CRC. To assess the expression of miR-145 in HCT116 and LOVO cells, qPCR was performed.

MiR-145 and a miR-non-targeting control (NTC) sequence were cloned into MG-1 using a previously published methodology, by inserting the specific 22nt into a pre-

miR-30 stem loop. [137] To confirm that miR-145 is processed into the mature 22nt miR-145-5p sequence following infection, qPCR was performed to assess the levels of miR-145-5p. HCT116 and LOVO triple culture spheroids were infected with MG-miR-NTC or MG-miR-145 at an MOI of 1 and left for 24 hours. MCTS were harvested and RNA was isolated, miRNA was converted to cDNA using a miRNA cDNA synthesis kit, briefly a Poly A tail was added to the 3'UTR using a Poly A polymerase, then cDNA made using specific adaptor primers. Analysis of miR-145-5p levels were compared to RNU6 (housekeeping control). **Figure 4.13** shows both the fold change in miR-145-5p expression compared to miR-NTC control (a) and the ΔCT values (b) for both LOVO and HCT-116 triple culture MCTS from one independent experiment. As is demonstrated in **Figure 4.13a)** the LOVO MCTS shows a 47-fold change in miR-145-5p expression, while HCT116 demonstrates a 9-fold change compared to miR-NTC control virus**. Figure 4.13b)** highlights the relative expression levels of miR-145-5p in the two cell lines. Interestingly, miR-145-5p expression levels, under control conditions, were much higher in the HCT116 (ΔCT =2.3) cells compared to LOVO (ΔCT =7.5), indicating that the expression of miR-145-5p was higher in the HCT116 cell line; however, to confirm this, the of miR-145 in mono-culture spheroids would be needed to be investigated. Due to the lower level of miR-145 expression in LOVO cells, this cell line was chosen for subsequent plaque assays assessment, for viral fitness, and combination experiments.

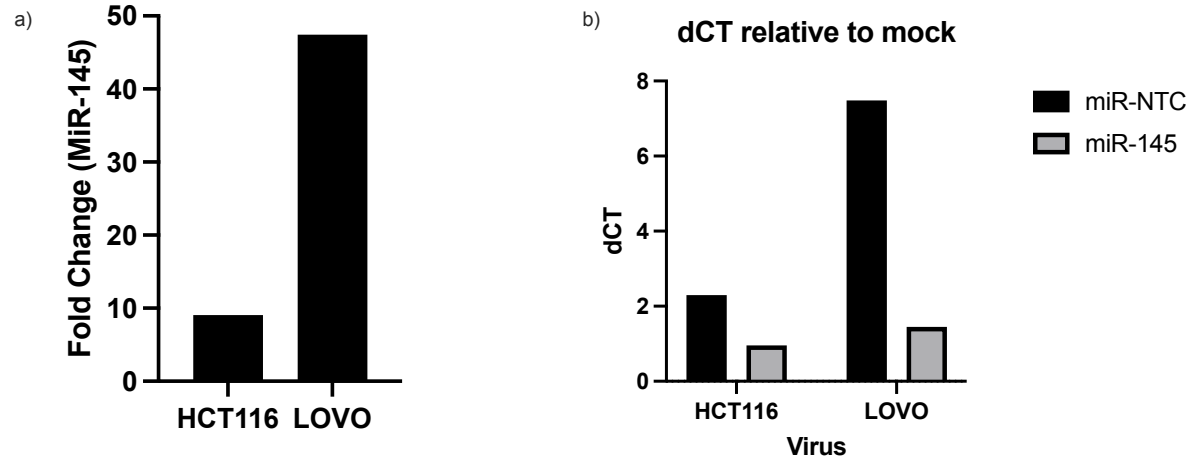

Figure 4-13. **qPCR data for HCT116 and LOVO cell lines in 3D culture.** HCT116, LOVO, HFF and CD14 cells were seeded at a 2:1:1 ratio in a 96 well ultra-low binding U bottom plate. Following incubation at 37°C for 7 days plates were infected with MG-miR-NTC and MG-miR-145 at an MOI of 1 for 24 hours. qPCR was then performed on isolated RNA. a) shows the fold change of MG-miR-145 expression in LOVO and HCT116 cell lines compared to MG-miR-NTC. b) shows the dCT figures relative to RNU6 (the house keeping gene) in LOVO and HCT116 cell lines. Results are (n=1)

4.12 MG-1 replication in LOVO cells assessed via plaque assay

Next, we sought to demonstrate whether the addition of miR-145 had any effect of the fitness of the virus. Viral replication of MG-miR145 was compared to control virus MG-miR-NTC in LOVO cells in 3D mono, double and triple culture. MTCS were infected with $5x10^4$ PFU/mL (which is approximately an MOI of 0.1) of both viruses and cell-free supernatants were collected at 24 hrs, viral titre was determined by plaque assay and calculated for this time point. **Figure 4.14** shows the PFU/mL of MG-miR-NTC and MG-miR-145 following infection of the MCTS from one independent experiment. The data demonstrates the two viruses in mono, double and triple culture over 24hrs. The input virus concentration is depicted with a dash line at $5x10^4$ pfu/ml. Comparing virus replication in the mono-culture spheroid model over 24hrs demonstrates viral replication, comparing levels of input virus (dash line), and no obvious differences in viral titre were observed when miR-145 was expressed.

The addition of fibroblasts and fibroblasts with monocytes appears to reduce viral replication when compared to viral replication in monocultures. Replication of MiR-145 in the triple culture models is reduced compared to replication of the control virus. However, this is one independent experiment and this would need to be repeated to confirm these initial preliminary findings.

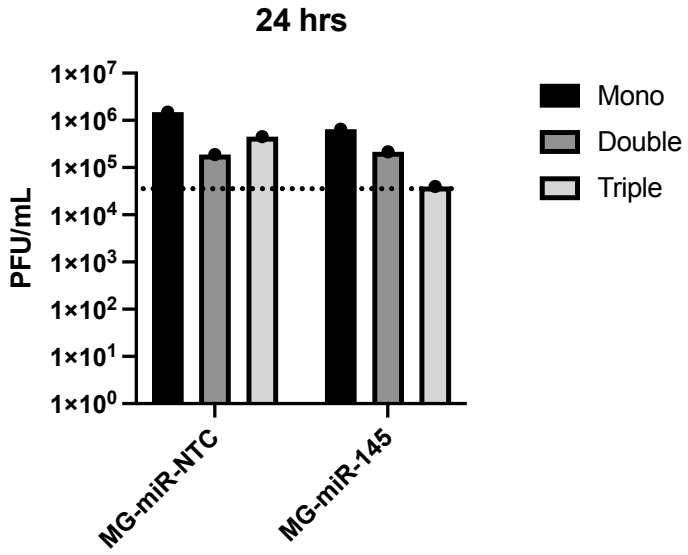

Figure 4-14. **MG-1 replication within LOVO cell lines.** Concentrations of MG-miR-NTC and MG-miR-145 (pfu/ml) were determined by plaque assay. Each spheroid contained $1x10^5$ cells therefore were treated with $5x10^4$pfu/ml of MG-miR-NTC and MG-miR-145. Supernatants were harvested at 24hrs, frozen at -80°C and plaque assays carried out. Figure 4.14 compares MG-miR-145 and MG-miR-NTC in mono, double and triple culture at 24 hours. Graphs show log values of viral titre (PFU/ml) for n=1 experiment.

4.13 Combination data for LOVO cells

Work in previous chapters has confirmed that CRC cells can be developed into a more representative model of cancer incorporating immune and stromal cells. This model in monoculture has shown to be sensitive to both 5-FU and MG-1. Similar to published literature the developed triple culture model has shown to be more resistant to 5-FU. Therefore, using this more complex model the OV MG-1 was used to deliver microRNA to restore chemosensitivity. As previously described in **Section**

4.1 MiR-145 is downregulated in CRC cells and upregulating this microRNA may enhance the treatment of CRC with 5-FU.

Having optimised the 3D MCTS CRC model and confirmed that these 3D cultures are susceptible to both 5-FU and MG-1 in **Figure 4.3 and Figure 4.9**, respectively. The combination of 5-FU with both MG-miR-NTC and MG-miR-145 was next investigated, to determine if expression of miR-145 from MG-1 enhanced tumour cell susceptibility to 5-FU, compared to control virus. Triple culture LOVO cell lines were initially infected with PBS (mock infected) or MG-miR-NTC or MG-miR-145 at an MOI of 0.1 for 30 hrs prior to the addition of 5-FU at varying concentrations (0, 50, 200 and 400μM) viability was then assessed as previously described at 72 hrs post 5-FU treatment. **Figure 4.15** shows the percentage of viable cells compared to PBS treated cells following infection with MG-miR-NTC and MG-miR-145 from two independent experiments for LOVO cell lines. LOVO MCTS displayed very little cytotoxic effects as single agent virus treatments however, a dose dependent decrease in cell viability was observed with 5-FU treatment. Unfortunately, no combination effects were observed.

In summary further optimisation of timings and doses are therefore needed to fully establish if restoring miR-145 expressing in CRC MCTS can enhance their susceptibility to 5-FU.

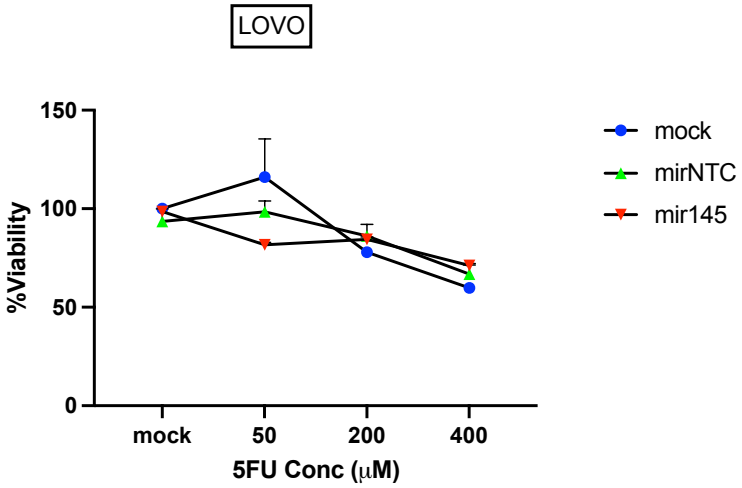

Figure 4-15. **Viability of LOVO 3D cell lines following combination treatment with virus and 5-FU.** LOVO, HFF and CD14 cells were seeded at a 2:1:1 ratio in 96 well ultra - low binding U bottom plates. Following incubation at 37°C for seven days cells were infected with miR-NTC and miR-145 at an MOI of 0.1 and incubated again at 37°C for 30 hrs. Following this, cells were treated with 5-FU at 0µM, 50µM, 200µM and 400µM for 72 hours. After treatment with virus and chemotherapy a CellTitre-Glo® Luminescent Cell Viability Assay was performed. The graph displays the viability of LOVO cells following infection with miR-NTC and miR-145. Date shows mean ± SEM for n=2.

4.14 Discussion

Drug discovery and therapeutic modalities used in cancer research rely on cell culture. However, as mentioned previously traditional 2D methods of cell culture have certain limitations. Therefore, there is a need for more a robust and reproducible cell culture akin to human disease to test anti-cancer therapies. As cancer cells develop resistance to commonly used agents, the drive to find new treatment modalities is continually evolving.

OVs are a novel treatment modality that have the potential to alter cancer progression and resistance. Advances in OV therapies have taken place over the last two decades and have shown promise, in that, clinical trials with OVs have shown little to no side effects in the human population. This is compared to the significant side effects observed with traditional anti-cancer therapies such as chemotherapy.

This is because OVs preferentially infect and kill tumour cells instead of healthy cells and because they can also be genetically modified to increase safety. [210] As well as reducing the harmful effects of some viruses, OV's can also be genetically engineered to enhance their potency. For example, Le Boeuf *et al* (2017) modified VSV with the p14 fusion protein which allowed cell fusion at a neutral pH. . Fusion at a neutral pH promoted higher viral yields and better dissemination in cancer cells and spheroids. In the CT26 CRC in vivo model, mice infected with VSV-p14 generated increased anti-tumour immunity, e.g., increased numbers of activated CD4+ and CD8+ T cells in the spleen, lymph nodes and tumours compared to controls. [211]

To date, there are no clinical studies investigating the OV potential of MG-1 in the treatment of CRC. However, studies have shown that MG-1 virus can be successfully genetically engineered to enhance viral replication. Previously, viral replication of MG-1 has been confirmed in a variety of cancer cell lines using the NCI-60 panel, which included five colon cancer cell lines (COLO205, HCT116, HCT15, HT29 and SW620). [15],[16] Pre- clinical studies have shown that in CT26-bearing mouse models, MG-1 can successfully infect and replicate in CT26 tumour, mice showed complete tumour regression of primary tumours, while extending the survival of mice with CRC lung metastasis. [212] Moreover, using a peritoneal carcinomatosis model of CRC intraperitoneal injection of MG-1 expressing IL-12 attracts activated natural killer (NK) cells to the peritoneal cavity. This study concluded that recruitment of NK cells reduced tumour burden; pivotally a complete response was demonstrated radiologically and 100% survival was displayed. [201] In line with the data presented in this chapter, these data also support the use of MG-1 for the treatment of CRC.

The treatment of CRC remains multi-factorial and surgery is the main stay of treatment for non-metastatic CRC. However, neoadjuvant and adjuvant chemo and radiotherapy remain important treatment options depending on severity and location of disease. Despite these tested treatment modalities being used in CRC a safer and more therapeutic modality is needed.

So far, there have been a number of Phase I trials for OVs in CRC and these show promising results. [12] One of these was a multicentre Phase I/II trial with HSV virus. Patients with metastatic CRC were given repeated doses of a genetically modified HSV (NV1020). This was administered over 10 minutes directly into the hepatic artery. Following administration, response was determined by growth of liver metastasis. Encouragingly, 50% of patients showed stable disease and importantly these results were achieved with minimal toxic side effects to the patients. [13] Another Phase I clinical trial using an adenovirus, Enadenotucirev (previously ColoAd1), also showed promising results. Enandenotucirev was injected prior to primary tumour resection. Results showed that Enandenotucirev was detected in tumour tissues but not in healthy tissue. There was also an increased level of CD8+ infiltration in tumour samples, suggesting possible activation of an anti-tumour immune response. Again, patients in this trial exhibited no side effects. [14] Collectively, these data support the potential us of OV, such as MG-1, for the treatment of CRC. However, it would be beneficial to use OVs in combination with standard therapies such as chemotherapy. In this regard, there have been a few ongoing trials investigating this dual treatment modality. For example, a recent Phase I/II trial has combined JX-594 (Pexa-Vec) with Irinotecan in CRC patients who are intolerant or refractory to standard therapies. [119] In addition, oncolytic reovirus has been evaluated in combination with Irinotecan, Leucovorin, 5-FU and Bevacizumab in patients with a KRAS mutated CRC. Results demonstrated that Reolysin used in combination with FOLFIRI (Folinic acid, fluorouracil and irinotecan) in CRC cancer patients that have a KRAS mutation, controlled disease in the majority of patients. [213]

The cytotoxic potential of 5-FU in 2D CRC cells was evaluated a dose dependent decrease in cell viability following treatment with 5-FU. These findings are in keeping with previous research by Mhaidat *et al* (2014) who displayed similar findings in CRC cell lines (SW480, SW620, HCT116 and HT29). Their results showed that 5-FU can induce apoptosis to varying degrees in CRC cells which was dependent on the activation of protein kinases C (PKC). Similarly, this study also used an MTT assay to examine cell viability, although cells were left for 72 hours post 5-FU treatment, at

doses 0, 1, 10, 25, 50, 100 and 200μM, rather than 96 hours post treatment, at doses 0, 10, 50, 100, 200, 400, 800μM, as used in **Figure 4.1**. Overall, similar results were concluded in that CRC cells were susceptible to the cytotoxic effects of 5-FU; however, this study determined that the HT29 cells were more sensitive cell to 5-FU than HCT116, which was the opposite of the findings in this study**.** It is possible that this difference could be due to the timing of 5-FU treatment or the density of CRC cells treated. [214]

As demonstrated in **Figures 4.2**, there appeared to be a difference in sensitivity to 5-FU in 2D and monoculture 3D cultures. For example, at 200μM HCT116 in 2D were 63.87% viable compared to 78.24% viable in 3D. Therefore, in summary **Figure 4.2** demonstrates that following treatment with 5-FU at varying concentrations the growth of tumour cells in a 3D model (monoculture) were more resistant that traditional 2D cancer models and therefore may represent a better model for testing novel therapeutic agents. These results were also confirmed by multiple studies including Lange *et al* (1992) and Koch *et al* (2021) which confirmed that CRC cells grown in 3D spheroids were resistant to 5-FU compared to 2D CRC grown in a monolayer. [215],[216]

3D CRC cells grown in mono, double and triple culture also showed a decrease in cell viability, in varying degrees, following treatment with 5-FU. The addition of fibroblasts and monocyte made no difference to the level of sensitivity to 5-FU. Although previously published work with 3D spheroids have not incorporated HFF and monocytes, these studies have reported differences in sensitivity to 5-FU in different CRC lines. [1, 27] For example, Virgone-Carlotta *et al* (2017) measured sensitivity to 5-FU in HT29, HCT116 and SW480 cell lines and found that 3D spheroids in SW480 were highly sensitive to 5-FU and HT29 cells were more resistant; HCT116 cells showed an intermediate level of sensitivity to 5-FU. [217] Unfortunately, it is difficult to make direct comparisons as the time point used in this study was 48 hours. Furthermore, tumour cell survival was measured differently, in this study a core volume measurement for cells in 3D and real cell time analysis methods for CRC cells in 2D culture were used.

As confirmed, MG-1 can infect CRC cells in the 2D model and CRC cell lines were susceptible to the cytotoxic effects of MG-1. Previous work by Zhang *et al* (2014) also confirmed that MG-1 has the potential to kill CT26 CRC cells, a murine CRC cell line. [218]

Similar to 2D cultures, 3D MCTS were also susceptible to MG-1 infection, regardless of the incorporation of fibroblast or monocytes. These results are similar to those reported by Lee *et al* (2020) who successfully infected 3D AF49 (lung cancer) cells (consisting of tumour, stromal and endothelial cells) with oncolytic vesicular stomatitis virus expressing GFP (oVSV-GFP). However, this study did not assess any differences when comparing mono culture spheroids with triple culture spheroids. [19] Tong *et al* (2015) also confirmed that MG-1 can rapidly enter mono culture ovarian cancer spheroids. Following entry, MG-1 spread through-out the spheroid and demonstrated rapid cytotoxic potential. [202]

Figure 4.9 shows the cytotoxic potential of MG-1 in 3D cultures and subtle differences were noted amongst cells in mono, double and triple culture. Of the four CRC cell lines tested in mono, double and triple culture the addition of HFF and monocytes in the HCT116 cell line made no difference in cell viability following infection with MG-1. The addition of HFF in double culture in the LOVO and HT29 offered a slight protective mechanism and more cells were viable in double culture compared to monoculture. However, addition of monocytes in HCA7-culture offered a possible protective mechanism against MG-1, which was not seen with the LOVO and HT29 cell lines. However, as these experiments (except for HCT116 cells) were only carried out once, further repeats are needed to confirm these preliminary findings.

Contrary to what has been presented in our study, previous work by Ilkow *et al* (2015) demonstrated that MG1-GFP showed enhanced infection and cytotoxicity when human pancreatic, ovarian and renal cell lines cancer cell lines were co-cultured with human GM38 fibroblasts. This study did, however, not focus on CRC cell lines and also used a different fibroblast cell line. Experiments were also performed on 2D

cultures instead of 3D cultures. It would therefore be interesting to test the cell lines used in this study either as 2D cultures or to investigate the cell lines used in the Ilkow study in our 3D MCTS model to gain a greater understanding of the mechanism of infection and how this is impacted by stromal compartments. [142] Furthermore, as the Ilkow study demonstrated that fibroblast growth factor 2 (FGF2) was a key soluble component to enhance the susceptibility of tumour cells to MG-1 infection, it would also be worthwhile investigating the production of this growth factor in our MCTS models. Moreover, to add to the complex interplay between tumour and stromal cells another study by Van Asten *et al* (2018) demonstrated that viral replication of VSV was inhibited by fibroblast growth factor 16 (FGF16). HAP1 cells treated with VSV expressing GFP in IFNB-1 conditioned medium did not show any signs of VSV infection. [219] These studies therefore suggest a number of mechanisms in which fibroblasts can modulate tumour cells that could either result in enhanced or reduced OV cytotoxicity, which is clearly evident even in our own studies between the four CRC used here.

To our knowledge this is the first time a multiplex cytokine analysis has been performed on 3D CRC cells incorporating immune and stromal cells and the effects of MG-1 on cytokine production determined. As is demonstrated in **Figure 4.11** and **Figure 4.12,** a variety of cytokines are expressed in 3D CRC cells depending on infection with MG-1. The production of IL-28 and IL-29 are the two cytokines that show interesting changes following infection although more biological replicates are required to validate these findings. IL-28 and IL-29 belong to the Interferon λ family and their immune response is similar to that found in type 1 IFN however, it is structurally similar to type II IFNs.[28] [29]Following infection with VSV, IFN- λ promotes anti-viral activity. [29] Studies have shown that IFN-λ offers a protective mechanism to HT29 cells that are infected with VSV. [30] However, as is demonstrated in **Figure 4.11** none of the 3D CRC cells produce IFNβ, therefore suggesting they have defective type I IFN pathways. IFN-α is usually produced by monocytes but as demonstrated in **Figure 4.11** no IFN-α were produced in the triple culture model. This would suggest monocytes in this model are unable to produce

IFN's due to M2 polarisation or they are embedded in an area of the spheroid that is unable to sense viral infection. By contrast, 3D cellular components could be producing small amounts of type I IFN's that are being used up by the cells and therefore are not released into the supernatant to be detected by multiplex assays. To investigate this further RT-qPCR could be performed to assess whether expression of IFNα/β was being induced but are below the detection limit of the assay, furthermore the induction of interferon simulated genes (ISGs) could also be assessed.

MG-1 infection induced the production of IL-28 in all three CRC cell lines tested. With the highest production seen in the monoculture model of HCT116 following infection. IL-28 is important in OV therapy as confirmed by Wongthida *et al* (2010). They demonstrated that tumour cells (B16 melanoma cells) within the TME, were sensitised to NK cell recognition by VSV-induced IL-28 production. They also confirmed that loss of IL-28 production decreased the VSV-induced NK cell killing. [220]

The production of IL-29 was more variable across all three CRC cell lines, however similar to IL-28, infection with MG-1 increased the production of IL-29 in the HCT116 and LOVO cell lines. In CRC IL-29 has been found to amplify the response of natural killer cells as well as upregulating the innate immune response. Sato *et al* (2006) successfully confirmed this by implanting mice with CT26 tumour cells that expressed mouse IFN-λ. Upregulation of IFN-λ induced apoptosis and NK cell-mediated tumour destruction. [221] To assess whether the different cell populations have an impact on IL-28/-29 production, stromal and immune cells cultured in 2D could be looked at in isolation and an ELISA assay performed to assess which cells expressed IL-28/-29.

As mentioned in **Chapter 3**, sCD163 is a myeloid specific marker that is solely expressed on monocytes and macrophages. [190] There is no literature to suggest that tumour cells can express it.[222] Studies have shown that sCD163 is an important predictor of CRC patient's prognosis and increased levels are associated with a poor prognosis; Krijgsman *et al* (2020) have confirmed that a higher level of

sCD163 in CRC patients was associated with a shorter overall and disease-free survival. [165] High levels of sCD163 imply that macrophages have undergone differentiation towards the M2 phenotype. [223] **Figure 4.11** suggests that sCD163 is produced in the HCT116 cell line following infection with MG-1. MG-1 infection in the double culture LOVO cell line also resulted in the production of sCD163. It can by hypothesised that MG-1 is a catalyst for sCD163 production in these cell lines. Moreover, it can also be hypothesised that infection with MG-1 could result in increase in production of MMPs, and hence cleave CD163 from the plasma membrane of CRC cell lines. To further evaluate this, CD163 expression either on the cell membrane or intra-cellular could be performed by flow cytometry, testing CRC cell lines under mock infected and MG1 infection to establish if CRC express CD163 under normal growth conditions or if it is induced following MG1 infection.

Finally, this chapter aimed to investigate whether incorporating miR-145 into MG-1 could improve the sensitivity of CRC MCTS to 5-FU treatment. Previous work in our laboratory has shown that pre-miRNA stem loops can be successfully incorporated into the rhabdovirus backbone, which are successfully processed and results in the generation of mature miRNA species. These miRNA sequences have been identified in both infected tumour cells and in extracellular vesicles isolated from the supernatant of infected cells. This then provides a mechanism in which knockdown of miRNA targets can occur in uninfected cells allowing for further dissemination within the TME. [137] As discussed in **Section 1.4,** microRNA regulate gene expression and can have tumour suppressor properties. OV and miRNA combination strategies have been investigated by two approaches, firstly as a way to target specific viral replication within a tumour cell and secondly to restore gene expression to improve combination therapies. This first strategy has been used in numerous pre-clinical studies and included encoding miRNA target sequences into the 3'untranslated region of viral genomes, for example, miRNA-145 driven viral replication of Adenovirus and HSV can target breast and lung cancer cells, respectively. The second approach has been less widely studied but has shown promise in the treatment of ARIDA1 wild-type tumours to sensitise cells to the small molecule inhibitor, GSK-126. Moreover, combining oncolytic virotherapy with

chemotherapy in CRC has previously shown promising results in various studies. For example, Ottolino-Perry *et al* (2015) investigated the potential of combining vaccinia virus (VV) with the chemotherapy agents oxaliplatin or SN-38 (active metabolite of irinotecan) in CRC cell lines. Results were promising in that cell killing in CRC cell lines was evident and median survival compared to monotherapy was significantly increased in the in vivo model. [224] Shen *at al* (2010) also confirmed the potential of combination OV therapy as a promising treatment option for CRC. A genetically modified adenovirus incorporating a Survivin targeted shRNA was tested alone as well as in combination with 5-FU. Results showed that combination therapy inhibited cancer metastasis in *in vivo*. Interestingly this effect was only displayed in combination therapy and monotherapy alone was ineffective. [225] Although MG-1 used in combination with 5-FU in CRC has yet to be investigated, Bourgeois-Daigneault *et al* (2016) confirmed that MG-1 can be used in combination with Paclitaxel in the breast cancer model. Results confirmed that combination therapy halted tumour growth and thus prolonged survival in murine models. [226]

MiR-145 is a tumour suppressor miRNA and is downregulated in CRC. Shen *et al* (2010) confirmed that the upregulation of miR-145 inhibited CRC cell invasion and migration in LOVO, HCT116 and HT29 CRC cells. [205] Moreover, restoring miR-145 also sensitised SW620 CRC cells to the cytotoxic effects of 5-FU. Studies have shown that reintroducing miR-145 into tumour cells enhances 5-FU sensitivity in CRC by directly targeting the RAD18 gene (DNA damage gene).[208] Due to the unstable nature of microRNA's a reliable delivery method is key. Recent studies have harnessed exosomes in the delivery of microRNA's. Sheykhhasan *et al* (2021) used MSC-derived exosomes to deliver miR-145 to T-47D breast cancer cells. Results showed that exosomes were statistically more efficient in delivery miR-145 cells compared to direct more standard transfection techniques ($p=0.033$). [227] Alternatively, Wedge *et al* (2022) confirmed that miRNA can be encoded and expressed by MG-1 can be packaged into exosomes which in turn are taken up by uninfected tumour cells. This can lead to those previously uninfected cells becoming sensitive to small molecule inhibition. [137]

To confirm an increase in expression levels of miR-145-5p following MG-miRNA infection preliminary qPCR analysis was performed on MCTS 24 hrs post infection and compared to the control virus, as is displayed in **Figure 4.13**. This demonstrated that miR-145 was successfully cloned into MG-1 and following infection mature miRNA species was identified in both LOVO and HCT116. Previous studies have investigated reintroducing miR-145 into the HCT116 cell line. For example, a study by Yu *et al* (2015) transfected HCT116 with a pCMV/miR145 plasmid and then subsequently quantified the expression of miR-145, this study found that following transfection miR145-5p was 4-fold higher in HCT116 cells than the control vector. [228] By contrast, results in **Figure 4.13** demonstrate a 9-fold change when using MG-1, this difference is most likely due to the difference in the mode of delivery. A fold increase of 47 was noted in the LOVO cells. This proof of principals confirms that miRNA delivery with MG-1 was more effective than previously reported transfection techniques.

Figure 4.14 shows that viral replication of both MG-miR-145 and MG-miR-NTC occurs in LOVO cells and these preliminary results suggest that expressing miR-145 from the viral backbone does not have a significant impact on viral replication. However, this needs to be repeated to confirm these preliminary findings. Whilst, definitive conclusions cannot be drawn from these preliminary findings previous unpublished work in our laboratory supports this data and confirm that miR-145 expression does not effect viral fitness in other cancer models.

Overall, it was hypothesised that restoring miR-145 expression using OV, either via either direct infection or by extracellular vesicle mediated transfer would lead to enhanced cell death following treatment with 5-FU.

To explore this possibility, 5-FU in combination with MG-miR-145 was tested in the 3D LOVO model. In order to achieve expression of MiR-145 to downregulate protein expression, cells were treated with the virus prior to treatment with 5-FU. Disappointingly, the addition of miR-145 did not improve 5-FU cytotoxicity. This could suggest that the miR-145 expressing virus did not replicate effectively in LOVO

MCTS and there was no expression of miR145. As was demonstrated in **Figure 4.8**, MG1-GFP only reached the periphery of the LOVO MCTS and therefore could suggest that viral replication in the spheroid core was impeded. This is confirmed in **Figure 4.14**, where no viral replication was seen in the LOVO triple culture model following infection with miR-145. Initially this was thought to be artifact which needed to be repeated, however, this could be due to viral replication being impeded in the MCTS when miR145 was encoded in the virus. The timing of viral infection and treatment with 5-FU could also be a factor. Cells were infected with an MOI of 0.1 at day seven and future experiments could infect cells with a higher MOI. Once 3D CRC cells were optimised, they were treated with virus at an MOI of 0.1 and incubated for thirty hours prior to treatment with 5-FU. Wang *et al* (2018) found that CRC cells that were pre-treated with oxaliplatin sensitised oxaliplatin resistant CRC cell to the cytotoxic effects of CVA11 infection (Coxsackievirus A11) both *in vitro* and *in vivo.* CRC cells WiDr cells were pre-treated with 50μM of oxaliplatin for 12 hours then infected with CVA11 at MOI's of 0, 0.01 and 0.001 and results confirmed that WiDr cells were more sensitive to combination therapy rather than either treatment in isolation. [229] Although direct comparison cannot be made these data do suggest that altering the timings and schedule of treatment could affect the results obtained.

The delivery strategy for upregulating miR-145 could also play a role in restoring chemosensitivity. Xu *et al* (2020) designed lipid-coated calcium carbonate nanoparticles (NPs) to co-transport both 5-FU and miR-375-3p into HT29 and HCT116 cells. These results demonstrated that the lipid coated NPs were rapidly and effectively released into the cells. Results showed that following delivery of the combined treatment in mouse models, the therapeutic effects were greater than that seen in mouse models treated with monotherapy. [230]

In conclusion, results from this chapter confirms that the more representative realistic model of CRC developed in chapter 3 was infected and killed with MG-1. However, unfortunately, further work is required to determine whether miR-145 delivery using MG-1 has the potential to enhance sensitivity to 5-FU chemotherapy. Future work would investigate the dose and timings of treatments/ infections and

explore the possibility of combination therapy using the alternative CRC models developed in chapter 3.

Chapter 5: Conclusion and future work

There has been continued advances in the treatment of CRC. However, the incidence continues to rise. Although, chemotherapy has been the mainstay of treatment for a number of decades a significant number of those patient treated with chemotherapy develop chemoresistance disease. It is for this reason a new treatment modality is needed. Ideally a combination therapy to harness the therapeutic features of chemotherapy would be advantageous. A number of OV's have been investigated in the treatment of CRC, however these trials are in the early stages. MG-1 has not been investigated in CRC and to date pre-clinical trials have focussed on 2D cell line models and mouse models which may not replicate human disease effectively. It is for this reason a more realistic model of cancer was developed to test the efficacy of MG-1 alone or in combination with . standard of care 5-FU chemotherapy. To date this is the first study to examine the role on Maraba with 5-FU in 3D CRC cells that have an immune and stromal component.

Within this study we have demonstrated that CRC cells can be grown in 3D cell culture. Moreover, within this model we are able to incorporate immune cells in the form of monocytes and stromal cells in the form of fibroblasts. We have also been able to develop a MCTS that is of a size that can be used to test anti-cancer therapies. Following the development of this 3D CRC MCTS we have demonstrated that 3D CRC in mono, double and triple culture have a different cytokine profile depending on the cells present within the model. Thereby confirming that the incorporation of monocytes and fibroblasts influenced the cytokine milieu that exist with the TME.

In addition to developing the 3D CRC MCTS spheroid model we also confirmed that cytotoxic potential of standard of care 5-FU. As expected, all four CRC cell lines in 2D were susceptible to the cytotoxic effects of 5-FU. Interestingly, 3D CRC cells were also susceptible to the cytotoxic effects of 5-FU. However, over-all when comparing 3D versus 2D cell models the 3D CRC model were more resistant to 5-FU than traditional

2D models and could therefore represent a better model to use to test novel anti-cancer therapies.

Following on from this, as MG-1 has never been used in the panel of CRC cells/MCTS in this project, virus infectibility was tested in the 2D CRC model and the 3D CRC model. Interestingly, MG-1 can infect and replicate in both 2D and 3D CRC models. MG-1 was also able to kill CRC in 2D and the addition of immune and stromal cells in the 3D HCT116 CRC model did not appear to impede the cytotoxic potential of MG-1. However, when comparing both models the 3D model was more resistant to the virus which is encouraging as the 3D model was developed in the hope that it was a more resistant model of CRC.

A Luminex assay confirmed that the addition of immune and stromal cells altered the production of cytokines (e.g IL-28, IL-29 and SCD163) following infection with MG-1. This is an interesting result and suggests that integrating different cellular components, to generate a more complex model of CRC would allow better characterisation of cancer therapeutics, not only in terms of cytotoxicity but also downstream effects on pro vs anti-inflammatory cytokines/chemokines.

MiR-145 is downregulated in chemo-resistant CRC. Therefore, the aim of this study, once a 3D model of CRC was established, was to generate proof of principle data showing that upregulation of miR-145 could be used to sensitise CRC to 5-FU. Disappointingly, in the LOVO cell line tested, no combination effects of treatment were observed.

Further optimisation of the timing of the virus doses as well as careful consideration of whether miR-145 is the correct miRNA to restored chemosensitivity should be made. Further replicates of the plaque assay would need to be performed in order to determine whether the addition of miR-145 impeded viral replication. As preliminary results confirmed that miR-145 had no effect on viral replication in monocultures but may be affected in triple culture spheroids.

Although, the combination data has been disappointing we have successfully developed a resistant 3D model of CRC. Further work would focus testing the miR-145 virus in the alternative CRC models developed and exploring whether alternative miRNA are downregulated in the CRC MCTS models. As we have demonstrated MG-1 has the ability to infect and replicate in this model, if miR145 remained ineffective at restoring chemosensitivity, future studies would focus on generating an alternative MG-1 vector that could work synergistically with standard of care chemotherapies, such as 5-FU or alternative chemotherapy agents.

APPENDIX

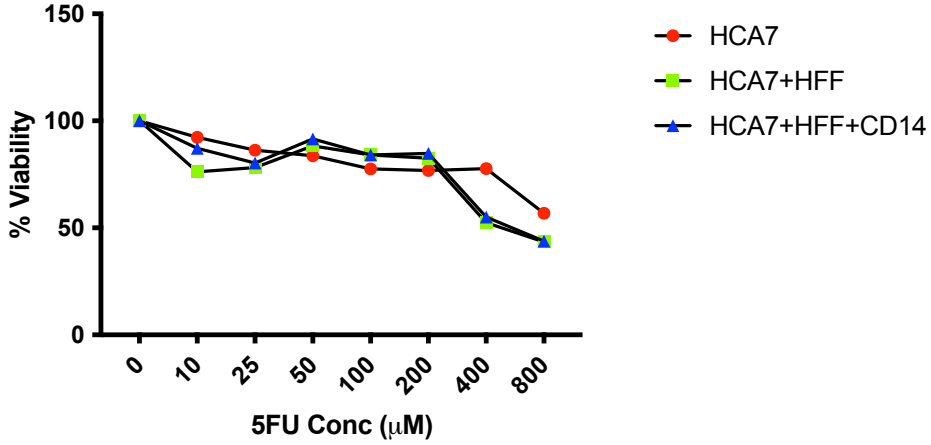

a)

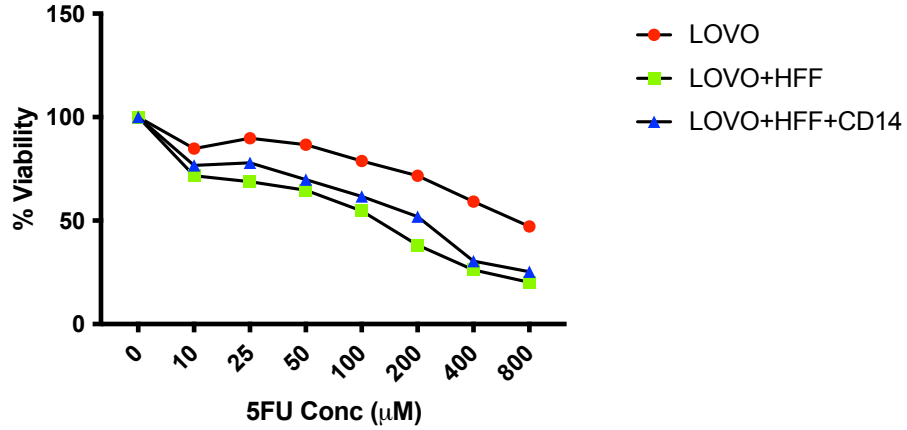

b)

***Figure 1*. Cytotoxicity of 5-FU in HCA7 and LOVO MCTS.** HCA7,LOVO, HFF and CD14 cells were seeded at ratios defined in chapter 3. Monoculture cells were seeded at $2.5x10^4$, double culture cells were seeded at a ratio of 2:1 and triple culture cells were seeded at a ratio of 2:1:1 in a 96 well ultra-low binding U bottom plate. Following incubation at 37°C for seven days cells were treated with 5-FU at 10, 25, 50, 100, 200, 400 and 800μM and incubated again for 96 hours at 37°C for a Cell-Titre-Glo® Luminescent Cell Viability Assay was performed. The graph shows mean % viability for ± SEM for n=1 for **a)** HCA7 and **b)** LOVO cells.

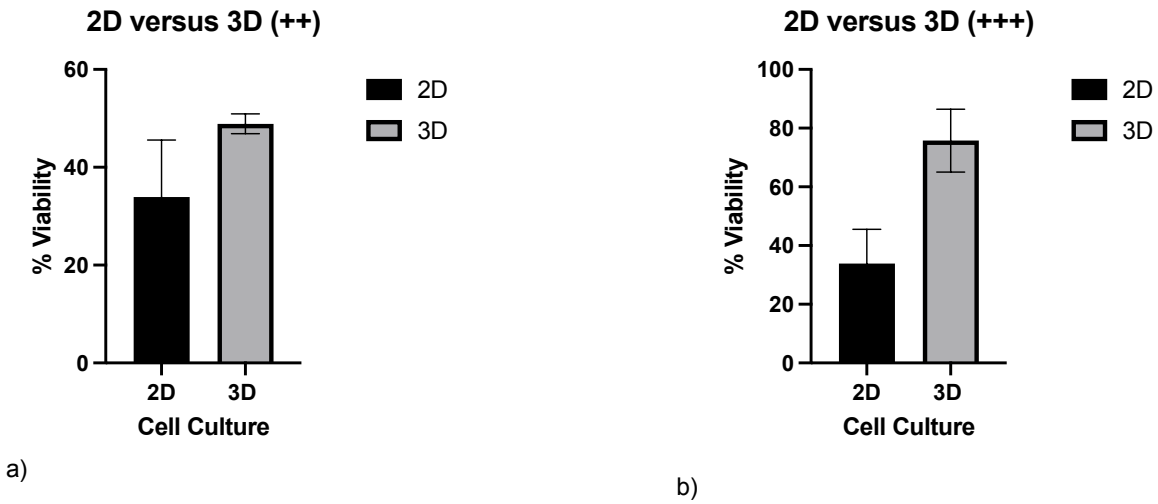

Figure 2. **Comparison of 2D versus 3D HCT116 cells with fibroblasts and monocytes following MG-1 infection.** HCT116 cells in 2D were seeded at $1.25x10^4$ cells/well in a 96 well flat bottom plate and HFF and CD14 cells were seeded at ratios defined in chapter 3. Double culture cells were seeded at a ratio of 2:1 and triple culture cells were seeded at a ratio of 2:1:1 in a 96 well ultra-low binding U bottom plate. Data shows the mean % viability of HCT116 cells in 2D and 3D 48hrs following infection with MG-1 at an MOI of 1, normalised to mock treated cells. Data shows mean ± SEM for n=4 independent experiments for 2D cells and n=2 for 3D cells. **a)** Shows 2D HCT116 cells compared to 3D HCT116 cells in double culture and **b)** shows 2D HCT116 cells compared to 3D HCT116 cells in triple culture. Statistical significance was calculated using the unpaired t-test and * denotes a statistically significant difference ($p<0.05$).

REFERENCES

1. Balkwill, F. and A. Mantovani, *Inflammation and cancer: back to Virchow?* Lancet, 2001. **357**(9255): p. 539-45.
2. Maibach, F., *Tumour-infiltrating Lymphocytes and Their Prognostic Value in Cutaneous Melanoma.* Front Immunol, 2020.
3. S, M., *Tumour host interaction: A Far-Reaching Relationship. .* Journal of Cancer Research and Clinical Oncology, 2010.
4. Klos, C.L. and S. Dharmarajan, *Polyp Genetics.* Clin Colon Rectal Surg, 2016. **29**(4): p. 289-295.
5. Kuipers, E.J., et al., *Colorectal cancer.* Nat Rev Dis Primers, 2015. **1**: p. 15065.
6. R, D., *Consensus molecular subtypes and the evaluation of precision medicine in colorectal cancer.* Nat Rev Cancer, 2017.
7. Baran, B., et al., *Difference Between Left-Sided and Right-Sided Colorectal Cancer: A Focused Review of Literature.* Gastroenterology Res, 2018. **11**(4): p. 264-273.
8. Pino, M.S. and D.C. Chung, *The chromosomal instability pathway in colon cancer.* Gastroenterology, 2010. **138**(6): p. 2059-72.
9. Kawakami, H., A. Zaanan, and F.A. Sinicrope, *Microsatellite instability testing and its role in the management of colorectal cancer.* Curr Treat Options Oncol, 2015. **16**(7): p. 30.
10. Afrasanie, V.A., et al., *KRAS, NRAS, BRAF, HER2 and microsatellite instability in metastatic colorectal cancer - practical implications for the clinician.* Radiol Oncol, 2019. **53**(3): p. 265-274.
11. Grady, W.M. and S.D. Markowitz, *The molecular pathogenesis of colorectal cancer and its potential application to colorectal cancer screening.* Dig Dis Sci, 2015. **60**(3): p. 762-72.
12. Yaeger, R. and R.B. Corcoran, *Targeting Alterations in the RAF-MEK Pathway.* Cancer Discov, 2019. **9**(3): p. 329-341.
13. Yang, D., et al., *Prognosis and clinical characteristics of colorectal cancer patients with KRAS gene mutation: a 5-year follow-up study.* Int J Clin Exp Pathol, 2019. **12**(2): p. 409-418.
14. Meng, M., et al., *The current understanding on the impact of KRAS on colorectal cancer.* Biomed Pharmacother, 2021. **140**: p. 111717.
15. Jones, R.P., et al., *Specific mutations in KRAS codon 12 are associated with worse overall survival in patients with advanced and recurrent colorectal cancer.* Br J Cancer, 2017. **116**(7): p. 923-929.
16. Caputo, F., et al., *BRAF-Mutated Colorectal Cancer: Clinical and Molecular Insights.* Int J Mol Sci, 2019. **20**(21).
17. Clarke, C.N. and E.S. Kopetz, *BRAF mutant colorectal cancer as a distinct subset of colorectal cancer: clinical characteristics, clinical behavior, and response to targeted therapies.* J Gastrointest Oncol, 2015. **6**(6): p. 660-7.
18. Koo, S., et al., *The NHS Bowel Cancer Screening Program: current perspectives on strategies for improvement.* Risk Manag Healthc Policy, 2017. **10**: p. 177-187.

19. Islam, Z., et al., *Prediabetes, Diabetes, and the Risk of All-Cause and Cause-Specific Mortality in a Japanese Working Population: Japan Epidemiology Collaboration on Occupational Health Study.* Diabetes Care, 2021. **44**(3): p. 757-764.
20. Church, D.N., R. Midgley, and D.J. Kerr, *Stage II colon cancer.* Chin Clin Oncol, 2013. **2**(2): p. 16.
21. Buturovic, S., *Colonoscopy as a method of choice in the diagnosis of colorectal cancer.* Acta Inform Med, 2014. **22**(3): p. 164-6.
22. Obenauf, A.C. and J. Massague, *Surviving at a Distance: Organ-Specific Metastasis.* Trends Cancer, 2015. **1**(1): p. 76-91.
23. Orr, F.W., et al., *Interactions between cancer cells and the endothelium in metastasis.* J Pathol, 2000. **190**(3): p. 310-29.
24. Langley, R.R. and I.J. Fidler, *The seed and soil hypothesis revisited--the role of tumor-stroma interactions in metastasis to different organs.* Int J Cancer, 2011. **128**(11): p. 2527-35.
25. Ribatti, D., G. Mangialardi, and A. Vacca, *Stephen Paget and the 'seed and soil' theory of metastatic dissemination.* Clin Exp Med, 2006. **6**(4): p. 145-9.
26. *Colorectal Cancer Survival by Stage-NCIN Data Briefing* 1996-2002.
27. Kopetz, S., et al., *Improved survival in metastatic colorectal cancer is associated with adoption of hepatic resection and improved chemotherapy.* J Clin Oncol, 2009. **27**(22): p. 3677-83.
28. Midgley, R.S. and D.J. Kerr, *Adjuvant chemotherapy for stage II colon cancer: less complicated than we thought.* J Clin Oncol, 2013. **31**(12): p. 1611.
29. Nordlinger, B., et al., *Perioperative chemotherapy with FOLFOX4 and surgery versus surgery alone for resectable liver metastases from colorectal cancer (EORTC Intergroup trial 40983): a randomised controlled trial.* Lancet, 2008. **371**(9617): p. 1007-16.
30. Iveson, T., et al., *Review of metastatic colorectal cancer treatment pathways and early clinical experience of trifluridine/tipiracil in the UK named patient programme.* BMC Cancer, 2020. **20**(1): p. 91.
31. Longley, D.B., D.P. Harkin, and P.G. Johnston, *5-fluorouracil: mechanisms of action and clinical strategies.* Nat Rev Cancer, 2003. **3**(5): p. 330-8.
32. Simpson, G.R., et al., *Cancer immunotherapy via combining oncolytic virotherapy with chemotherapy: recent advances.* Oncolytic Virother, 2016. **5**: p. 1-13.
33. Geretto, M., et al., *Resistance to cancer chemotherapeutic drugs is determined by pivotal microRNA regulators.* Am J Cancer Res, 2017. **7**(6): p. 1350-1371.
34. Hu, H., et al., *Loss of ABCB4 attenuates the caspase-dependent apoptosis regulating resistance to 5-Fu in colorectal cancer.* Biosci Rep, 2018. **38**(1).
35. Tie, Y., et al., *Upregulation of let-7f-5p promotes chemotherapeutic resistance in colorectal cancer by directly repressing several pro-apoptotic proteins.* Oncol Lett, 2018. **15**(6): p. 8695-8702.
36. Meads, M.B., R.A. Gatenby, and W.S. Dalton, *Environment-mediated drug resistance: a major contributor to minimal residual disease.* Nat Rev Cancer, 2009. **9**(9): p. 665-74.

37. Blondy, S., *5-Fluorouracil resistance mechanisms in colorectal cancer: From classical pathways to promising processes.* Cancer Sci, 2020.
38. Li, Z., et al., *Participation of CCL1 in Snail-Positive Fibroblasts in Colorectal Cancer Contribute to 5-Fluorouracil/Paclitaxel Chemoresistance.* Cancer Res Treat, 2018. **50**(3): p. 894-907.
39. Chen, F., et al., *New horizons in tumor microenvironment biology: challenges and opportunities.* BMC Med, 2015. **13**: p. 45.
40. M, O.B., *Apoptosis: A review of pro-apoptotic and anti-apoptotic pathways and dysregulation in disease.* Journal of Veterinary Emergency and Critical Care, 2008.
41. Ramesh, P. and J.P. Medema, *BCL-2 family deregulation in colorectal cancer: potential for BH3 mimetics in therapy.* Apoptosis, 2020. **25**(5-6): p. 305-320.
42. Das, P.K., F. Islam, and A.K. Lam, *The Roles of Cancer Stem Cells and Therapy Resistance in Colorectal Carcinoma.* Cells, 2020. **9**(6).
43. Wen, X.Q., et al., *MicroRNAs: Multifaceted Regulators of Colorectal Cancer Metastasis and Clinical Applications.* Onco Targets Ther, 2020. **13**: p. 10851-10866.
44. Thomas, J., et al., *MicroRNAs: Clinical Relevance in Colorectal Cancer.* Int J Mol Sci, 2015. **16**(12): p. 28063-76.
45. Zhu, J., et al., *MicroRNAs Associated With Colon Cancer: New Potential Prognostic Markers and Targets for Therapy.* Front Bioeng Biotechnol, 2020. **8**: p. 176.
46. Peng, Y. and C.M. Croce, *The role of MicroRNAs in human cancer.* Signal Transduct Target Ther, 2016. **1**: p. 15004.
47. Michael, M.Z., et al., *Reduced accumulation of specific microRNAs in colorectal neoplasia.* Mol Cancer Res, 2003. **1**(12): p. 882-91.
48. Xu, W.X., et al., *MiR-145: a potential biomarker of cancer migration and invasion.* Am J Transl Res, 2019. **11**(11): p. 6739-6753.
49. Kent, O.A., K. Fox-Talbot, and M.K. Halushka, *RREB1 repressed miR-143/145 modulates KRAS signaling through downregulation of multiple targets.* Oncogene, 2013. **32**(20): p. 2576-85.
50. Weinmann, H., *Therapeutic Areas II: Cancer, Infectious Diseases, Inflammation and Immunology and Dermatology*, in *Comperhensive Medicinal Chemistry II*. 2007, Elsevier.
51. Zhang, X., et al., *PAK4 regulates G6PD activity by p53 degradation involving colon cancer cell growth.* Cell Death Dis, 2017. **8**(5): p. e2820.
52. Ren, Y., et al., *TUSC3 induces drug resistance and cellular stemness via Hedgehog signaling pathway in colorectal cancer.* Carcinogenesis, 2020. **41**(12): p. 1755-1766.
53. Xu, Q., et al., *MiR-145 directly targets p70S6K1 in cancer cells to inhibit tumor growth and angiogenesis.* Nucleic Acids Res, 2012. **40**(2): p. 761-74.
54. Liang, X., et al., *An Enhancer-Driven Stem Cell-Like Program Mediated by SOX9 Blocks Intestinal Differentiation in Colorectal Cancer.* Gastroenterology, 2022. **162**(1): p. 209-222.
55. Dunn, T.A., et al., *A novel role of myosin VI in human prostate cancer.* Am J Pathol, 2006. **169**(5): p. 1843-54.

56. Lomperta, K., et al., *Insulin receptor substrate 1 may play divergent roles in human colorectal cancer development and progression.* World J Gastroenterol, 2020. **26**(28): p. 4140-4150.
57. Vu, T. and P.K. Datta, *Regulation of EMT in Colorectal Cancer: A Culprit in Metastasis.* Cancers (Basel), 2017. **9**(12).
58. Shioiri, M., et al., *Slug expression is an independent prognostic parameter for poor survival in colorectal carcinoma patients.* Br J Cancer, 2006. **94**(12): p. 1816-22.
59. Findlay, V.J., et al., *SNAI2 modulates colorectal cancer 5-fluorouracil sensitivity through miR145 repression.* Mol Cancer Ther, 2014. **13**(11): p. 2713-26.
60. Zhu, Y., et al., *miR-145 Antagonizes SNAI1-Mediated Stemness and Radiation Resistance in Colorectal Cancer.* Mol Ther, 2018. **26**(3): p. 744-754.
61. Yokoyama, W.M., *Natural killer cell immune responses.* Immunol Res, 2005. **32**(1-3): p. 317-25.
62. Amarante-Mendes, G.P., et al., *Pattern Recognition Receptors and the Host Cell Death Molecular Machinery.* Front Immunol, 2018. **9**: p. 2379.
63. Moretti, J. and J.M. Blander, *Insights into phagocytosis-coupled activation of pattern recognition receptors and inflammasomes.* Curr Opin Immunol, 2014. **26**: p. 100-10.
64. Marshall, J.S., et al., *An introduction to immunology and immunopathology.* Allergy Asthma Clin Immunol, 2018. **14**(Suppl 2): p. 49.
65. Actor, J., *Elsevier's Integrated Review Immunology and Microbiology*. 2012: London. p. 43-51.
66. Al Ahmad, M., et al., *Electrical Detection of Innate Immune Cells.* Sensors (Basel), 2021. **21**(17).
67. B, A., *Molecular Biology of the cell*. 2002.
68. Muenst, S., et al., *The immune system and cancer evasion strategies: therapeutic concepts.* J Intern Med, 2016. **279**(6): p. 541-62.
69. Pandya, P.H., et al., *The Immune System in Cancer Pathogenesis: Potential Therapeutic Approaches.* J Immunol Res, 2016. **2016**: p. 4273943.
70. Prakash, O., J. Gill, and G. Farr, *Immune disorders and susceptibility to neoplasms.* Ochsner J, 2002. **4**(2): p. 107-11.
71. Li, K., et al., *Myeloid-derived suppressor cells as immunosuppressive regulators and therapeutic targets in cancer.* Signal Transduct Target Ther, 2021. **6**(1): p. 362.
72. Kim, R., M. Emi, and K. Tanabe, *Cancer immunoediting from immune surveillance to immune escape.* Immunology, 2007. **121**(1): p. 1-14.
73. Norton, S.E., et al., *Immune cell interplay in colorectal cancer prognosis.* World J Gastrointest Oncol, 2015. **7**(10): p. 221-32.
74. O'Malley, G., et al., *Mesenchymal stromal cells (MSCs) and colorectal cancer: a troublesome twosome for the anti-tumour immune response?* Oncotarget, 2016. **7**(37): p. 60752-60774.
75. Peddareddigari, V.G., D. Wang, and R.N. Dubois, *The tumor microenvironment in colorectal carcinogenesis.* Cancer Microenviron, 2010. **3**(1): p. 149-66.

76. Williams, C.S., M. Mann, and R.N. DuBois, *The role of cyclooxygenases in inflammation, cancer, and development.* Oncogene, 1999. **18**(55): p. 7908-16.
77. Kitadai, Y., et al., *Targeting the expression of platelet-derived growth factor receptor by reactive stroma inhibits growth and metastasis of human colon carcinoma.* Am J Pathol, 2006. **169**(6): p. 2054-65.
78. Chen, Y., *Tumour-associated macrophages: an accomplie in solid tumour progression.* J Biomed Science, 2019.
79. chen, y., y. song, and W. Du, *Tumour-associated macrophages: an accomplice in solid tumour progression.* Journal of Biomedical Science, 2019.
80. Wang H, T.T., Zhang J, *Tumour-Associated Macrophages (TAMs) in Colorectal Cancer (CRC): From Mechanism to Therapy and Prognosis.* Internation Journal of Molecular Science, 2021.
81. Pinto, M.L., et al., *The Two Faces of Tumor-Associated Macrophages and Their Clinical Significance in Colorectal Cancer.* Front Immunol, 2019. **10**: p. 1875.
82. Forssell, J., et al., *High macrophage infiltration along the tumor front correlates with improved survival in colon cancer.* Clin Cancer Res, 2007. **13**(5): p. 1472-9.
83. Kang, J.C., et al., *Intratumoral macrophage counts correlate with tumor progression in colorectal cancer.* J Surg Oncol, 2010. **102**(3): p. 242-8.
84. Dost Gunay, F.S., et al., *Tumor-associated Macrophages and Neuroendocrine Differentiation Decrease the Efficacy of Bevacizumab Plus Chemotherapy in Patients With Advanced Colorectal Cancer.* Clin Colorectal Cancer, 2019. **18**(2): p. e244-e250.
85. Kumar, V., et al., *The Nature of Myeloid-Derived Suppressor Cells in the Tumor Microenvironment.* Trends Immunol, 2016. **37**(3): p. 208-220.
86. Chun, E., et al., *CCL2 Promotes Colorectal Carcinogenesis by Enhancing Polymorphonuclear Myeloid-Derived Suppressor Cell Population and Function.* Cell Rep, 2015. **12**(2): p. 244-57.
87. Sieminska, I. and J. Baran, *Myeloid-Derived Suppressor Cells in Colorectal Cancer.* Front Immunol, 2020. **11**: p. 1526.
88. Ma, P., et al., *Circulating Myeloid Derived Suppressor Cells (MDSC) That Accumulate in Premalignancy Share Phenotypic and Functional Characteristics With MDSC in Cancer.* Front Immunol, 2019. **10**: p. 1401.
89. Youn, J.I. and D.I. Gabrilovich, *The biology of myeloid-derived suppressor cells: the blessing and the curse of morphological and functional heterogeneity.* Eur J Immunol, 2010. **40**(11): p. 2969-75.
90. Heine, A., et al., *Targeting myeloid derived suppressor cells with all-trans retinoic acid is highly time-dependent in therapeutic tumor vaccination.* Oncoimmunology, 2017. **6**(8): p. e1338995.
91. Juno, J.A., et al., *Cytotoxic CD4 T Cells-Friend or Foe during Viral Infection?* Front Immunol, 2017. **8**: p. 19.
92. Tay, R.E., E.K. Richardson, and H.C. Toh, *Revisiting the role of CD4(+) T cells in cancer immunotherapy-new insights into old paradigms.* Cancer Gene Ther, 2021. **28**(1-2): p. 5-17.

93. Grizzi, F., et al., *Prognostic value of innate and adaptive immunity in colorectal cancer.* World J Gastroenterol, 2013. **19**(2): p. 174-84.
94. Zhang, X., et al., *The functional and prognostic implications of regulatory T cells in colorectal carcinoma.* J Gastrointest Oncol, 2015. **6**(3): p. 307-13.
95. Terme, M., et al., *VEGFA-VEGFR pathway blockade inhibits tumor-induced regulatory T-cell proliferation in colorectal cancer.* Cancer Res, 2013. **73**(2): p. 539-49.
96. Maby, P., et al., *Correlation between Density of CD8+ T-cell Infiltrate in Microsatellite Unstable Colorectal Cancers and Frameshift Mutations: A Rationale for Personalized Immunotherapy.* Cancer Res, 2015. **75**(17): p. 3446-55.
97. de Vries, N.L., et al., *The Immunogenicity of Colorectal Cancer in Relation to Tumor Development and Treatment.* Int J Mol Sci, 2016. **17**(7).
98. Frantz, C., K.M. Stewart, and V.M. Weaver, *The extracellular matrix at a glance.* J Cell Sci, 2010. **123**(Pt 24): p. 4195-200.
99. Manoukian, P., M. Bijlsma, and H. van Laarhoven, *The Cellular Origins of Cancer-Associated Fibroblasts and Their Opposing Contributions to Pancreatic Cancer Growth.* Front Cell Dev Biol, 2021. **9**: p. 743907.
100. Sahai, E., et al., *A framework for advancing our understanding of cancer-associated fibroblasts.* Nat Rev Cancer, 2020. **20**(3): p. 174-186.
101. Kim, I., et al., *Cancer-Associated Fibroblasts in the Hypoxic Tumor Microenvironment.* Cancers (Basel), 2022. **14**(14).
102. Santi, A., F.G. Kugeratski, and S. Zanivan, *Cancer Associated Fibroblasts: The Architects of Stroma Remodeling.* Proteomics, 2018. **18**(5-6): p. e1700167.
103. Glabman, R.A., P.L. Choyke, and N. Sato, *Cancer-Associated Fibroblasts: Tumorigenicity and Targeting for Cancer Therapy.* Cancers (Basel), 2022. **14**(16).
104. Deng, L., et al., *The Versatile Roles of Cancer-Associated Fibroblasts in Colorectal Cancer and Therapeutic Implications.* Front Cell Dev Biol, 2021. **9**: p. 733270.
105. Yuan, Q., et al., *MyD88 in myofibroblasts enhances colitis-associated tumorigenesis via promoting macrophage M2 polarization.* Cell Rep, 2021. **34**(5): p. 108724.
106. Wang, Y., et al., *Cancer-Associated Fibroblast Risk Model for Prediction of Colorectal Carcinoma Prognosis and Therapeutic Responses.* Mediators Inflamm, 2023. **2023**: p. 3781091.
107. Nishina, T., et al., *Interleukin-11-expressing fibroblasts have a unique gene signature correlated with poor prognosis of colorectal cancer.* Nat Commun, 2021. **12**(1): p. 2281.
108. Ham, I.H., D. Lee, and H. Hur, *Cancer-Associated Fibroblast-Induced Resistance to Chemotherapy and Radiotherapy in Gastrointestinal Cancers.* Cancers (Basel), 2021. **13**(5).
109. Gu, J., *Response prediction to oxaliplatin plus 5-fluorouracil chemotherapy in patients with colorectal cancer using a four-protein immunohistochemical model* Oncol Lett, 2019.

110. Tuomisto, A.E., M.J. Makinen, and J.P. Vayrynen, *Systemic inflammation in colorectal cancer: Underlying factors, effects, and prognostic significance.* World J Gastroenterol, 2019. **25**(31): p. 4383-4404.
111. Xing, F., J. Saidou, and K. Watabe, *Cancer associated fibroblasts (CAFs) in tumor microenvironment.* Front Biosci (Landmark Ed), 2010. **15**(1): p. 166-79.
112. Morini, S.R., et al., *Metalloproteinases and colorectal cancer. Correlation of gene expression and clinical-pathological parameters.* Acta Cir Bras, 2020. **35**(7): p. e202000707.
113. Fan, A., et al., *Immunotherapy in colorectal cancer: current achievements and future perspective.* Int J Biol Sci, 2021. **17**(14): p. 3837-3849.
114. Johdi, N.A. and N.F. Sukor, *Colorectal Cancer Immunotherapy: Options and Strategies.* Front Immunol, 2020. **11**: p. 1624.
115. Kelly, E. and S.J. Russell, *History of oncolytic viruses: genesis to genetic engineering.* Mol Ther, 2007. **15**(4): p. 651-9.
116. Hemminki, O., J.M. Dos Santos, and A. Hemminki, *Oncolytic viruses for cancer immunotherapy.* J Hematol Oncol, 2020. **13**(1): p. 84.
117. Pelin, A., et al., *The importance of imaging strategies for pre-clinical and clinical in vivo distribution of oncolytic viruses.* Oncolytic Virother, 2017. **7**: p. 25-35.
118. Marchini, A., E.M. Scott, and J. Rommelaere, *Overcoming Barriers in Oncolytic Virotherapy with HDAC Inhibitors and Immune Checkpoint Blockade.* Viruses, 2016. **8**(1).
119. Park, S.H., et al., *Phase 1b Trial of Biweekly Intravenous Pexa-Vec (JX-594), an Oncolytic and Immunotherapeutic Vaccinia Virus in Colorectal Cancer.* Mol Ther, 2015. **23**(9): p. 1532-40.
120. Fukuhara, H., Y. Ino, and T. Todo, *Oncolytic virus therapy: A new era of cancer treatment at dawn.* Cancer Sci, 2016. **107**(10): p. 1373-1379.
121. Ren, Y., et al., *Oncolytic viruses combined with immune checkpoint therapy for colorectal cancer is a promising treatment option.* Front Immunol, 2022. **13**: p. 961796.
122. Geevarghese, S.K., et al., *Phase I/II study of oncolytic herpes simplex virus NV1020 in patients with extensively pretreated refractory colorectal cancer metastatic to the liver.* Hum Gene Ther, 2010. **21**(9): p. 1119-28.
123. Ling, Q., et al., *The employment of vaccinia virus for colorectal cancer treatment: A review of preclinical and clinical studies.* Hum Vaccin Immunother, 2022. **18**(6): p. 2143698.
124. Samson, A., et al., *Neoadjuvant Intravenous Oncolytic Vaccinia Virus Therapy Promotes Anticancer Immunity in Patients.* Cancer Immunol Res, 2022. **10**(6): p. 745-756.
125. Lee, Y.S., et al., *Oncolytic vaccinia virus reinvigorates peritoneal immunity and cooperates with immune checkpoint inhibitor to suppress peritoneal carcinomatosis in colon cancer.* J Immunother Cancer, 2020. **8**(2).
126. Gong, J. and M.M. Mita, *Activated ras signaling pathways and reovirus oncolysis: an update on the mechanism of preferential reovirus replication in cancer cells.* Front Oncol, 2014. **4**: p. 167.

127. Fogel, E.J., et al., *Transcriptome Signature of Immune Cells Post Reovirus Treatment in KRAS Mutated Colorectal Cancer.* Cancer Manag Res, 2021. **13**: p. 6743-6754.
128. Adair, R.A., et al., *Cell carriage, delivery, and selective replication of an oncolytic virus in tumor in patients.* Sci Transl Med, 2012. **4**(138): p. 138ra77.
129. Zemp, F., J. Rajwani, and D.J. Mahoney, *Rhabdoviruses as vaccine platforms for infectious disease and cancer.* Biotechnol Genet Eng Rev, 2018. **34**(1): p. 122-138.
130. Brun, J., et al., *Identification of genetically modified Maraba virus as an oncolytic rhabdovirus.* Mol Ther, 2010. **18**(8): p. 1440-9.
131. Chiu, M., et al., *Combination therapy with oncolytic viruses and immune checkpoint inhibitors.* Expert Opin Biol Ther, 2020. **20**(6): p. 635-652.
132. Pol, J.G., et al., *Preclinical evaluation of a MAGE-A3 vaccination utilizing the oncolytic Maraba virus currently in first-in-human trials.* Oncoimmunology, 2019. **8**(1): p. e1512329.
133. Fernandez, M., et al., *Genetically engineered vesicular stomatitis virus in gene therapy: application for treatment of malignant disease.* J Virol, 2002. **76**(2): p. 895-904.
134. Li, Z., et al., *FSCN1 acts as a promising therapeutic target in the blockade of tumor cell motility: a review of its function, mechanism, and clinical significance.* J Cancer, 2022. **13**(8): p. 2528-2539.
135. Le Boeuf, F., et al., *Oncolytic Maraba Virus MG1 as a Treatment for Sarcoma.* Int J Cancer, 2017. **141**(6): p. 1257-1264.
136. Stewart, J.H.t., et al., *Vesicular stomatitis virus as a treatment for colorectal cancer.* Cancer Gene Ther, 2011. **18**(12): p. 837-49.
137. Wedge, M.E., et al., *Virally programmed extracellular vesicles sensitize cancer cells to oncolytic virus and small molecule therapy.* Nat Commun, 2022. **13**(1): p. 1898.
138. Sun, Y., et al., *The Influence of Cell Cycle Regulation on Chemotherapy.* Int J Mol Sci, 2021. **22**(13).
139. Jung, K.H., et al., *Oncolytic adenovirus expressing relaxin (YDC002) enhances therapeutic efficacy of gemcitabine against pancreatic cancer.* Cancer Lett, 2017. **396**: p. 155-166.
140. Zhang, B. and P. Cheng, *Improving antitumor efficacy via combinatorial regimens of oncolytic virotherapy.* Mol Cancer, 2020. **19**(1): p. 158.
141. Gomez-Gutierrez, J.G., et al., *Combined therapy of oncolytic adenovirus and temozolomide enhances lung cancer virotherapy in vitro and in vivo.* Virology, 2016. **487**: p. 249-59.
142. Ilkow, C.S., et al., *Reciprocal cellular cross-talk within the tumor microenvironment promotes oncolytic virus activity.* Nat Med, 2015. **21**(5): p. 530-6.
143. Filley, A.C. and M. Dey, *Immune System, Friend or Foe of Oncolytic Virotherapy?* Front Oncol, 2017. **7**: p. 106.
144. Sant, S. and P.A. Johnston, *The production of 3D tumor spheroids for cancer drug discovery.* Drug Discov Today Technol, 2017. **23**: p. 27-36.
145. Tammela, T. and J. Sage, *Investigating Tumor Heterogeneity in Mouse Models.* Annu Rev Cancer Biol, 2020. **4**(1): p. 99-119.

146. Usui, T., et al., *Establishment of a Novel Model for Anticancer Drug Resistance in Three-Dimensional Primary Culture of Tumor Microenvironment.* Stem Cells Int, 2016. **2016**: p. 7053872.
147. Kimlin, L.C., G. Casagrande, and V.M. Virador, *In vitro three-dimensional (3D) models in cancer research: an update.* Mol Carcinog, 2013. **52**(3): p. 167-82.
148. Clevers, H., *Modeling Development and Disease with Organoids.* Cell, 2016. **165**(7): p. 1586-1597.
149. Lee, S.H., et al., *Colorectal cancer-derived tumor spheroids retain the characteristics of original tumors.* Cancer Lett, 2015. **367**(1): p. 34-42.
150. Nath, S. and G.R. Devi, *Three-dimensional culture systems in cancer research: Focus on tumor spheroid model.* Pharmacol Ther, 2016. **163**: p. 94-108.
151. Browning, A.P., et al., *Quantitative analysis of tumour spheroid structure.* Elife, 2021. **10**.
152. Valcarcel, M., et al., *Three-dimensional growth as multicellular spheroid activates the proangiogenic phenotype of colorectal carcinoma cells via LFA-1-dependent VEGF: implications on hepatic micrometastasis.* J Transl Med, 2008. **6**: p. 57.
153. Kondo, J., et al., *High-throughput screening in colorectal cancer tissue-originated spheroids.* Cancer Sci, 2019. **110**(1): p. 345-355.
154. Dardousis, K., et al., *Identification of differentially expressed genes involved in the formation of multicellular tumor spheroids by HT-29 colon carcinoma cells.* Mol Ther, 2007. **15**(1): p. 94-102.
155. Dolznig, H., et al., *Modeling colon adenocarcinomas in vitro a 3D co-culture system induces cancer-relevant pathways upon tumor cell and stromal fibroblast interaction.* Am J Pathol, 2011. **179**(1): p. 487-501.
156. Bauleth-Ramos, T., et al., *Colorectal cancer triple co-culture spheroid model to assess the biocompatibility and anticancer properties of polymeric nanoparticles.* J Control Release, 2020. **323**: p. 398-411.
157. Habanjar, O., et al., *3D Cell Culture Systems: Tumor Application, Advantages, and Disadvantages.* Int J Mol Sci, 2021. **22**(22).
158. Cui, X., Y. Hartanto, and H. Zhang, *Advances in multicellular spheroids formation.* J R Soc Interface, 2017. **14**(127).
159. Edmondson, R., et al., *Three-dimensional cell culture systems and their applications in drug discovery and cell-based biosensors.* Assay Drug Dev Technol, 2014. **12**(4): p. 207-18.
160. Gialeli, C., A.D. Theocharis, and N.K. Karamanos, *Roles of matrix metalloproteinases in cancer progression and their pharmacological targeting.* FEBS J, 2011. **278**(1): p. 16-27.
161. Liu, B., Y. Zhao, and L. Guo, *Increased serum pentraxin-3 level predicts poor prognosis in patients with colorectal cancer after curative surgery, a cohort study.* Medicine (Baltimore), 2018. **97**(40): p. e11780.
162. Gallagher, G., et al., *Human interleukin-19 and its receptor: a potential role in the induction of Th2 responses.* Int Immunopharmacol, 2004. **4**(5): p. 615-26.

163. Holt, P.R., P. Kozuch, and S. Mewar, *Colon cancer and the elderly: from screening to treatment in management of GI disease in the elderly.* Best Pract Res Clin Gastroenterol, 2009. **23**(6): p. 889-907.
164. Kapalczynska, M., et al., *2D and 3D cell cultures - a comparison of different types of cancer cell cultures.* Arch Med Sci, 2018. **14**(4): p. 910-919.
165. Li, Y., et al., *Functional and Therapeutic Significance of Tumor-Associated Macrophages in Colorectal Cancer.* Front Oncol, 2022. **12**: p. 781233.
166. Wei, C., et al., *M2 macrophages confer resistance to 5-fluorouracil in colorectal cancer through the activation of CCL22/PI3K/AKT signaling.* Onco Targets Ther, 2019. **12**: p. 3051-3063.
167. Wang, Q., et al., *Drug Resistance in Colorectal Cancer: From Mechanism to Clinic.* Cancers (Basel), 2022. **14**(12).
168. Gencoglu, M.F., et al., *Comparative Study of Multicellular Tumor Spheroid Formation Methods and Implications for Drug Screening.* ACS Biomater Sci Eng, 2018. **4**(2): p. 410-420.
169. Mittler, F., et al., *High-Content Monitoring of Drug Effects in a 3D Spheroid Model.* Front Oncol, 2017. **7**: p. 293.
170. Wanigasekara, J., et al., *Three-Dimensional (3D) in vitro cell culture protocols to enhance glioblastoma research.* PLoS One, 2023. **18**(2): p. e0276248.
171. Bresciani, G., et al., *Evaluation of Spheroid 3D Culture Methods to Study a Pancreatic Neuroendocrine Neoplasm Cell Line.* Front Endocrinol (Lausanne), 2019. **10**: p. 682.
172. Zanoni, M., et al., *3D tumor spheroid models for in vitro therapeutic screening: a systematic approach to enhance the biological relevance of data obtained.* Sci Rep, 2016. **6**: p. 19103.
173. Mehta, G., et al., *Opportunities and challenges for use of tumor spheroids as models to test drug delivery and efficacy.* J Control Release, 2012. **164**(2): p. 192-204.
174. Tan, Y., et al., *Human fibroblast-macrophage tissue spheroids demonstrate ratio-dependent fibrotic activity for in vitro fibrogenesis model development.* Biomater Sci, 2020. **8**(7): p. 1951-1960.
175. Zoetemelk, M., et al., *Short-term 3D culture systems of various complexity for treatment optimization of colorectal carcinoma.* Sci Rep, 2019. **9**(1): p. 7103.
176. Yau, J.N.N. and G. Adriani, *Three-dimensional heterotypic colorectal cancer spheroid models for evaluation of drug response.* Front Oncol, 2023. **13**: p. 1148930.
177. Yakavets, I., et al., *Stroma-Rich Co-Culture Multicellular Tumor Spheroids as a Tool for Photoactive Drugs Screening.* J Clin Med, 2019. **8**(10).
178. Montalban-Hernandez, K., et al., *Colorectal Cancer Stem Cells Fuse with Monocytes to Form Tumour Hybrid Cells with the Ability to Migrate and Evade the Immune System.* Cancers (Basel), 2022. **14**(14).
179. Han, S.J., S. Kwon, and K.S. Kim, *Challenges of applying multicellular tumor spheroids in preclinical phase.* Cancer Cell Int, 2021. **21**(1): p. 152.
180. Fang, G., et al., *Gradient-sized control of tumor spheroids on a single chip.* Lab Chip, 2019. **19**(24): p. 4093-4103.

181. Ward, J.P. and J.R. King, *Mathematical modelling of drug transport in tumour multicell spheroids and monolayer cultures.* Math Biosci, 2003. **181**(2): p. 177-207.
182. Jeppesen, M., et al., *Short-term spheroid culture of primary colorectal cancer cells as an in vitro model for personalizing cancer medicine.* PLoS One, 2017. **12**(9): p. e0183074.
183. Bar, S.I., B. Biersack, and R. Schobert, *3D cell cultures, as a surrogate for animal models, enhance the diagnostic value of preclinical in vitro investigations by adding information on the tumour microenvironment: a comparative study of new dual-mode HDAC inhibitors.* Invest New Drugs, 2022. **40**(5): p. 953-961.
184. Rios de la Rosa, J.M., et al., *Colorectal tumor 3Din vitromodels: advantages of biofabrication for the recapitulation of early stages of tumour development.* Biomed Phys Eng Express, 2018. **4**(4).
185. Yeung, T.M., et al., *Cancer stem cells from colorectal cancer-derived cell lines.* Proc Natl Acad Sci U S A, 2010. **107**(8): p. 3722-7.
186. Liu, B., et al., *TSG-6 promotes Cancer Cell aggressiveness in a CD44-Dependent Manner and Reprograms Normal Fibroblasts to create a Pro-metastatic Microenvironment in Colorectal Cancer.* Int J Biol Sci, 2022. **18**(4): p. 1677-1694.
187. Webster, N.L. and S.M. Crowe, *Matrix metalloproteinases, their production by monocytes and macrophages and their potential role in HIV-related diseases.* J Leukoc Biol, 2006. **80**(5): p. 1052-66.
188. Kessenbrock, K., V. Plaks, and Z. Werb, *Matrix metalloproteinases: regulators of the tumor microenvironment.* Cell, 2010. **141**(1): p. 52-67.
189. Honda, T., I. Yamamoto, and H. Inagawa, *Angiogenesis-, metastasis- and signaling pathway-related factor dynamics in human colon cancer cells following interaction with monocytes.* Anticancer Res, 2013. **33**(7): p. 2895-900.
190. Krijgsman, D., et al., *CD163 as a Biomarker in Colorectal Cancer: The Expression on Circulating Monocytes and Tumor-Associated Macrophages, and the Soluble Form in the Blood.* Int J Mol Sci, 2020. **21**(16).
191. Franze, E., et al., *Role of Interleukin-34 in Cancer.* Cancers (Basel), 2020. **12**(1).
192. Franze, E., et al., *Interleukin-34 sustains pro-tumorigenic signals in colon cancer tissue.* Oncotarget, 2018. **9**(3): p. 3432-3445.
193. Baghdadi, M., et al., *Chemotherapy-Induced IL34 Enhances Immunosuppression by Tumor-Associated Macrophages and Mediates Survival of Chemoresistant Lung Cancer Cells.* Cancer Res, 2016. **76**(20): p. 6030-6042.
194. Ahmmed, B., et al., *Tunicamycin enhances the suppressive effects of cisplatin on lung cancer growth through PTX3 glycosylation via AKT/NF-kappaB signaling pathway.* Int J Oncol, 2019. **54**(2): p. 431-442.
195. Doni, A., et al., *The Long Pentraxin PTX3 as a Link Between Innate Immunity, Tissue Remodeling, and Cancer.* Front Immunol, 2019. **10**: p. 712.

196. Chang, X., et al., *Pentraxin 3 is a diagnostic and prognostic marker for ovarian epithelial cancer patients based on comprehensive bioinformatics and experiments.* Cancer Cell Int, 2021. **21**(1): p. 193.
197. Giacomini, A., et al., *Long pentraxin 3: A novel multifaceted player in cancer.* Biochim Biophys Acta Rev Cancer, 2018. **1869**(1): p. 53-63.
198. Rakina, M., et al., *Spheroid Formation and Peritoneal Metastasis in Ovarian Cancer: The Role of Stromal and Immune Components.* Int J Mol Sci, 2022. **23**(11).
199. Lazzari, G., et al., *Multicellular spheroid based on a triple co-culture: A novel 3D model to mimic pancreatic tumor complexity.* Acta Biomater, 2018. **78**: p. 296-307.
200. Ren, Y., *Oncolytic viruses combined with immune checkpoint therapy for colorectal cancer is a promising treatment option* Front Immunol, 2022.
201. Alkayyal, A.A., et al., *NK-Cell Recruitment Is Necessary for Eradication of Peritoneal Carcinomatosis with an IL12-Expressing Maraba Virus Cellular Vaccine.* Cancer Immunol Res, 2017. **5**(3): p. 211-221.
202. Tong, J.G., et al., *Evidence for differential viral oncolytic efficacy in an in vitro model of epithelial ovarian cancer metastasis.* Mol Ther Oncolytics, 2015. **2**: p. 15013.
203. Blondy, S., et al., *5-Fluorouracil resistance mechanisms in colorectal cancer: From classical pathways to promising processes.* Cancer Sci, 2020. **111**(9): p. 3142-3154.
204. Jung, E., et al., *MicroRNA-Based Therapeutics for Drug-Resistant Colorectal Cancer.* Pharmaceuticals (Basel), 2021. **14**(2).
205. Shen, X., et al., *MicroRNA-145 Inhibits Cell Migration and Invasion in Colorectal Cancer by Targeting TWIST.* Onco Targets Ther, 2019. **12**: p. 10799-10809.
206. Li, S., et al., *miR-145 suppresses colorectal cancer cell migration and invasion by targeting an ETS-related gene.* Oncol Rep, 2016. **36**(4): p. 1917-26.
207. Zheng, R.P., et al., *MiR-145 Regulates the Chemoresistance of Hepatic Carcinoma Cells Against 5-Fluorouracil by Targeting Toll-Like Receptor 4.* Cancer Manag Res, 2020. **12**: p. 6165-6175.
208. Liu, R.L., et al., *Tumor suppressor miR-145 reverses drug resistance by directly targeting DNA damage-related gene RAD18 in colorectal cancer.* Tumour Biol, 2015. **36**(7): p. 5011-9.
209. Langhans, S.A., *Three-Dimensional in Vitro Cell Culture Models in Drug Discovery and Drug Repositioning.* Front Pharmacol, 2018. **9**: p. 6.
210. Buijs, P.R., et al., *Oncolytic viruses: From bench to bedside with a focus on safety.* Hum Vaccin Immunother, 2015. **11**(7): p. 1573-84.
211. Le Boeuf, F., et al., *Reovirus FAST Protein Enhances Vesicular Stomatitis Virus Oncolytic Virotherapy in Primary and Metastatic Tumor Models.* Mol Ther Oncolytics, 2017. **6**: p. 80-89.
212. Pol, J.G., et al., *Development and applications of oncolytic Maraba virus vaccines.* Oncolytic Virother, 2018. **7**: p. 117-128.
213. Maitra, R., et al., *Oncolytic reovirus preferentially induces apoptosis in KRAS mutant colorectal cancer cells, and synergizes with irinotecan.* Oncotarget, 2014. **5**(9): p. 2807-19.

214. Mhaidat, N.M., M. Bouklihacene, and R.F. Thorne, *5-Fluorouracil-induced apoptosis in colorectal cancer cells is caspase-9-dependent and mediated by activation of protein kinase C-delta.* Oncol Lett, 2014. **8**(2): p. 699-704.
215. Lange, C.S., B. Djordjevic, and W.A. Brock, *The hybrid spheroid clonogenic assay for the intrinsic radio- and chemo-sensitivities of human tumors.* Int J Radiat Oncol Biol Phys, 1992. **24**(3): p. 511-7.
216. Koch, J., et al., *Three dimensional cultivation increases chemo- and radioresistance of colorectal cancer cell lines.* PLoS One, 2021. **16**(1): p. e0244513.
217. Virgone-Carlotta, A., et al., *In-depth phenotypic characterization of multicellular tumor spheroids: Effects of 5-Fluorouracil.* PLoS One, 2017. **12**(11): p. e0188100.
218. Zhang, J., et al., *Maraba MG1 virus enhances natural killer cell function via conventional dendritic cells to reduce postoperative metastatic disease.* Mol Ther, 2014. **22**(7): p. 1320-1332.
219. van Asten, S.D., et al., *Secretome Screening Reveals Fibroblast Growth Factors as Novel Inhibitors of Viral Replication.* J Virol, 2018. **92**(16).
220. Wongthida, P., et al., *Type III IFN interleukin-28 mediates the antitumor efficacy of oncolytic virus VSV in immune-competent mouse models of cancer.* Cancer Res, 2010. **70**(11): p. 4539-49.
221. Sato, A., *Anti-tumour activity of IFN-lamda in murine tumour models.* Journal of Immunology, 2006: p. 7686-7694.
222. Garvin, S., *Tumour cell expression of CD163 is associated to postoperative radiotherapy and poor prognosis in patients with breast cancer treated with breast-conserving surgery.* Journal of Cancer Research and Clinical Oncology, 2018: p. 1253-1263.
223. Yu, X., et al., *Scavenger Receptors: Emerging Roles in Cancer Biology and Immunology.* Adv Cancer Res, 2015. **128**: p. 309-64.
224. Ottolino-Perry, K., et al., *Oncolytic vaccinia virus synergizes with irinotecan in colorectal cancer.* Mol Oncol, 2015. **9**(8): p. 1539-52.
225. Shen, W., et al., *Oncolytic adenovirus mediated Survivin RNA interference and 5-fluorouracil synergistically suppress the lymphatic metastasis of colorectal cancer.* Oncol Rep, 2010. **24**(5): p. 1285-90.
226. Bourgeois-Daigneault, M.C., et al., *Combination of Paclitaxel and MG1 oncolytic virus as a successful strategy for breast cancer treatment.* Breast Cancer Res, 2016. **18**(1): p. 83.
227. Sheykhhasan, M., et al., *Exosomes of Mesenchymal Stem Cells as a Proper Vehicle for Transfecting miR-145 into the Breast Cancer Cell Line and Its Effect on Metastasis.* Biomed Res Int, 2021. **2021**: p. 5516078.
228. Yu, Y., et al., *miR-21 and miR-145 cooperation in regulation of colon cancer stem cells.* Mol Cancer, 2015. **14**: p. 98.
229. Wang, B., et al., *A Novel Combination Therapy for Human Oxaliplatin-resistant Colorectal Cancer Using Oxaliplatin and Coxsackievirus A11.* Anticancer Res, 2018. **38**(11): p. 6121-6126.
230. Xu, F., et al., *MicroRNA-375-3p enhances chemosensitivity to 5-fluorouracil by targeting thymidylate synthase in colorectal cancer.* Cancer Sci, 2020. **111**(5): p. 1528-1541.